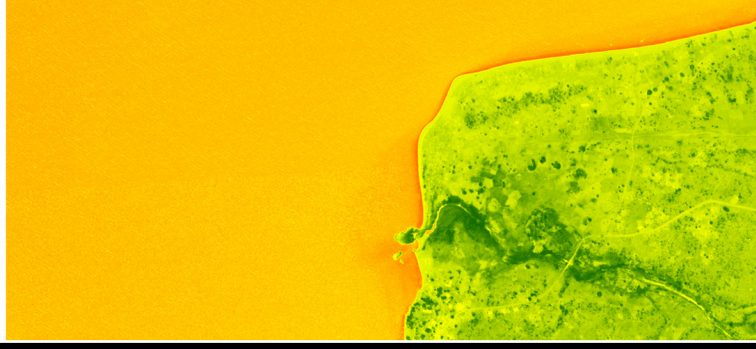

4

CONSERVATION TECHNOLOGY

# SATELLITE REMOTE SENSING

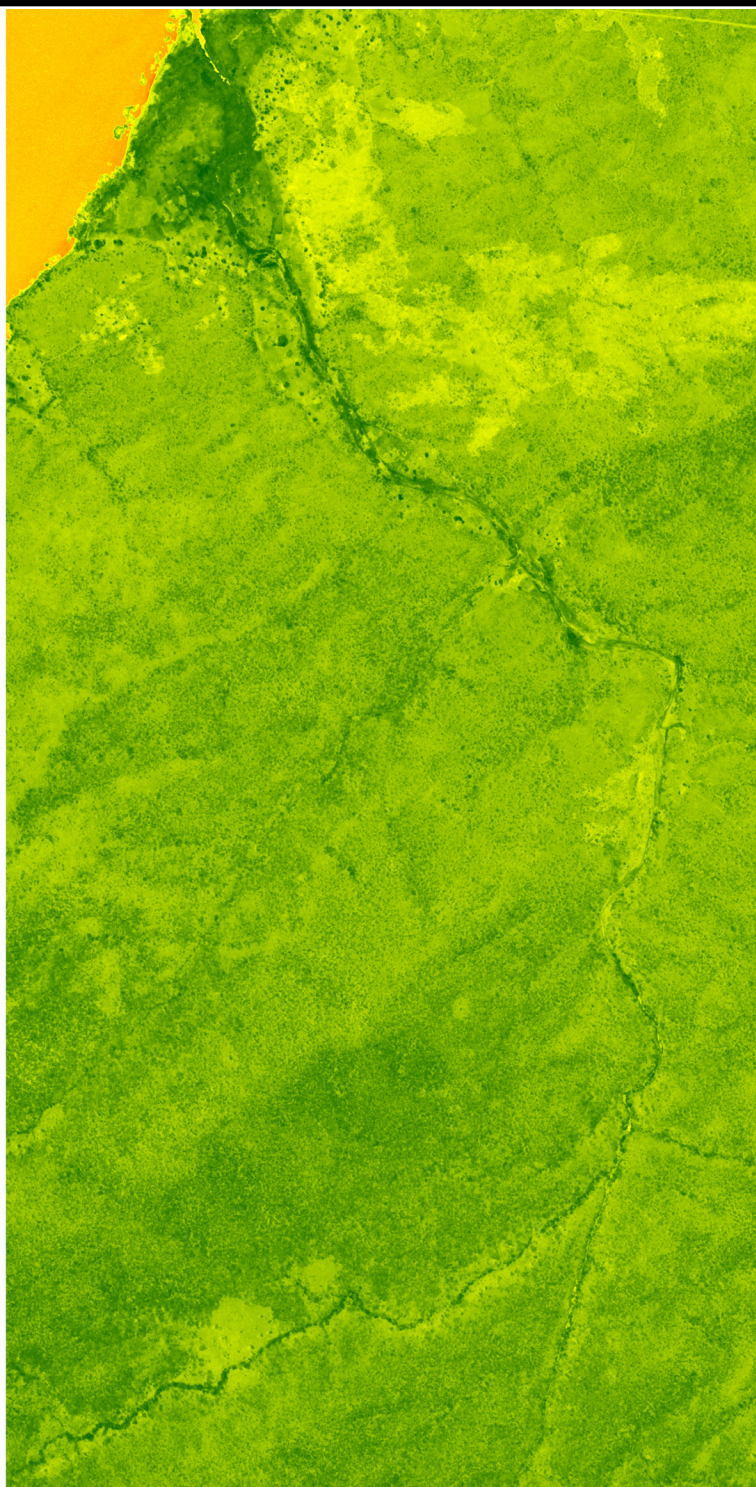

4

CONSERVATION TECHNOLOGY

SATELLITE REMOTE SENSING

# Satellite remote sensing for conservation

Nathalie Pettorelli, Henrike Schulte to Bühne, Aurélie C. Shapiro & Paul Glover-Kapfer.
2018. WWF Conservation Technology Series 1(4).



Cover image: Lake Niassa in Mozambique. The left panel contains a true colour composite, similar to how we would perceive the scene. The forests appear in green, bare areas in white, whereas agriculture and dry vegetation appear brown. The water grades from deep blue to turquoise at shallower depths. The right panel depicts the Normalized Difference Vegetation Index (NDVI), which captures information about the amount of photosynthetically active vegetation for the same area. Water has low NDVI values (yellow and red tones) whilst vegetation has higher values (green). The fringing forested wetlands appears dark green along the coast, indicating lush vegetation. Both sides of this image were derived from data acquired by the IKONOS satellite, which carries a multispectral sensor with a spatial resolution of 3 meters, in 2009.

Report designed by Volta Jazz.

Recommended Citation: Pettorelli, N., Schulte toBühne, H., Shapiro, A. C., & Glover-Kapfer, P. 2018. Satellite Remote Sensing for Conservation. WWF Conservation Technology Series 1(4). WWF.

# SATELLITE REMOTE SENSING FAQ

***What is satellite remote sensing?***

Remote sensing refers to the process of acquiring information about an object without coming into direct contact with it. Your vision could be considered one form of remote sensing because you are constantly acquiring information about many things in your environment without coming into contact with them! Satellite remote sensing refers to the acquisition of information via satellite-mounted sensors that measure the intensity of radiation in a particular range of the electromagnetic spectrum. Some of these sensors measure visible light or near-infrared radiation (multi- and hyperspectral remote sensing, LiDAR), whereas others measure microwave radiation (radar). This information is delivered in scenes (or images) which provide snapshots of a particular area of the Earth's surface from above. Satellite remote sensing allows monitoring of many aspects of the Earth system, including oceans, land surface and cryosphere. See **Chapter 2** for an overview of the different types of satellite remote sensing.

***What is the difference between radar and multispectral satellite remote sensing, and why does it matter?***

Multispectral remote sensors measure radiance in a small number of well-defined ranges of wavelengths ("spectral bands"). They are passive sensors, meaning they rely on an external source of energy (e.g. the sun or artificial light), and record the radiation reflected by the Earth's surface to produce an image. Radar sensors, by contrast, are active sensors, which emit energy in the microwave part of the electromagnetic spectrum, and measure the amount of energy reflected back at them. Multispectral and radar sensors record different characteristics of the Earth's surface: multispectral sensors generally respond to reflected light or colour, or chemical composition and temperature, whereas radar sensors respond to moisture content, orientation, surfaces and volume of objects in their field of view. Importantly, multispectral sensors cannot "see" through (penetrate) clouds, whereas radar sensors can. See **Chapter 2** for a short introduction to multispectral and radar remote sensors, and **Chapter 3** for a description of currently available multispectral and radar satellite remote sensing data.

***What kind of satellite remote sensing data exist?***

There are a large number of Earth-observing satellites currently in orbit, all of which carry multispectral or radar sensors (new satellites carrying LiDAR and hyperspectral sensors should be launched soon, see **Chapter 6**). Satellite sensors vary in the spatial resolution of the data they collect (from kilometre to sub-meter), the (overpass) frequency with which they collect data at a particular location (from monthly to daily), as well as the spectral characteristics (number of spectral bands and wavelength width for multispectral sensors; wavelength and polarisation modes for radar; see **Chapter 2**). Many of the organizations that own or operate spaceborne sensors provide open-access data, though some (especially those with higher spatial resolution) sell their data commercially. In addition to the "raw" satellite remote sensing data, a range of derived data products exist, including vegetation indices, land cover and fire maps, among others. **Chapter 3** provides an overview of the most commonly used satellite remote sensing data and derived products.

***How can satellite remote sensing be useful in conservation?***

Satellite remote sensing has become a standard tool in conservation science and practice for supporting large-scale monitoring of the extent and condition of ecosystems and habitats (see **Chapters 5.1** and **5.2**), as well as detecting threats to biodiversity (see **Chapter 5.3**) across land and marine biomes. Satellite remote sensing possesses several attributes that makes the approach particularly advantageous. First, spatial coverage is nearly continuous across large extents, and the data are of relatively high spatial resolution. Second, repeat ”snapshots” of the same geographic location produce multiple measures over time, thereby allowing time series analyses. Such spatially continuous time series data with potentially high spatial resolution allows trends in biodiversity to be detected at large scales, supporting global biodiversity monitoring initiatives and helping nations meet their reporting requirements. Spaceborne sensors can also be useful at more local scales, e.g. to help characterise changes in vegetation types or structure, to map roads or houses, or to detect individual species and organisms (see **Chapter 5.4**).

***Is it possible to detect subtle ecosystem/habitat degradation when it occurs in the absence of outright habitat loss, using satellite remote sensing methods?***

In addition to detecting change (loss or gain) in ecosystem or habitat distribution, satellite remote sensing can detect changes in the structure, composition and function of these ecological entities (see **Chapters 5.2** and **5.3**), which frequently indicate ecosystem or habitat degradation. Examples for this include mapping small gaps in forest canopies, identifying changes in biomass or primary productivity (including net primary productivity of vegetation, or eutrophication of freshwater or coastal water bodies) and tracking changes in the distribution of invasive species.

***Many parts of the world are persistently cloudy, blocking visible light. What technological and analytical methods are available to circumvent this?***

Sensors acquiring information in the visible and near-infrared part of the electromagnetic spectrum – e.g. multispectral or Light Detection and Ranging (LiDAR) – are sensitive to cloud cover. In contrast, radar remote sensing can penetrate clouds. Spaceborne radar is for example often used – alone or in combination with multispectral imagery – to monitor tropical forests (see **Chapter 5**), where availability of multispectral satellite remote sensing data can be limited by cloud cover. An alternative approach is to choose a multispectral sensor which revisits the same geographic location frequently (e.g. daily). This means that the sensor has more opportunities to view cloud-free openings (see **Chapter 3.1** for an overview of temporal resolutions of spaceborne multispectral sensors). Image compositing (i.e. selecting and combining cloud-free pixels across a longer time period such as weeks or months) can also help close data gaps.

***How far back in time do satellite remote sensing datasets go?***

Although coverage is not global, the Landsat mission provides multispectral imagery from as early as 1973, and the first civilian radar satellite, SEASAT, was launched in 1978. Earth observation satellites, together with the range of spectral, spatial and temporal resolutions of the datasets they are able to collect, rapidly increased in number after 2000. **Figure 3.3** provides an overview of the active periods of commonly used satellite remote sensors, including the estimated time period each sensor was active; this may vary locally because not all satellites (especially early satellites) have routinely acquired imagery over the entire globe.

***What is the cost of satellite remote sensing?***

A large number of satellite remote sensing datasets and products are open-access, or free to use, including data gathered by the Landsat, MODIS and the Sentinel missions. In some cases, commercial satellite data can be obtained for non-commercial or research applications by submitting a proposal to the institution which holds the data (such as the DigitalGlobe Foundation, ALOS PALSAR from the Japanese Space Agency or various data from the European Space Agency). Some satellites, especially those with high spatial resolutions, are primarily provided commercially, and range in cost from $1 to $20 per square kilometre. The **Appendix** lists most of the widely used satellite remote sensing data sets which are free of charge.

***How can I access satellite remote sensing data?***

EarthExplorer
http://earthexplorer.usgs.gov/

Copernicus Open Access Hub
https://scihub.copernicus.eu/

Open-access satellite remote sensing data can be downloaded from a large range of sources, including EarthExplorer (United States Geological Survey) and the Copernicus Open Access Hub (European Space Agency). Data from commercial providers is available through their respective websites. Download can be manual (choosing and downloading each scene by hand) or automated using scripts, bulk downloaders or programmed software. An overview of these sources is provided in **Table 3.1**.

***What kind of uncertainty is associated with different types of satellite data imagery, how is it quantified, and how will this influence my analyses?***

There are two key sources of uncertainty associated with satellite remote sensing imagery. Radiometric uncertainty comes from errors in measuring the signal (the radiation recorded by the sensor), whereas geometric uncertainty comes from errors in assigning a signal to its correct position on the Earth's surface. Radiometric and geometric precision are commonly reported in user handbooks, and vary between sensors. Many aspects of satellite remote sensing data pre-processing (see **Chapter 4.2**) aim to reduce the impact of radiometric or geometric uncertainty on analytical outcomes.

***What kind of uncertainty is associated with different types of products derived from satellite remote sensing (such as land cover maps), how is it quantified, and how does this affect comparability of different datasets?***

The accuracy of satellite remote sensing products is commonly assessed by comparison with independent data sets, either from field observations (ground-truthing data) or from other remote sensing data (such as high spatial resolution imagery, e.g. from Google Earth). For land cover maps, accuracy is quantified by comparing predicted and observed land cover. There are three measures of accuracy that are commonly reported (all are expressed in percent): first, the overall proportion of correctly identified pixels (called overall accuracy); second, the user accuracy (proportion of pixels that have been correctly labelled with a given land cover class); third, the producer accuracy (proportion of pixels belonging to a given land cover class that have been correctly labelled as such). For continuous variables, such as vegetation cover, accuracy can be quantified e.g. via root mean square error, or the coefficient of determination ($R^2$). Satellite remote sensing products are generated using a wide variety of methods and for different purposes, and their accuracy may vary depending on spatial scales, geographical location, and time. Where available, users should consult product handbooks and other literature for information about accuracy assessments, or validate products using ground-truthing data and standard methods for assessing statistical accuracy.

***What software do I need to analyse satellite remote sensing data?***

There are many types of software with satellite imagery processing and geospatial analysis capabilities. The most common software packages used for image processing include R (with added raster and remote sensing packages), QGIS, ArcGIS, ERDAS Imagine or ENVI. Processing large amounts of data efficiently or automation of processing might require use of programming languages such as Python, with processing commands from GDAL or GRASS GIS (see **Chapter 4.3**).

***How much computing power is required for analysing large satellite remote sensing datasets?***

The size of satellite remote sensing data sets increases with the area covered and the spatial, temporal and spectral resolutions considered. A single scene from Sentinel 1 corresponds to 1 GB of data and covers 10,000 km$^2$, whereas global coverage or dense time series typically require terabytes of data. The exact computing power requirements depend on the efficiency of the processing chain, such as whether parallel processing is used (see **Chapter 6**). In cases with large data processing requirements, cloud computing services or platforms such as Google Earth Engine (see **Box E**) provide access to greater computing power where necessary.

***What are the main classification methods used to convert raw remote-sensing data into land cover maps?***

Unsupervised and supervised image classification techniques are the two most common approaches to mapping land cover (see **Chapters 4.3** and **5.1**). Unsupervised classification is the simplest and quickest method, where the pixels in an image are separated into a pre-defined number of clusters or groups by an algorithm. The aim is to assign pixels with similar spectral properties to the same group; this approach is called unsupervised because no external information about land cover classes is provided. These clusters can later be assigned to different land cover classes. Supervised classification is when a machine learning algorithm is trained to distinguish discrete classes of land cover based on samples e.g. from ground-truthing data. Another increasingly commonly used approach for high resolution imagery is object segmentation, in which an algorithm identifies clusters of pixels that are more similar to each other than to the surrounding pixel; these clusters (or objects) can then be labelled by assigning them land cover classes.

***What is the difference between raster data and vector data (such as points, lines or shapes) derived from satellites, and why does it matter?***

Satellite data is provided in raster format, which means that it consists of a grid of pixels, each of which is associated with a measurement such as radiance. Pixels are georeferenced, which means they are associated with a location on a reference grid describing the Earth's surface. By contrast, vector data are used to store geospatial information in point, line or polygon format. Imagery in raster format can be converted into vector format, and vector data can likewise be converted to raster. For instance, all pixels in a raster image that cover a forest can be used to create a polygon of that forest, or all pixels that cover a river can be used to produce a line that corresponds to this river. Vector data are useful for calculating area-based statistics, e.g. the mean reflectance within a given radius around a line, or the most common land cover class in a polygon. By contrast, satellite remote sensing data has to be in raster format to generate band ratios or vegetation indices (see **Chapter 2.3**), to carry out supervised and unsupervised land cover classifications (**Chapter 4.4**), and to produce true-colour images of an area.

***What are the most important things for a new user to keep in mind when starting to work with satellite remote sensing data for the first time?***

As with all research and conservation endeavours, it is critical to have a clearly defined question, and identify time and budget constraints in order to select relevant imagery and analyses. What feature or element is the user trying to map, and what methods, software and hardware are available? This will greatly affect the selection of data and analytical technique. For instance, it might be tempting to assume that whichever satellite remote sensing data have the highest spatial resolution will be the most appropriate; however, if the aim is to map forest extent across an entire country or region, high spatial resolution may not be necessary, and may in fact put unnecessary strain on budget, time and computing resources. Some key considerations for choosing and pre-processing satellite remote sensing data are covered in **Chapter 4**.

Secondly, locating the right resources – such as available software, online software tutorials or user forums – will greatly simplify the process. This includes connecting with people working on the same kind of data, using similar software, and trying to answer similar questions. StackOverflow, GeoNet and OSGeo are good starting points for finding support and information about satellite remote sensing imagery processing and geospatial analysis. Groups connecting scientists and practitioners who apply satellite remote sensing in ecological and conservation contexts include the Remote Sensing Conservation Network (CRSnet) and CEOS Biodiversity.

Thirdly, it is important to remember that satellite remote sensing data is only one piece of the puzzle – ground-truthing data is indispensable to validate or interpret results in their geographic or ecological context. This means that sourcing existing or gathering new ground-truthing data is a key step in satellite remote sensing applications in conservation and ecology.

**StackOverflow**
www.stackoverflow.com

**GeoNet**
https://geonet.esri.com

**OSGeo**
www.osgeo.org

**CRSnet**
http://remote-sensing-biodiversity.org/networks/crsnet/

**CEOS Biodiversity**
http://remote-sensing-biodiversity.org/networks/ceos-biodiversity/

This is the first photograph of Earth ever taken from space, on 24 October 1946.
The image shows for the first time the curvature of the earth as seen by a V2 rocket, 105 km above the ground. Credit:  White Sand Missile Range /Applied Physics Laboratory

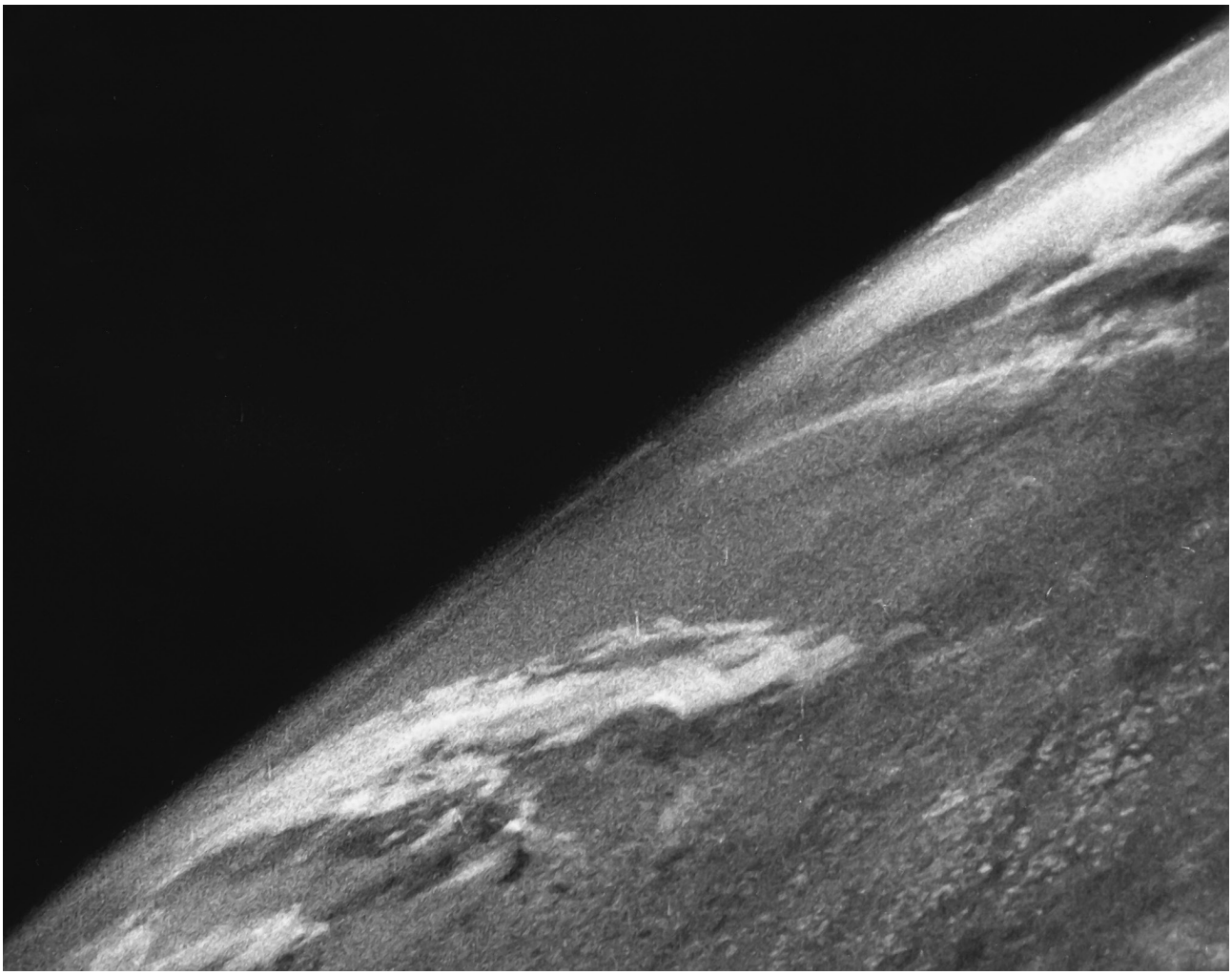

# TABLE OF CONTENTS

Polar bears (indicated by the yellow circle) in an SRS image with very high spatial resolution (< 1 m). Partial reproduction from Stapleton et al. 2014; satellite imagery printed under a CC BY license, with permission from DigitalGlobe ©2013.

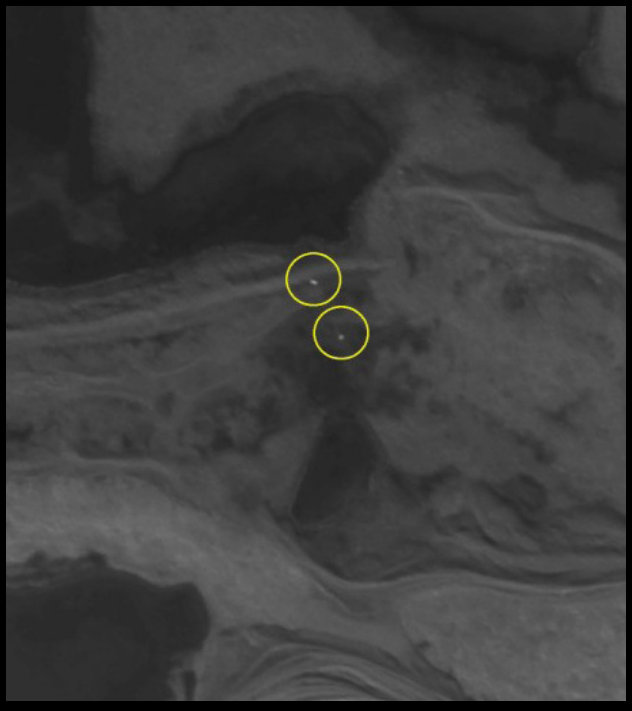

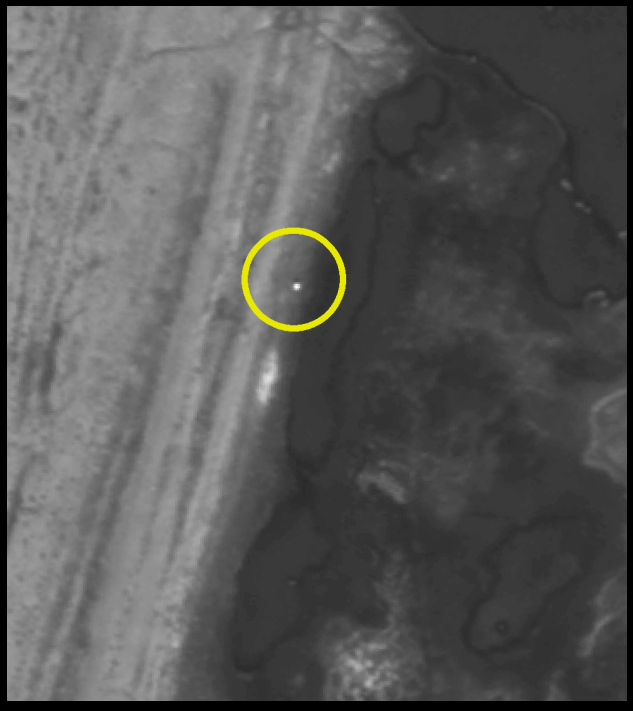

# 1 PREFACE

## 1.1 Aim of this guide

Humans are precipitating a global biodiversity crisis. Habitat loss and degradation, climate change, overexploitation, and invasive species threaten the survival of ecosystems and species worldwide (Butchart *et al.* 2010; Venter *et al.* 2016). The need for evidence-based conservation action has been widely recognised by conservation scientists, practitioners and policy-makers alike. Satellite Remote Sensing (SRS) offers a unique source of information about the biosphere, providing spatially explicit insights into biodiversity patterns and processes, and the threats and pressures they are experiencing, at multiple spatiotemporal scales. It is also a key source of repeated observations necessary to monitor our rapidly changing environment. As a result, SRS is an indispensable tool for developing and targeting evidence-based solutions, and monitoring their impacts. Although ecologists and conservation practitioners increasingly possess the technical skills required to effectively use satellite imagery, significant barriers to its use remain. This guide aims to familiarise prospective users in the conservation community with SRS technology and its applications (focusing on the two most widely used types of SRS: multispectral and radar), introduce terminology and principles behind SRS data and its analysis, support conservation practitioners in identifying where and how SRS could benefit their work, and give an overview of the resources (including software) needed for using SRS data.

## 1.2 Structure of this guide

The first half of this guide provides a primer on the most commonly used SRS data and their application in conservation science and practice. Though key terms and ideas are introduced primarily in **Chapter 2**, it is not necessary to read this guide in order, as a **Glossary** is provided. **Chapter 2** introduces SRS, defining terminologies as well as principles behind multispectral and radar SRS. This is followed by a review of available SRS data, focussing on open-access datasets and data products in **Chapter 3**. **Chapter 4** provides guidance on how to choose appropriate SRS data, and common pre-processing and analysis techniques, as well as software requirements for processing and analysis.

The second half of this guide focuses on best-practice information aimed at conservation practitioners who wish to begin exploring and using SRS data in their work. **Chapter 5** provides a broad overview of SRS-based opportunities for mapping and monitoring ecosystem and habitat extent and condition, species distributions, and threats to biodiversity. A brief introduction to advanced SRS data types and analysis techniques, which are beyond the scope of this guide, is offered in **Chapter 6**. **Chapter 7** outlines limitations of SRS that should be considered for SRS-based work, such as data resolution, availability and accessibility. Throughout this guide, there are descriptions of case studies illustrating how SRS data has been used to inform real-world conservation issues by WWF: mapping mangroves in Mozambique (**Box B**), degradation of palm swamp forest in Indonesia (**Box A**), and coral reefs in a marine protected area (**Box C**), as well as monitoring ecosystem functioning across the Arctic (**Box D**), and using Big Data to monitor land degradation in a transfrontier conservation complex (**Box E**).

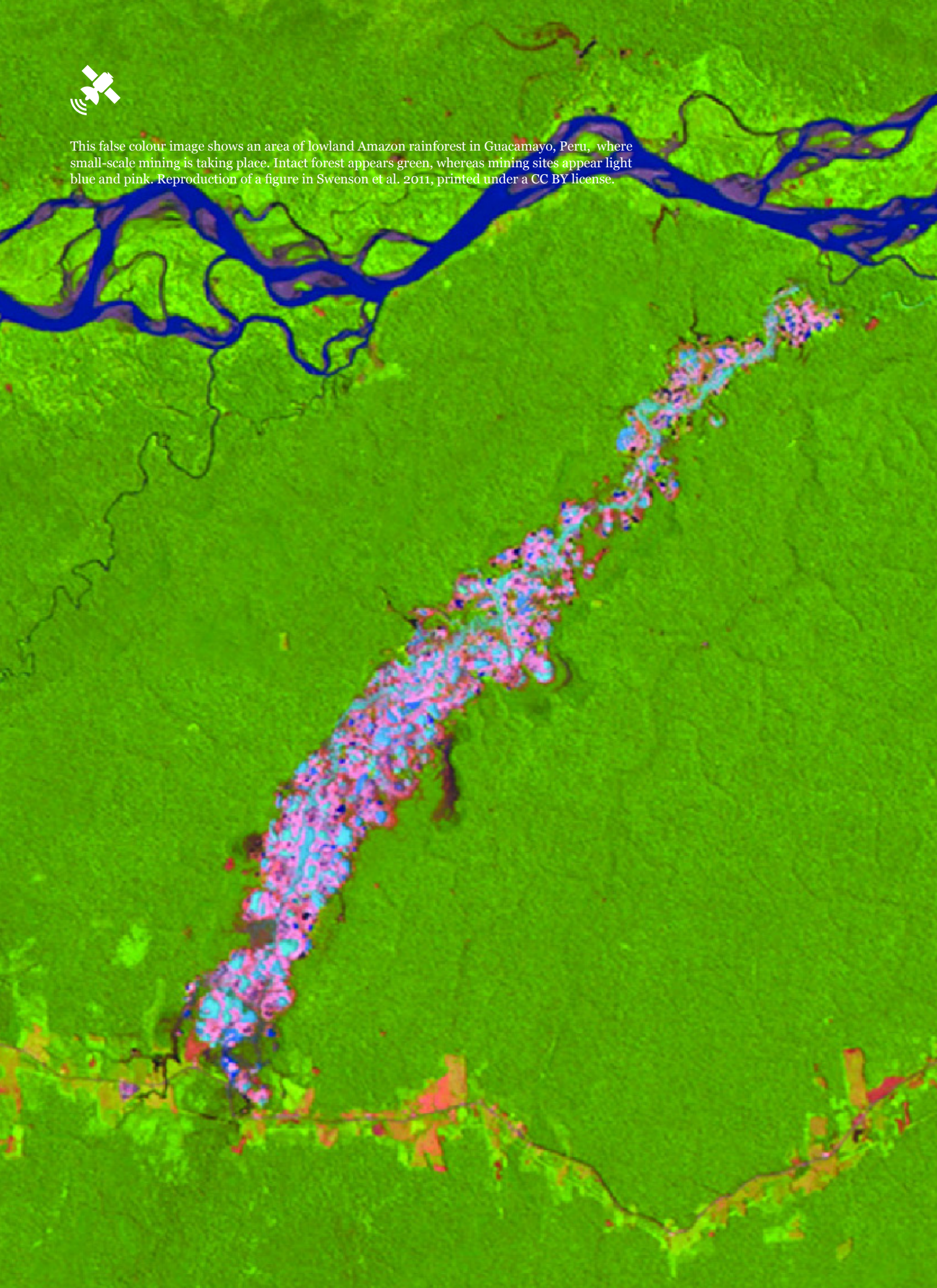

This false colour image shows an area of lowland Amazon rainforest in Guacamayo, Peru, where small-scale mining is taking place. Intact forest appears green, whereas mining sites appear light blue and pink. Reproduction of a figure in Swenson et al. 2011, printed under a CC BY license.

# 2 INTRODUCTION TO SATELLITE REMOTE SENSING

## HIGHLIGHTS

- Remote sensing is the process of identifying, observing, and measuring an object without coming into contact with it.
- Satellite remote sensing originated in the mid-20th century and measures electromagnetic radiation reflected off of objects, which is influenced by the object's size, shape, orientation, temperature, and chemical composition.
- Remote sensors are characterized by their spatial, temporal, spectral, and radiometric resolutions.
- There are two types of remote sensors: passive and active. Passive remote sensors do not emit radiation but instead measure reflected, emitted, or scattered radiation from other sources. In contrast, active remote sensors emit radiation and then measure that radiation as it is reflected.

Remote sensing refers to the process of identifying, observing and measuring an object without coming into contact with it (Pettorelli *et al.* 2015). Remote sensing thus includes acoustic monitoring of the environment (Blumstein *et al.* 2011), but the term is commonly used in reference to the measurement of electromagnetic radiation. Eyes, like cameras, are remote sensors (see **Glossary**). Remote sensing is based on the principle that all objects interact with incident radiation: they absorb, reflect, refract or scatter it (Campbell 1996) How much radiation an object reflects back at a remote sensor depends on its surface properties, like its size, orientation and chemical composition (Jackson & Huete 1991). Simply put, a tree has a different reflectance signature (or spectrum) than a rock under the same environmental conditions (**Figure 2.1**). This means it is possible to distinguish the two by sampling the radiation they reflect. Of course, the reflectance spectrum also depends on the incident radiation: a tree at dusk has a very different reflectance spectrum than a tree in the midday sun. Additionally, objects above absolute zero emit radiation themselves (Campbell 1996), which depends on their temperature, i.e. hot objects can be distinguished from cold objects.

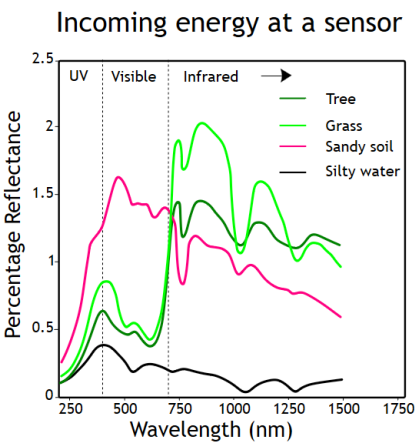


**Figure 2.1.** Different reflectance spectra (or curves) for different types of land cover. Vegetation typically has a large difference between reflectance in the red (approximately 620 – 750 nm) and the infrared compared to other types of land cover, a property that is exploited by vegetation indices. Image from Anthony Beck, published under CC-BY 3.0 license (adapted).

Humans can see electromagnetic radiation in wavelengths between approximately 400 nm and 750 nm, known as the visible spectrum. Remote sensors can measure radiation not only in the visible, but also at much larger wavelengths (infrared (700 nm – 1 mm), microwave (1 mm – 1 m), radio (1 m – 100,000 km)). Smaller-than-visible wavelengths (i.e. ultraviolet (10 nm – 400 nm)) are largely scattered by the Earth's atmosphere, and are therefore not used for remote sensing (**Figure 2.2**; Campbell 1996).

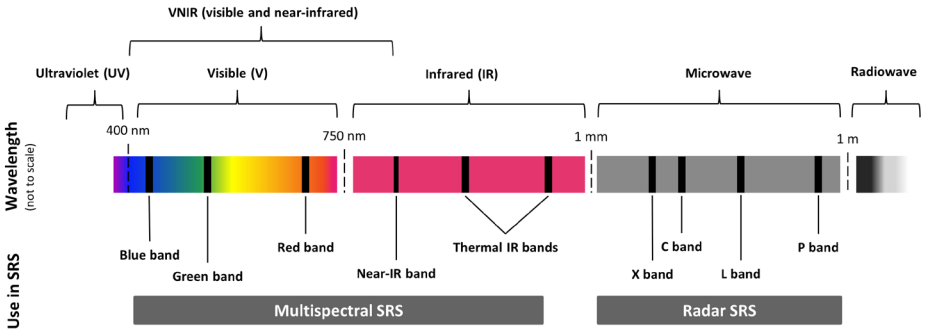


**Figure 2.2.** The spectrum of electromagnetic radiation (not to scale), and its use in satellite remote sensing.

Remote sensors can be located on the ground or deployed on aircrafts or satellites. Ground-based sensors range from hand-held spectrometers to camera traps (Burton *et al.* 2015) and weather radar stations. Airborne sensors are deployed on aircrafts or drones to gather remote sensing data with high spatial, spectral and/or temporal resolution (see below), but their use is normally restricted over relatively small areas.

Spaceborne remote sensors are deployed on satellites orbiting the Earth at heights of 500 to 800 km. A satellite earth observation mission has three basic components: *a space segment* (including the satellite, one or several sensors which measure electromagnetic radiation from the Earth's surface, and any other instruments needed for its operation); *a ground segment* (the ground stations which receive the data from the satellite via microwave downlink, pre-process and distribute the data, and control satellite operation, e.g. changes in orbit); and the *user segment* (databases accessible for end users). SRS imagery was first developed in the middle of the 20$^{th}$ century (Campbell 1996) and – in addition to its use by militaries and in disaster response – is today used in geology, geography and the environmental sciences, to monitor weather as well as terrestrial and marine resources (Morain 1998). Sensors onboard satellites are able to repeatedly gather standardized data from all points on the Earth's surface. This characteristic makes them an invaluable source of information to understand patterns and processes of the atmosphere, the biosphere, land surface, and the oceans, all of which fall under the umbrella term "Earth Observation".

## 2.1 Key concepts in remote sensing

Remote sensors are characterised by their spatial, temporal, spectral and radiometric resolutions (see **Glossary**, **Figure 2.3**):

- **Spatial** resolution refers to size of the smallest object that can be identified by a given sensor and corresponds to the size of an individual pixel. Spatial resolution is not only determined by sensor specifics, but also the height of the sensor above the Earth's surface (Latty *et al.* 1985). A low spatial resolution corresponds to a larger pixel size.

- **Temporal** resolution is the time between two successive images, and is given by the overpass frequency of a satellite (i.e. how often a satellite passes over the same location on the Earth's surface) which is determined by the sensor's orbit. Temporal coverage is determined by the launch and decommission dates.

- **Spectral** resolution is the smallest difference in wavelength that can be distinguished by a sensor. In the visible spectrum, this can be thought of as the number of different individual colours that can be detected.

- **Radiometric** resolution refers to the smallest difference in the intensity of radiation that can be distinguished by a sensor. This is akin to the number of grey values in a black-and-white photograph – the more different grey values there are, the finer the differences that can be distinguished.

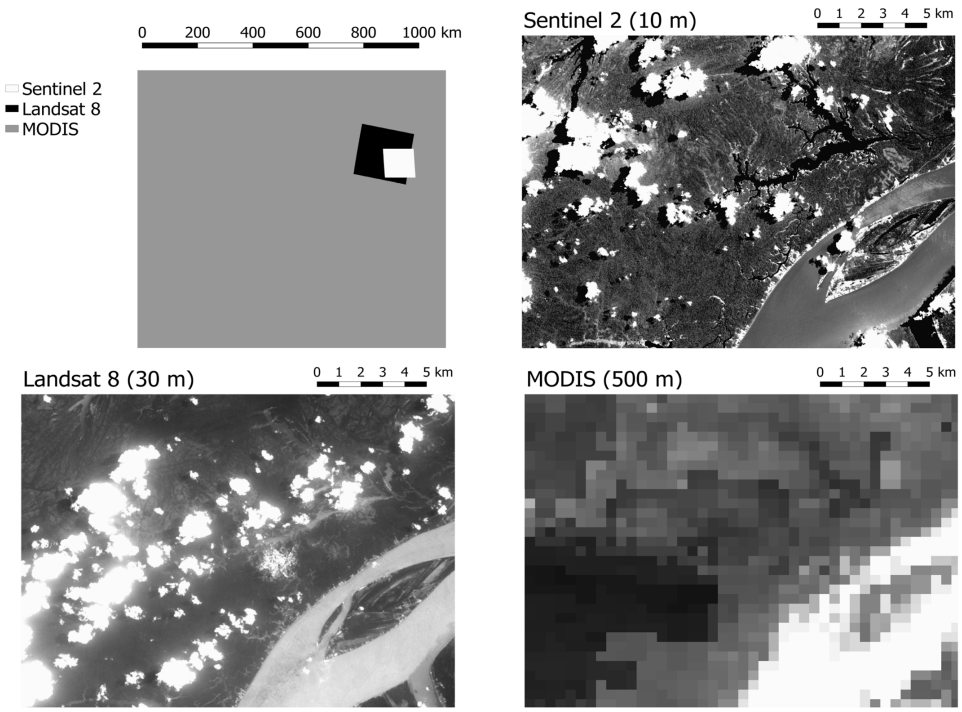


**Figure 2.3.** Clockwise from top left: Comparison of the footprint of three scenes from different multispectral spaceborne sensors; these vary in size from 100 x 100 km (Sentinel 2 Level 1C) to 1015 x 1015 km (MODIS MOD09A1 Surface Reflectance product). Three satellite images acquired over the same area, by three multispectral sensors, showing the different level of detail captured by different spatial resolutions.

It should be noted that temporal resolution and spatial resolution are often negatively correlated – the satellites with higher overpass frequency tend to have a higher orbit, and lower spatial resolution. Likewise, higher temporal resolution is not associated with large spatial extents, as sensors with a high spatial resolution often cover a smaller footprint. Satellites are typically intended to provide imagery across the entire Earth's surface, which is achieved by a polar orbit. In polar orbit, the satellite passes over, or near, the poles during each orbit as the Earth rotates. As a result, the satellite crosses the equator at different longitudes over time, so that it eventually canvasses all points on Earth. If the orbit is sun-synchronous, it means that the satellite passes over a given location on the Earth's surface at the same solar time in every orbit. To achieve this, the orbit rotates once around the earth's axis during one solar year. Satellites in geostationary orbits fly along the equator in such a way that they seem to rest above a given location on the Earth's surface. These satellites have a fixed view, but their signal is easier to capture by ground stations because it comes from the same relative position at all times. By contrast, polar-orbiting satellites change their position relative to ground stations and the antennae which receive their signals have to track the satellite as it flies overhead.

## 2.2 How remote sensing works: passive and active sensors

Remote sensors can be classified into two categories: passive and active (see **Figure 2.4**). Passive remote sensors do not emit radiation themselves, but instead measure radiation which is reflected, emitted or scattered by an object (Campbell 1996). In SRS, the source for this radiation is the sun, thermal energy or other sources such as anthropogenic light (for sensors collecting at night). Active remote sensors, by contrast, emit radiation themselves, and then measure the returning signal or echo.

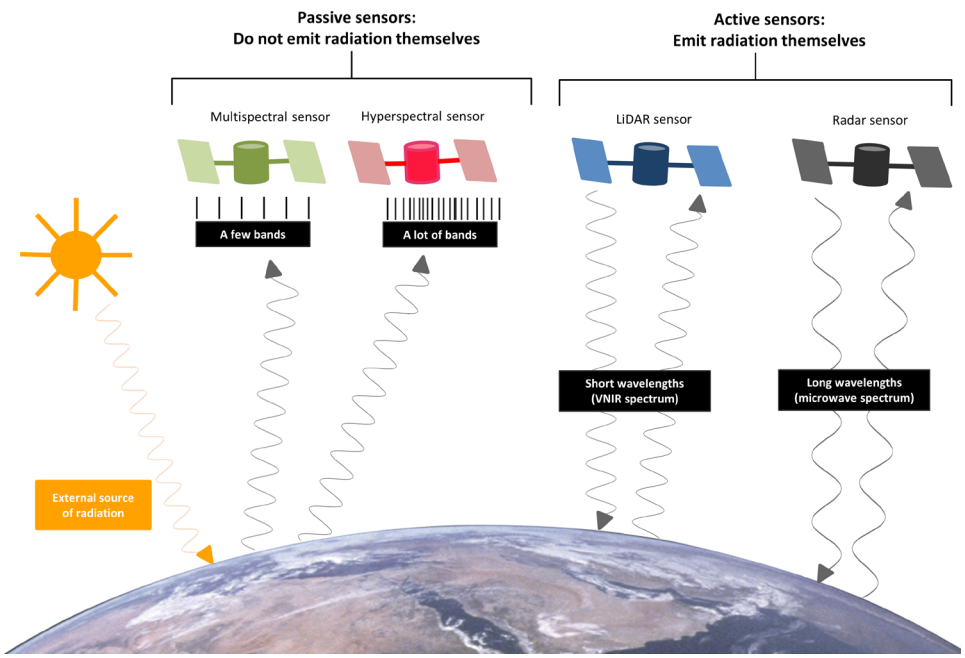


**Figure 2.4.** The difference between four major types of remote sensors: passive sensors (multispectral and hyperspectral) do not emit radiation themselves, but active sensors (LiDAR and radar) do. The passive modes are distinguished by the number of bands across which they measure radiance, whereas the active modes are distinguished by the wavelength of the radiation which they emit. Image: Astronaut photograph AS17-148-22727 courtesy NASA Johnson Space Center Gateway to Astronaut Photography of Earth.

*Passive remote sensing*

The most common type of passive remote sensing is multispectral remote sensing. The key parameter measured by multispectral sensors is radiance or radiant flux, which is the amount of radiation reflected from a unit surface area, as detected by the sensor (measured in power per solid angle and unit area [$W \cdot sr^{-1} \cdot m^{-2}$]). This is also referred to as the reflectance or brightness. If the amount of radiation hitting an object is known, he reflectance is the proportion of the radiation that is reflected by an object, instead of being absorbed or transmitted. For instance, if we know the time at which an image was acquired, and the position of the satellite, we can work out the illumination conditions, and then derive reflectance. Because multispectral sensors depend on the sun as a source of radiation, they are not used at night, though there are some sensors which detect artificial light emitted from cities or infrastructure.
Multispectral sensors measure brightness in a limited number of relatively broad bands (**Figure 2.2**). These bands are generally found in the visible and near to mid-infrared parts of the spectrum ("thermal" bands). Typically, some bands correspond to colours that humans can perceive (red (R), green (G), blue (B) bands), allowing the reconstruction of RGB images, which are very close to how humans perceive the environment (**Figure 2.5**). However, the exact width of each band varies from sensor to sensor.

- **Blue** bands (approximately 450–495 nm) are the most sensitive to atmospheric scattering, and are often used to correct for optical properties of the atmosphere, such as haze (Kaufmann & Tanre 1992).

- **Green** bands (approximately 495–570 nm) help visualize vegetation, since green light is strongly reflected by photosynthetic vegetation.

- Light in the **Red** band (approximately 620–750 nm) is strongly absorbed by vegetation, and as a result, this band is often used for monitoring vegetation condition or health, e.g. as part of vegetation indices (Vogelmann *et al.* 1993; see **Chapter 2.3**).

- **Near-infrared** bands (approximately 780–1400 nm) are useful for identification of water bodies, which strongly absorb radiation in this part of the spectrum (Ruddick *et al.* 2006; see **Chapter 2.3**).

- **Short to mid-infrared** bands (approximately 1.4–3 μm and 3–8 μm respectively) are sensitive to water content (in soils, Lobell & Asner 2002, or vegetation, Tucker 1980), including clouds (Horning 2004).

- **Thermal** bands (approximately 3 μm –1 mm) are sensitive to temperature, and are used e.g. to detect fires, or clouds (Zhu & Woodcock 2012; see **Chapter 3.3**).

Additionally, multispectral sensors often have a single brightness band with a higher spatial resolution referred to as the **panchromatic** band because it covers a much larger range of wavelengths than the others. This band can be used to "pansharpen" other bands, a process in which the brightness values of the bands with lower spatial resolution are substituted for those of the panchromatic band, resulting in an image with higher spatial resolution. Finally, some passive sensors measure radiation at much longer wavelengths (i.e. < 300 μm wavelength up to microwaves), which are primarily used for weather observations.

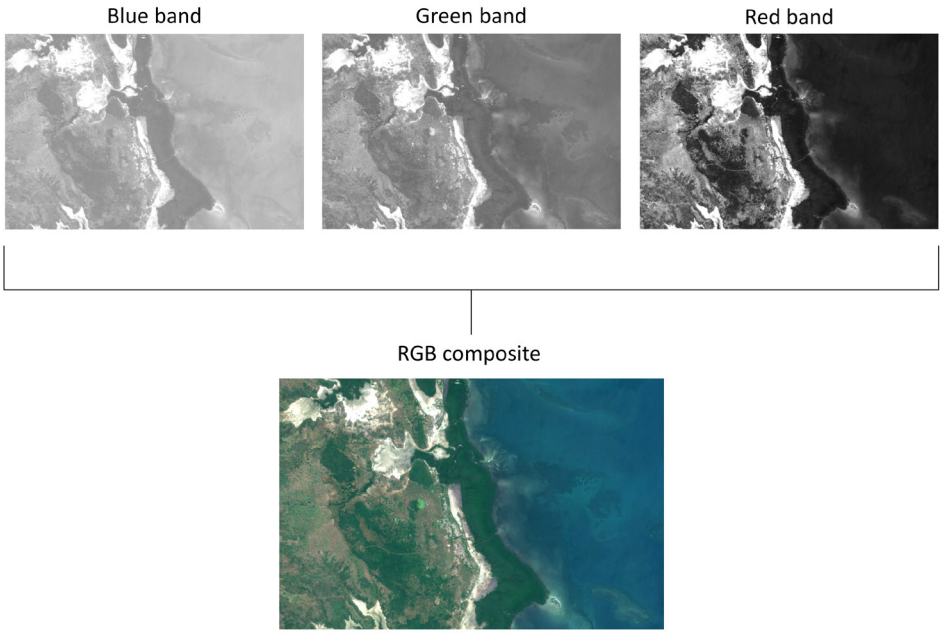


**Figure 2.5.** The top row consists of three bands of Sentinel 2 imagery of coastal mangrove forests in Mozambique. Each band contains information about the reflectance of the Earth's surface in a different segment of the visible spectrum. The images have a standardized grey scale (lighter colours = more reflectance). The blue band is the lightest overall, likely because light with short wavelengths is scattered quite strongly in the atmosphere (and is thus reflected back at the sensor). Water and vigorous vegetation (such as mangroves) have the lowest red values as most light in these wavelengths is absorbed instead of reflected. The red-green-blue (RGB) composite in the lower row is closer to how humans experience colour.

Hyperspectral sensors are much like multispectral sensors, in that they passively measure reflectance (Pettorelli *et al.* 2014a). However, unlike multispectral sensors, which typically acquire information across a limited number of bands (typically between 4 and 12), hyperspectral sensors collect information across hundreds of spectral bands, splitting the spectrum into much narrower slices. This distinction is somewhat arbitrary but not unimportant as hyperspectral data allow reconstructing reflectance across a continuous spectrum, whereas multispectral data gives "snapshots" of reflectance at discrete points.

*Active remote sensing*

There are two types of active sensors: Radar (Radio Detection and Ranging) and LiDAR (Light Detection and Ranging). Because they emit their own radiation, they can "see" independently of other sources of radiation, such as the sun. Interpreting imagery from active sensors is less intuitive than for multispectral imagery because these sensors do not perceive colour per se, but rather respond to surface geometry, texture, three dimensional structure and water content.

Radar sensors emit radiation at long wavelengths, i.e. in the microwave or radiowave part of the electromagnetic spectrum. This radiation interacts with objects in its path: it is either transmitted (e.g. through the atmosphere), reflected, or scattered by rocks, vegetation, or other scatterers. The radar sensor, specifically its antenna, then receives information about two aspects of this returning radiation, or backscatter:

1) The ***relative phase shift***. As the radar sensor controls the timing of the outgoing radiation, it can compare the wavephase – the position of a point in time along the wave – of the outgoing to that of the incoming radiation. This phase shift is determined by the time between emission and reception of the signal, which in turn depends on the distance between an object and the sensor. As a result, information about the phase shift can be used to reconstruct a three dimensional model of the environment, e.g. a digital elevation model. This process is called inferometry (Hooper *et al.* 2004; Prati *et al.* 2010).

2) The ***intensity***. The intensity measures how much radiation returns to the sensor, relative to the amount emitted. In the context of microwave radiation, this is referred to as backscatter (rather than reflectance, which is used in the context of multispectral sensors). It is affected by the surface characteristics of the objects/features scattering the emitted signal (or "scatterers"), specifically, a) their volumetric distribution (the size and arrangement of scatterers in space), and b) their chemical composition (in particular, their water content; **Figure 2.6**). The size of an object determines how much of the radiation it scatters. Objects that are larger, or of a similar size compared to the wavelength of the radiation, scatter a lot of radiation; smaller objects do not interact as much with the radiation, allowing it to be transmitted further. For instance, a signal with a small wavelength (such as X-band; see **Table 2.1**) will be scattered by small objects in a canopy, such as leaves, whereas longer wavelengths will penetrate dense canopies, and even the ground (Campbell 1996), but might be scattered by large tree trunks. As a result, a surface will appear "smooth" in a radar image if its topography varies on a scale smaller than the radiation wavelength. This is also the reason why radar sensors can "see" through (penetrate) clouds: the water droplets contained in clouds are almost always too small to scatter the signal (though in rare circumstances, very large clouds have been observed in radar imagery). Finally, the intensity of the returning signal is higher if the scatterer has a high water content. Water bodies themselves reflect a large amount of radiation, and radar cannot penetrate water beyond a few millimeters.

**Table 2.1.** Names and wavelengths of radar bands (Moreira *et al.* 2013). Bands in bold are frequently used for environmental and ecological applications (see **Figure 2.2**).

| NAME | WAVELENGTH |
|---|---|
| P-band | 120 - 60 cm |
| L-band | 30 - 15 cm |
| S-band | 15 - 8 cm |
| C-band | 8 - 4 cm |
| X-band | 4 - 2.5 cm |
| Ku-band | 2.5 - 1.7 cm |
| Ka-band | 1.2 - 0.75 cm |

Another source of information about the Earth's surface comes from the polarization of the signal. Electromagnetic energy can be thought of as oscillating waves that travel forward. Radar sensors emit polarised electromagnetic energy, i.e. the waves all oscillate within a single plane. Sensors can transmit horizontally (H) or vertically (V) polarized radiation. Similarly, they can receive the returning signal in horizontal or vertical orientation (receiver polarization).

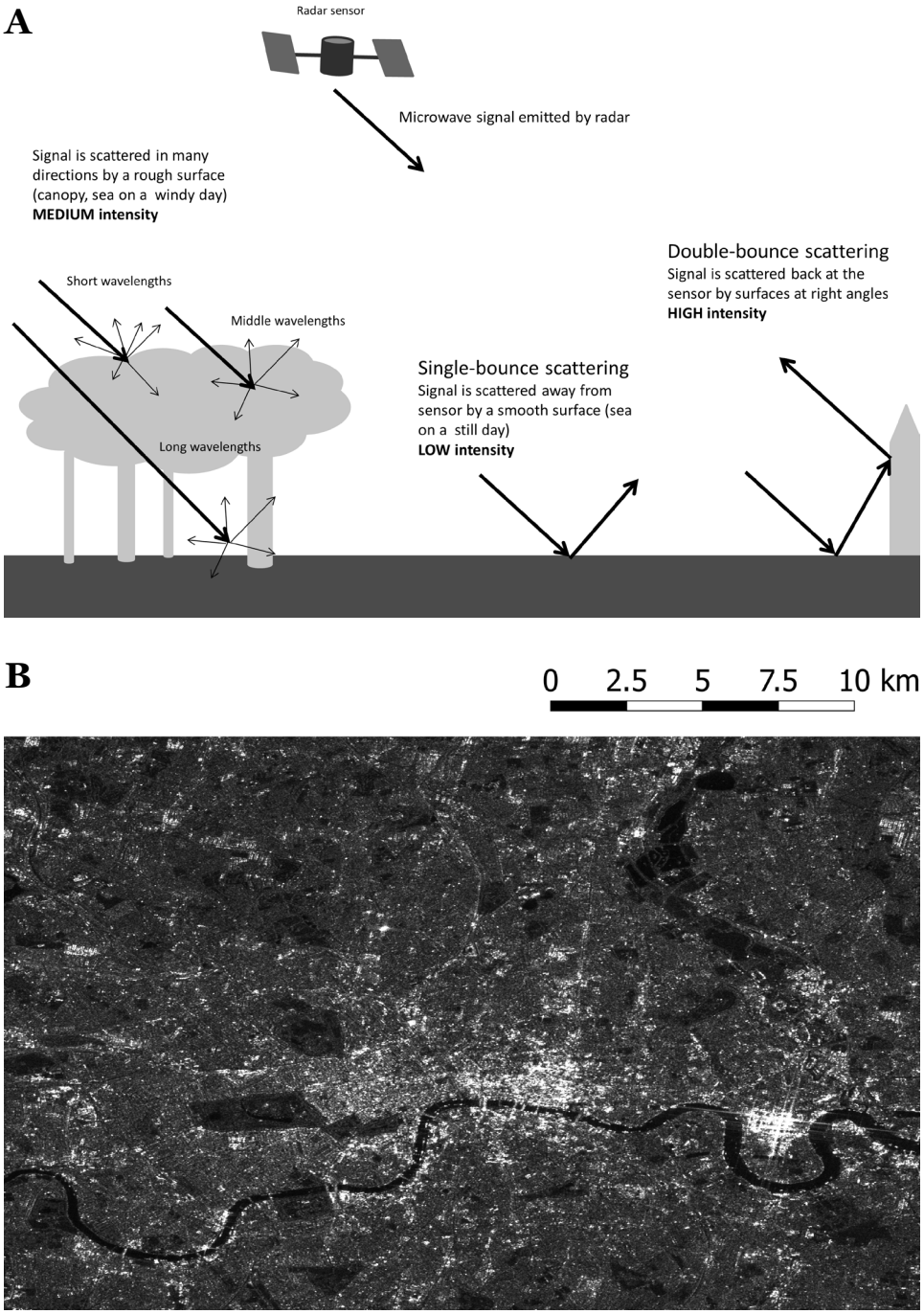


**Figure 2.6.** (A) An overview of common backscatter mechanisms. Longer wavelengths can penetrate canopies and are scattered by tree trunks (and large branches), whilst shorter wavelengths are scattered within the canopy, or (for the shortest wavelengths) the top of the canopy. Smooth surfaces result in very low backscatter coefficients (intensity) because the signal is mainly directed away from the sensor, whereas surfaces at right angles (such as buildings on a road) produce very strong backscatter coefficients. (B) A radar image from the Sentinel 1B satellite acquired over London, United Kingdom, in 2017. Note the lower backscatter from the river Thames (smooth water) and the large parks (relatively rough vegetation), and the higher backscatter from areas with a lot of buildings due to double bounce. The large buildings in Canary Wharf (bottom right) produce very intense backscatter, resulting in a star-like artefact.

Altogether, there are four possible polarization modes: HH and VV (like-polarized); and HV and VH (cross-polarised), though not all sensors are capable of all four modes. Comparing the intensity of backscatter across the same area between polarization modes allows discriminating surfaces with different orientation and volume of scatterers (Lönnqvist *et al.* 2010). This is because the emitted signal can be depolarized by interacting with the objects in its path. For instance, depolarization tends to occur over rough surfaces or if the radar signal has penetrated the canopy or the soil before being backscattered to the sensor (Campbell 1996). Comparing the intensity of the signal received in different polarization modes helps to distinguish different types of surfaces, though inferences about the mechanism that caused depolarization can be difficult.

At a given distance from an object, the spatial resolution of a radar sensor is limited by the size of its antenna, i.e. its aperture. The maximum spatial resolution is constrained by the diffraction limit, which is in turn determined by the distance between the sensor and the object (object-sensor distance), the wavelength of emitted radiation, and the length of the aperture:

$$D=R.\lambda/a$$

Where D= diffraction limit, R= object-sensor distance, $\lambda$ = wavelength and a = size of the antenna.

This relationship implies that, at a given wavelength and sensor-object distance, the spatial resolution of a radar sensor will increase with the length of its antenna. However, given that spaceborne sensors orbit the Earth at height of 100s of kilometers, associated antennae would have to be enormous to give a reasonable spatial resolution to investigate surface processes. For example, a satellite with a C-band sensor, emitting radiation with a wavelength of 6 cm, which orbits the Earth at a height of 693 km would require an antenna 416 km in length to achieve a spatial resolution of 10 m. In fact, there is a C-band satellite orbiting the Earth at a height of 693 km: it corresponds to either of the twin satellites in the Sentinel 1 mission, recently launched by the European Space Agency (ESA). Their antennae are 12.3 m long, yet provide imagery with a spatial resolution of 10m – but how? The answer is that spaceborne satellites mimic having a sufficiently large antenna by acquiring lots of images as the sensor moves along the satellite flight path, or azimuth (**Figure 2.7**); this method is called Synthetic Aperture radar (SAR). The same object is thus imaged numerous times. Because the time when the radiation is emitted and its wavelength are known, it is then possible to combine these images into a composite image which shows the original relative position of the objects. All spaceborne radar sensors are SAR sensors, but we will use the broader term (radar) throughout this text.

LiDAR is another type of active remote sensor that relies on much shorter wavelengths than radar, i.e. laser beams. Airborne terrestrial LiDAR mostly uses infrared wavelengths (Nayegandhi 2006). Its sensors emit a laser beam, which is reflected when it comes into contact with an object. The returning signal allows measurement of the distance between the sensor and the object, which is then used to build a three-dimensional model of the environment (Dubayah & Drake 2000; **Figure 2.4**). Since this guide is focusing on multispectral and radar SRS, we refer the reader to Melin *et al.* (2017), who provide an accessible, comprehensive overview of LiDAR technology and applications.

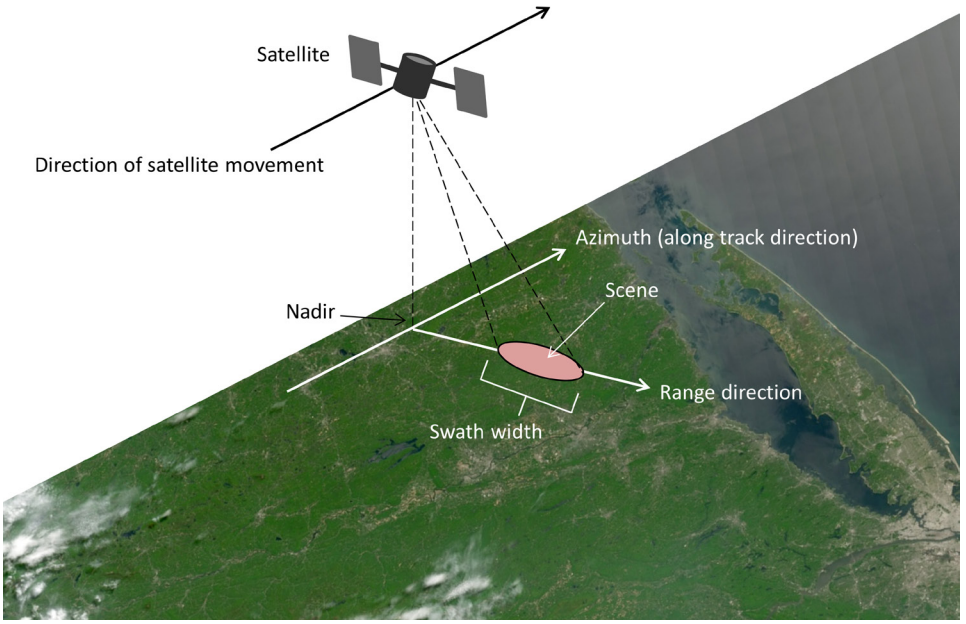


**Figure 2.7.** View geometry of a SAR satellite. The satellite moves above the nadir in azimuth direction, imaging a part of the Earth's surface to its side. The size of the scene is limited by the swath width, and extends in azimuth and range direction. Image: NASA Earth Observatory image by Jesse Allen, using data from the Land Atmosphere Near real-time Capability for EOS (LANCE), showing hardwood forest near a lake in North America.

## 2.3 Band ratios, vegetation indices and biophysical parameters derived from SRS

One way to distinguish objects with different spectral characteristics is to construct band ratios. For instance, field measurements of the transparency of water bodies using Secchi disks correlates strongly with the red/blue ratio (Kloiber *et al.* 2002), whereas short-wave infrared (SWIR) and near-infrared (NIR) or red/NIR ratios are sensitive to photosynthetically active vegetation (Green *et al.* 1998). For visual interpretation of the images, it can be useful to calculate these band ratios, or combinations of more than two bands (such as RGB images, see **Figure 2.5**; Horning 2004). However, it is often preferable to retain as much spectral information as possible for quantitative analysis, which is why band ratios are often used in conjunction with the original bands, rather than alone (see **Chapter 4.4**).

Vegetation indices are linear combinations of radiation captured in different bands by passive sensors (both multispectral and hyperspectral). They are sensitive to variation in vegetation "greenness", and provide synoptic views of vegetation dynamics. The Normalised Difference Vegetation Index (NDVI) is the most widely used vegetation index (**Figure 2.8**). Its applications include (a) mapping ecosystem extent and condition; (b) modelling species distributions; and (c) informing conservation in practice, from monitoring protected areas to supporting future conservation planning (Pettorelli 2013). The NDVI is calculated from the red (R) and the near-infrared (NIR) band as:

$$NDVI = (NIR - R) / (NIR + R)$$

This is based on the observation that photosynthetically active vegetation strongly absorbs red light and reflects near-infrared radiation. A closed canopy that is photosynthetically active will produce NDVI values close to 1, whereas areas with fewer (or less vigorous) vegetation will produce lower NDVI values. Water reflects little red and near-infrared radiation, resulting in NDVI values close to 0.

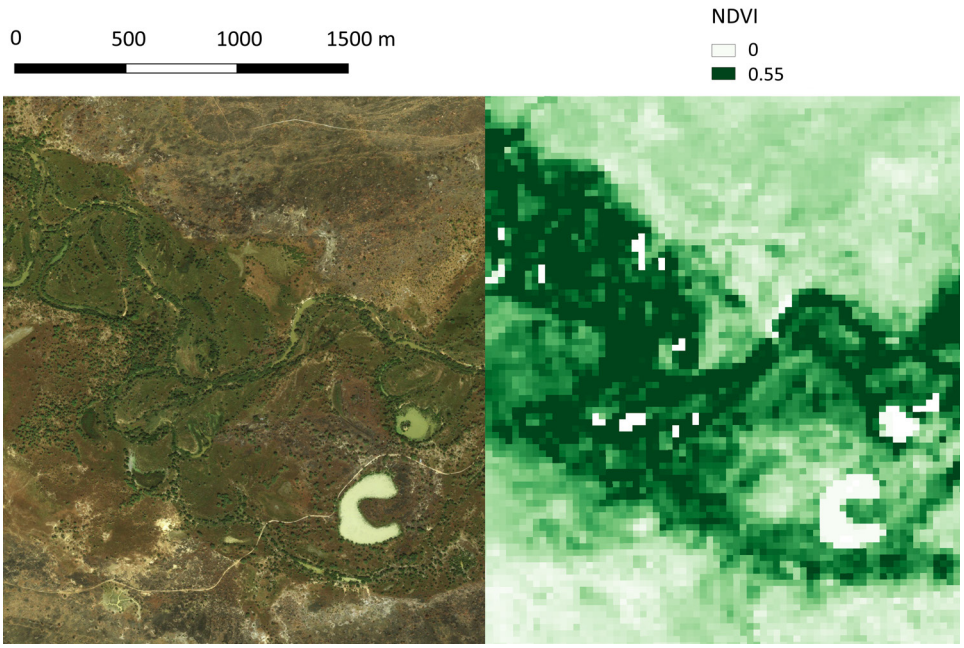


**Figure 2.8.** NDVI derived from Landsat 8 in a savannah landscape during the dry season. The (relatively) lush vegetation around the river running diagonally across the image has higher NDVI values (indicated by darker NDVI) then the rest of the savannah. Water has an NDVI of 0, so pools of water appear white. Image: Landsat 8 (United States Geological Survey), © 2017 DigitalGlobe & Microsoft Corporation.

Passive sensors are sensitive to atmospheric constituents, such as gasses, water vapour or aerosols, and these consequently have a strong influence on measured vegetation indices (Pettorelli 2013). To address this sensitivity, the Enhanced Vegetation Index (EVI) was developed from the NDVI, using the blue band to correct atmospheric influences (Huete *et al.* 2002). EVI has been shown to be correlated with photosynthesis and plant transpiration (Huete *et al.* 2010), and is expected to be more sensitive to changes in vegetation at high biomass than the NDVI (Huete *et al.* 2002, 2010). However, this vegetation index is very sensitive to the atmospheric correction of the blue band. This means that if there is a lot of haze in the imagery, the EVI might not provide reliable information about the vegetation.

There have also been attempts to correct for effects of soil reflectance on the NDVI, which are pronounced when vegetation is scarce. The Soil-Adjusted Vegetation Index (SAVI) proposes to correct the NDVI by a factor L in the denominator. This factor varies between 1 (for sparse vegetation) to 0 (for high density vegetation); SAVI is equivalent to NDVI in the latter case. However, it can be difficult to estimate the effects of soil background reflectance on the NDVI to identify an appropriate correction factor (Pettorelli 2013). Lastly, the Normalised Water Difference Index is calculated like the NDVI, but instead of

the red band, a shortwave infrared band is used; this index is sensitive to vegetation water content, and is thus useful in monitoring vegetation health or to delineate open water features (Gao 1996; Xu 2006; Tripathi *et al.* 2013).

Similar to NDVI and NDVI-related vegetation indices, tasselled cap indices allow characterising vegetation cover. Tasselled cap indices are linear combinations of multispectral bands using pre-defined coefficients, which yield three parameters: greenness, brightness, and wetness. The coefficients needed to calculate tasselled caps vary between sensors, and have to be derived empirically and vary by sensor (Crist & Cicone 1984; Huang *et al.* 2002; Baig *et al.* 2014; Rocchini *et al.* 2016).

Apart from vegetation indices, biophysical parameters such as Leaf Area Index (LAI; De Kauwe *et al.* 2011) or chlorophyll-α concentration (Hu *et al.* 2012) can be derived from SRS. Unlike vegetation indices, which either do not have units (e.g. NDVI) or units of radiance or reflectance (e.g. Green Vegetation Index, Tucker 1979), these parameters have different units from the underlying SRS data (e.g. [$m^2$ $m^{-2}$] for LAI). Many of these parameters are being routinely produced because they are Essential Climate Variables, which form the basis for global climate observations (GCOS 2010). However, they are also useful for characterising ecosystem and habitat properties. For instance, SRS-derived LAI can be used as a proxy for ecosystem structure (Morton *et al.* 2014) and primary productivity (Asner *et al.* 2003). Chlorophyll-α concentration is useful for monitoring marine primary productivity and ecosystem condition of coastal and marine waters (Gohin *et al.* 2008).

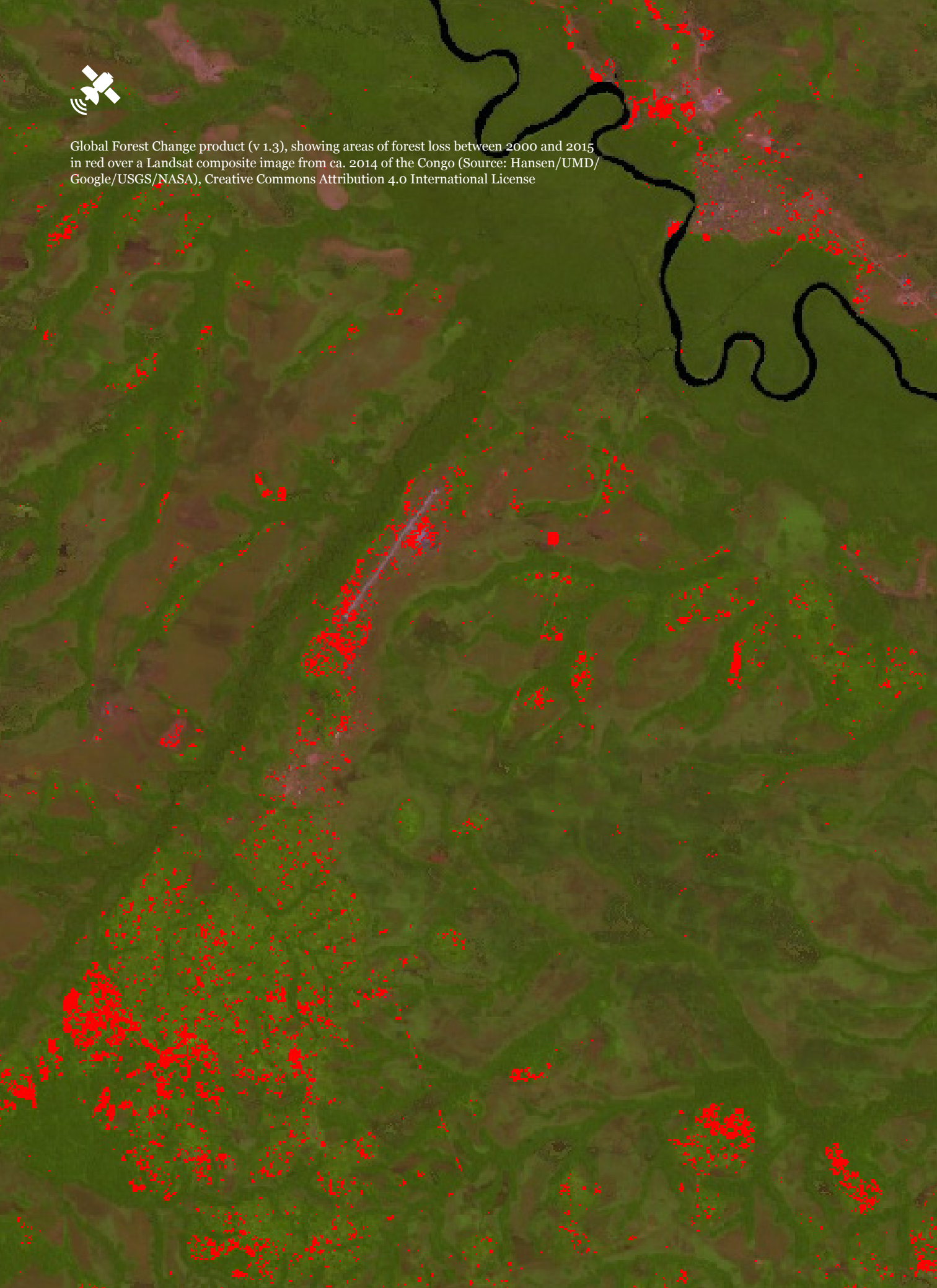

Global Forest Change product (v 1.3), showing areas of forest loss between 2000 and 2015 in red over a Landsat composite image from ca. 2014 of the Congo (Source: Hansen/UMD/ Google/USGS/NASA), Creative Commons Attribution 4.0 International License

# 3 WHAT SATELLITE IMAGERY IS CURRENTLY AVAILABLE?

## HIGHLIGHTS

- There is a wide variety of multispectral low (kilometres) to high (< 30 m) resolution open-access satellite remotely sensed data, with some imagery available as far back as 1972.
- However, satellite data with very high spatial (< 5 m) resolutions typically must be purchased from commercial providers.
- Like multispectral data, radar data are available across a wide range of resolutions. Unlike multispectral data however, radar sensors have a much lower spectral resolution, emitting and measuring radiation in a single wavelength.
- An alternative to processing raw data collected by remote sensors is to instead use one of the many derived products, such as vegetation indices (e.g. Normalized Difference Vegetation Index), biophysical parameters (e.g. Leaf Area Index), and land cover (e.g.CORINE Land Cover). Whilst these derived products are readily accessible to non-experts, that they aren't tailored to specific contexts may limit their applicability in some cases.

Observation Portal
https://directory.eoportal.org/web/eoportal/satellite-missions

The sky is home to many satellites. The Earth Observations Portal's Satellite Missions Database lists hundreds, the oldest of which were launched as far back as 1959. However, the number of satellites which collect data commonly used in ecology or conservation is much smaller. This chapter gives a short overview of these satellites and the data they provide, focusing on satellites equipped with multispectral (**Chapter 3.1**) and radar sensors (**Chapter 3.2**). The **Appendix** provides a comprehensive list of these satellites, including their respective sensor specifications, spatio-temporal resolution and coverage, and also details how to access the data they collect, imagery costs, and examples of applications. This section provides examples of open-access products derived from raw SRS data, including vegetation indices, fire products and land cover maps; these are also summarised in **Chapter 3.3**.

There are about as many ways to access SRS data as there are types of SRS data. Whereas the **Appendix** provides a single point of access for each type of data or product, **Table 3.1** gives a short, non-exhaustive overview of the most common SRS data hubs, for both open access and commercial SRS data and products. These can be useful starting points for exploring the types of SRS data available for an area of interest. Many of these sources provide additional geospatial data, such as digital elevation models (DEMs) or aerial imagery. Most of the open-access data hubs require the user to register, and download scenes manually, which can be time-consuming and cumbersome when many SRS images are required. In this case, downloading open-access SRS imagery can be automatized using batch scripts, or bulk downloaders, which also facilitates setting the desired data parameters (e.g. spatial extent, time period).

### 3.1 Multispectral SRS data

Open-access multispectral data are probably the most widely used type of satellite data for environmental and ecological applications, especially when dealing with large spatial scales (Hansen & Loveland 2012). The United States Geological Survey's (USGS) Landsat archive provides imagery of the Earth's surface at moderate spatial resolution (30 m) going back to 1972 (Wulder *et al.* 2012a). Landsat imagery has been open access since 2008 (Woodcock *et al.* 2008), arguably resulting in the remarkable expansion of SRS

data use for environmental applications (Wulder *et al.* 2012a). Multispectral SRS has thus far informed conservation science and practice in a large number of ways – ranging from ecosystem mapping (Cohen & Goward 2004), monitoring ecosystem condition (Pasquarella *et al.* 2016), to modelling species distributions (Shirley *et al.* 2013). There have been eight Landsat satellites in total, of which two (Landsat 7 ETM+ and Landsat 8 OLI/TIRS) are currently in orbit. Landsat 7 and 8 each have a panchromatic band, which allows pan-sharpening the other bands to increase their spatial resolution to 15 m (see **Glossary**), as well as a higher number of bands than their previous incarnations (Young *et al.* 2017). In May 2003, Landsat 7's Scan Line Corrector failed, which has resulted in strips of lost data, affecting about 22% of each scene (Loveland & Dwyer 2012; **Figure 3.1**). Several gap filling methods have been developed since, based on spatial or temporal interpolation, or by using imagery from another satellite (e.g. Landsat 5 or MODIS). The USGS does not currently produce a gap-filled version of Landsat 7 (Zhang *et al.* 2007; Roy *et al.* 2008b).

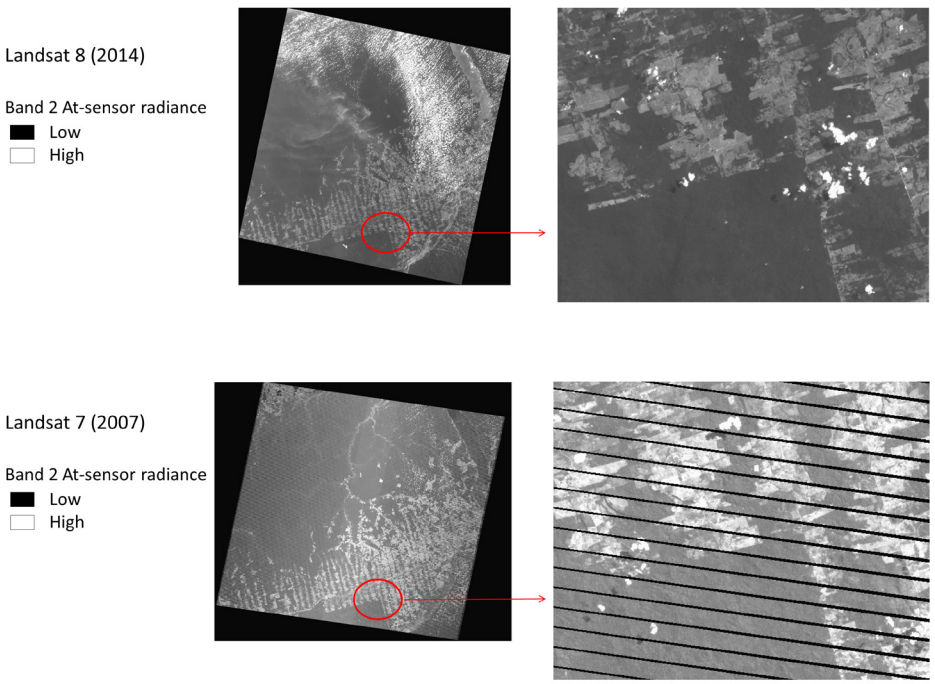


**Figure 3.1.** The Scan Line Corrector of Landsat 7 failure, resulting in strips of data gaps in all imagery collected after May 31, 2003. This figure shows the same scene, from Landsat 8 (top row) and Landsat 7 (below), which has the characteristic "stripes".

MODIS data have a lower spatial resolution than Landsat (between 250 and 5,600 m, depending on the band and the type of pre-processing applied; **Figure 3.2**), but much higher temporal and spectral resolutions, providing daily images of every point on the Earth's surface across 36 bands. As a result of this, MODIS is often used for time series analysis, e.g. many repeated images to capture information on vegetation phenology (Pennec *et al.* 2011). It is also a key source of cloud-free SRS-derived products such as the NDVI (Landmann & Dubovyk 2014), biophysical parameters such as the LAI (Zhu *et al.* 2013), as well as maps of active fires (Oom & Pereira 2012; Giglio *et al.* 2016), burned areas (Roy *et al.* 2008a) and land cover (Friedl *et al.* 2010; Klein *et al.* 2012).

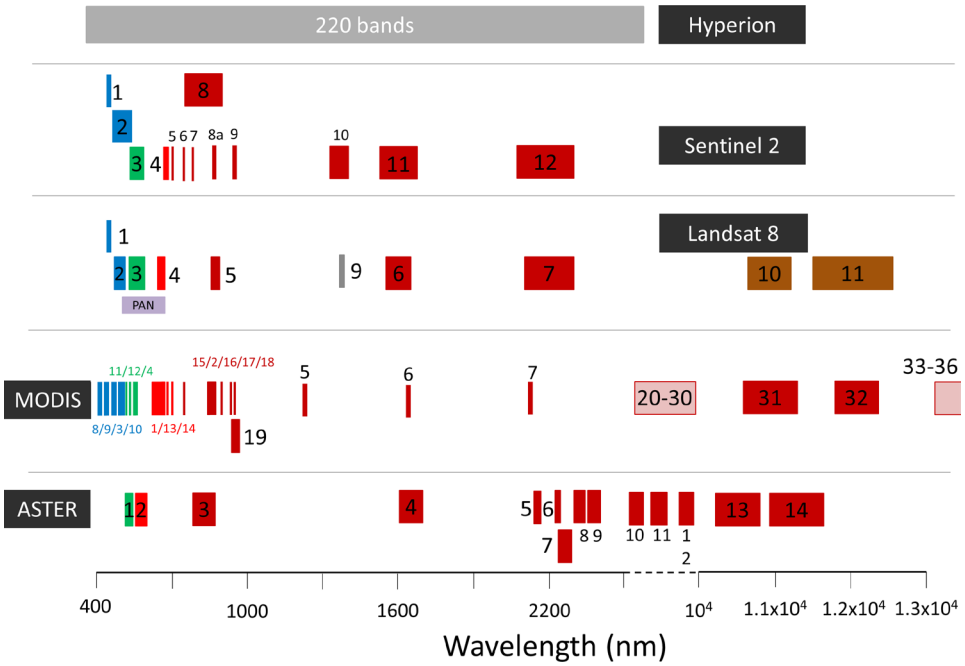


**Figure 3.2.** Comparison of band widths of spaceborne multispectral sensors and one hyperspectral sensor, Hyperion. In contrast to the multispectral sensors (which each have at most a few dozen bands), Hyperion had 220 narrow bands between 357 and 2576 nm (its satellite, EO-1, was decommissioned in April 2017). Each rectangle corresponds to a band, and its width is approximately proportional to the range of wavelengths that it covers. The numbers are the band designations, which vary between sensors. For instance, the Landsat 8 sensor has one green band called Band 3, whereas MODIS has several green bands (Bands 4, 11 and 12). Bands are shifted vertically if they overlap.

SRS imagery with similarly high temporal resolution (daily) has been provided by the sensor AVHRR since 1979, but at lower spatial and spectral resolutions (AVHRR has a spatial resolution of 1.1 km and a spectral resolution of 6 bands; **Appendix**). Like MODIS, AVHRR imagery has been an important source of information for NDVI time series (Beck *et al.* 2011), and has formed the basis for early global land cover products (Herold *et al.* 2008). The sensors ENVISAT MERIS and OrbView-2 SeaWiFS also fall in the category of multispectral sensors with coarse spatial resolution. Whereas ENVISAT MERIS imagery has been applied to investigations of primary productivity distribution, both in the terrestrial and the marine realms (Tüshaus *et al.* 2014; Palmer *et al.* 2015), SeaWiFS has been primarily used in the marine and coastal realm (Werdell *et al.* 2009; Siegel *et al.* 2013).

Multispectral SRS data with higher spatial resolution than Landsat, such as imagery from the SPOT 1-4 satellites or the RapidEye fleet (which have spatial resolutions between 6.5 and 10 metres, **Appendix**), allows mapping of finer-scale environmental features (Salajanu & Olson Jr. 2001; Castillo-Santiago *et al.* 2010). Sentinel 2, part of ESA's Sentinel fleet of Earth Observation satellites, is a recent addition to the range of multispectral satellites providing open access data, and provides imagery with a maximum spatial resolution of 10 m (4 bands in the visible and near-infrared spectrum; other bands have a spatial resolution of 20 m and 60 m, ESA 2015; **Appendix**). It consists of two

satellites (A and B), launched in 2015 and 2017 respectively. The satellites are in the same orbit, but phased 180° from each other. Whereas each twin passes a given location once every 10 days, the repeat frequency is 5 days over the equator when both satellites are considered, and the repeat frequency is even less at higher latitudes. Sentinel 2's data is expected to enable the routine production of well-known biophysical parameters such as LAI, as well as land cover maps, at finer spatial resolutions (Drusch *et al.* 2012). Since 2000, Terra ASTER has provided multispectral imagery at a similar spatial resolution as Sentinel 2 (15 m; Abrams 2000). Unlike Sentinel 2, however, it does not systematically acquire imagery at every location, but instead, ASTER has focused collections over protected areas, and new data can be requested, or historical imagery can be downloaded. This means that, although ASTER can in theory acquire imagery over each point on the Earth's surface, it only does so above particular areas for each overpass. As a result, the coverage of ASTER SRS imagery is not continuous.

Since the beginning of the 21st century, multispectral SRS with very high spatial resolution (i.e. pixel resolution < 10 m) has become available (**Figure 3.3**; **Appendix**), including the IKONOS, the Pléiades 1A and 1B twin satellites, QuickBird, GeoEye and WorldView satellites. SPOT 5-7 also fall into this category when pansharpened (see **Glossary**). Their sensors tend to have low spectral resolution (i.e. only four or five bands, except WorldView), but very high spatial resolution (all < 3.2 m, some < 1 m when pansharpened) and temporal resolution (up to daily for Pléiades and WorldView-2/3; **Appendix**). This very high temporal resolution is achieved using different means: WorldView satellites fly at a high altitude to increase the spatial coverage of their imagery, whereas the Pléiades twin satellites are phased at 180° to each other. They are unique among existing satellites in providing imagery capable of detecting single, large animals (this is reviewed in more details in **Chapter 5.4**). This imagery is available from commercial providers, with costs typically around $20 km$^{-2}$ with a minimum purchase of 25 km$^2$ (Marvin *et al.* 2016).

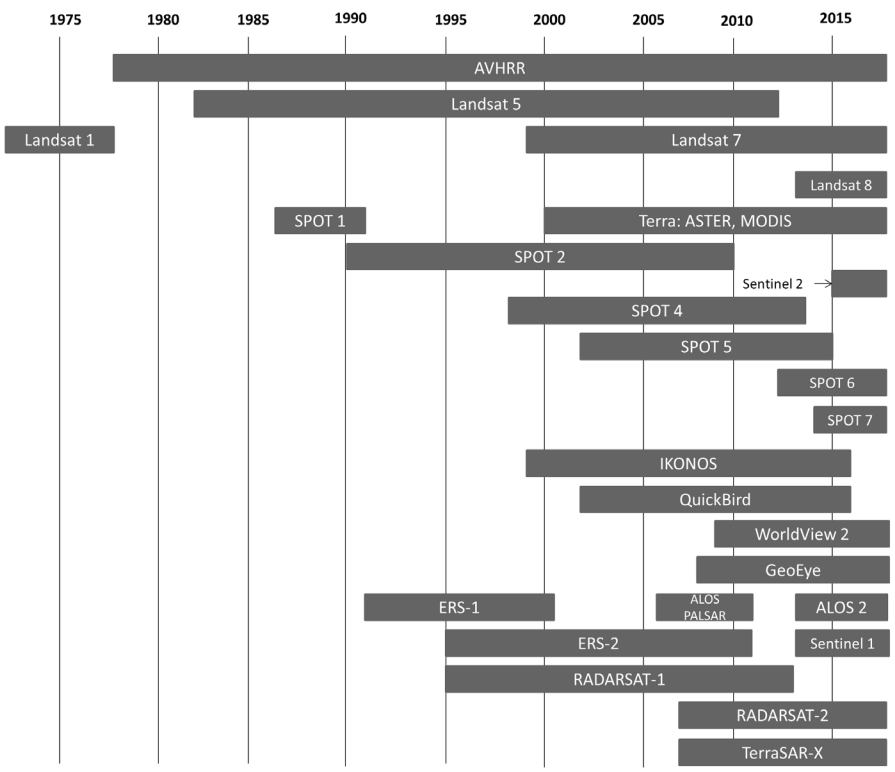


**Figure 3.3.** Timeline of satellite missions.

## 3.2 Radar SRS data

Like multispectral sensors, radar sensors acquire data with a large range of spatial resolutions (0.25 m – 50 km). SRS data from the same sensor is typically available at different spatial resolutions, depending on acquisition mode (see **Chapter 4.1**), though few have very high spatial resolutions (exceptions are TerraSAR-X, RADARSAT-1 and 2 and ALOS-2). Unlike multispectral SRS sensors, radar sensors have a much lower spectral resolution, emitting and measuring radiation in a single wavelength (or band). In the following section, available radar SRS will be ordered by their wavelength, from long to short, since this characteristic tends to guide applications (more so than spatial resolution considerations). There is currently no satellite carrying a P-band sensor, though ESA is planning to launch a P-band satellite called BIOMASS in 2021 to monitor biomass and forest height at a global scale (Le Toan *et al.* 2011). The lack of P-band earth observation mission is due to a relative lack of free bandwidth; P-band radar is frequently used by governments for military purposes and thus not widely available for civilian remote sensing. L-band sensors include JERS-1, ALOS PALSAR, and ALOS-2, of which only ALOS-2 is currently in orbit. Radar utilizing this wavelength is scattered by large surface elements such as tree trunks or large branches, but is relatively insensitive to smaller elements such as leaves (Campbell 1996). The most widely used L-band satellite is ALOS PALSAR and its follow-up satellite, ALOS-2, which has increased temporal and spatial resolutions. C-band sensors such as ERS-1 and 2, RADARSAT-2, and ENVISAT ASAR are scattered by smaller elements than L-band (Sinha *et al.* 2015). The latest addition to the fleet of C-band satellites is ESA's Sentinel 1, which, like Sentinel 2, consists of twin satellites in the same orbit. Sentinel 1A was launched in 2014, Sentinel 1B in 2016. Together these satellites provide imagery at high spatial resolution (between 5 and 40 m depending on the acquisition mode), comparable to older C-band satellites. However, their temporal resolution is much higher: They provide repeated imagery of the Earth's surface every six days over the equator (each satellite on its own has a repeat frequency of 12 days), and every one to three days at higher latitudes. Sentinel 1 thus offers opportunities for a much more detailed view of surface dynamics, including soil moisture retrieval at high spatial and temporal resolution (Paloscia *et al.* 2013; Mattia *et al.* 2015). Satellites with X-band radar sensors, such as TerraSAR-X and TanDEM-X, collect data originating from the scattering of very small surface elements. These two satellites (which have virtually identical sensor specifications) fly close together, and acquire imagery at the same time, in the same area, but at different view angles. This unique property allows their imagery to be used for radargrammetry, where backscatter intensity from two images with different view geometries is used to reconstruct the three-dimensional position of a target (Karjalainen *et al.* 2012). A digital elevation model has been constructed from TanDEM-X imagery, and is available for free. Other TerraSAR-X and TanDEM-X data can be acquired from Airbus (see **Appendix**).

**Table 3.1.** Common sources of satellite remote sensing data.

| NAME | WHICH SRS DATA? | WEBSITE |
|---|---|---|
| OPEN-ACCESS DATA | | |
| Earth Explorer | Landsat 4-8, MODIS data and products, ASTER, AVHRR, among other data sets | https://earthexplorer.usgs.gov/ |
| Copernicus Open Access Hub | Sentinel 1, 2, 3 | https://scihub.copernicus.eu/ |
| GloVis | Landsat 4-8, Sentinel 2, ASTER, EO-1, among others sets | https://glovis.usgs.gov/ |
| Google Earth Engine | Landsat 4-8, MODIS data and products, Sentinel-1, Sentinel-2, DMSP-OLS, among others | https://earthengine.google.com |
| QGIS Semi-Automatic classification plugin | Landsat 4-8; Sentinel 2; ASTER | https://plugins.qgis.org/plugins/ |
| 'MODIS' package in R | MODIS data and products | https://cran.r-project.org/web/packages/MODIS/MODIS.pdf |
| COMMERCIAL DATA PROVIDERS | | |
| Digital Globe | QuickBird (archive only), GeoEye-1, WorldView 1-3 | https://www.digitalglobe.com/ |
| Planet (subsumes Terra Bella, formerly SkyBox) | RapidEye, Planetscope, amongst other data sets | https://www.planet.com/https://www.planet.com/terrabella/ |
| Airbus Geostore | Pléiades, TerraSAR-X, SPOT | http://www.intelligence-airbusds.com/geostore/ |
| Satellite Imaging Corporation | WorldView 1-4, Pléiades, IKONOS, SPOT 6-7, TerraSAR-X, among other datasets | https://www.satimagingcorp.com/ |
| Appollo Mapping | WorldView, Pléiades, IKONOS, Geo-Eye 1, SPOT, RapidEye, among other data sets | https://apollomapping.com/ |

## 3.3 SRS-derived products

Many users of SRS imagery start working with the radiance or backscatter provided by individual satellites, processing them across their area of interest to derive a custom product. This requires time, appropriate hardware, software and expertise. An alternative is using SRS-derived products – including vegetation indices such as the NDVI or the EVI, biophysical parameters such as the LAI, and fire and land cover products, produced by agencies such as the USGS. SRS products are intended to be used directly without more image processing required, and there are often a range of case studies available to illustrate their utility. The drawbacks are that they are often global in scope, making them less accurate locally. Additionally, their spatial or temporal resolution, and aspects of processing and validation, can make them inadequate in certain contexts. For instance, many SRS products are derived from MODIS data, so although their temporal resolution can be high (daily to monthly), their spatial resolution is 250 m or coarser (see **Appendix**). Land cover products are central to assessments of land cover change, a major driver of global biodiversity loss (Sala *et al.* 2000) and climate change (Brovkin *et al.* 2004). A range of global and regional land cover products exists. Many of these have been generated for a single time period (Bontemps *et al.* 2011), or for a limited number of time periods (e.g. the CORINE European

land cover product exists for 1985, 2000, 2006, 2012), whereas the MODIS land cover product is generated annually (Friedl *et al.* 2010). The land cover products presented in **Table 3.2** either map several different land cover classes (such as University of Maryland Department of Geography Land cover), or the cover of a single land cover class, such as tree cover (e.g. Landsat Global Forest Change). Global land cover products have been used in assessments of human pressure on natural ecosystems (Sanderson *et al.* 2002), habitat fragmentation (Li *et al.* 2010), as well as environmental predictors for species distribution modelling (Fourcade *et al.* 2014). However, these land cover products may have low local accuracy and should be used with caution. Congalton *et al.* (2014) assessed the accuracy of four major global land cover products (see **Table 3.2**), finding that they had accuracies between ca. 67% and 79% (depending on how accuracy was assessed), whereas the MODIS 500 m land cover product has a global accuracy of 75% (Friedl *et al.* 2010). Accuracy tends to be low in areas that are characterised by mixtures of land covers (such as mixed trees and shrubs) rather than homogenous cover (e.g. closed canopy forest or snow fields; Herold *et al.* 2008; **Appendix**).

**Table 3.2.** Accuracy of global land cover products.

| NAME | GLOBAL ACCURACY | ASSESSED BY |
|---|---|---|
| International Geosphere-Biosphere Programme (IGBP) DISCover | 66 - 78% | Herold et al. 2008; Congalton et al. 2014 |
| University of Maryland Land Cover | 69% | Herold et al. 2008; Congalton et al. 2014 |
| Global Land Cover 2000 | 68% | Herold et al. 2008; Congalton et al. 2014 |
| GlobCover 2009 | 67% | Congalton et al. 2014 |
| MODIS 500 m land cover product | 75% | Friedl et al. 2010 |
| MODIS 1 km land cover product | 78% | Herold et al. 2008 |

Artist's rendition of Landsat 8. The Landsat mission of satellites has provided imagery of the Earth's surface since 1972. A key step in the mainstreaming of satellite remote sensing for ecological applications occurred in 2008, when the Landsat archives were made open-access.
Source: NASA.

# 4 SELECTING AND PROCESSING SRS DATA TO INFORM CONSERVATION

## HIGHLIGHTS

- Determining which satellite remote sensing data are appropriate depends on the question you are seeking to answer, the features being mapped, or processes of interest.
- The spatial and temporal resolution of remotely sensed data should be as low as possible in to minimize the time and budget required for processing and analysis.
- As a rule of thumb, the spatial resolution is appropriate if the smallest feature of interest (ecosystem or habitat patch, animal, or patch made up of a target plant species) is roughly the size of, or larger than, a single pixel.
- The ability of multispectral satellite remote sensing to distinguish between different classes of land cover or detect changes in continuous traits (e.g. woody vegetation cover) depends on whether these elements have a unique spectral signature. As a result the choice of multispectral sensor depends on whether its bands capture the electromagnetic spectrum which differentiates features of interest.
- Longer wavelengths penetrate the canopy more (and sometimes even the ground) than do shorter wavelengths, which tend to be scattered at the top of the canopy. Consequently, which radar sensor is appropriate depends on whether the feature of interest occurs above or below the canopy.
- The radiation that is captured by a space-borne multispectral sensor is affected by the type of land cover, sensor characteristics, and solar (such as differences in Earth-sun distance), atmospheric (such as haze or clouds), and topographic effects (hilly or rugged terrain which can create shadows), and these must be corrected for.
- Radiometric corrections adjust for mismeasurements of reflected radiation, whereas geometric corrections address the geographic or spatial accuracy of observations.
- Radar imagery tends to have a "salt and pepper" effect (speckle) that is reduced during pre-processing and, like multispectral imagery, radar data have to be corrected for topographic effects.
- Common analytical techniques include the generation of statistics that capture spatial context (i.e. textures), extraction of information from many different bands (i.e. dimensionality reduction), and image classification.

SRS is a valuable tool for informing and supporting conservation, but to leverage its full utility, it is necessary to choose the right type of imagery and process it appropriately (**Figure 4.1**). What SRS data are "right" to answer a given question depends on the features or processes that are of interest. The choice of data type (e.g. multispectral vs radar) is primarily guided by the type of surface feature or process to be examined.

Both multispectral and radar SRS data are available in a range of temporal or spatial resolutions. Guidance on how to choose between these is provided in **Chapter 4.1.** Whether and how to pre-process SRS imagery, or what type of pre-processed data to choose, is discussed in **Chapter 4.2**. **Chapter 4.3** gives a short overview of SRS data

sources and appropriate software, and **Chapter 4.4** provides an introduction to the most common SRS analysis techniques (including land cover classification). The choice of SRS data, processing protocol and software is constrained by factors that have nothing to do with the type of research questions being asked: time, budget, hardware resources, and individual expertise all shape what is and is not feasible. Where possible, the impact of these factors will be illustrated throughout this chapter.

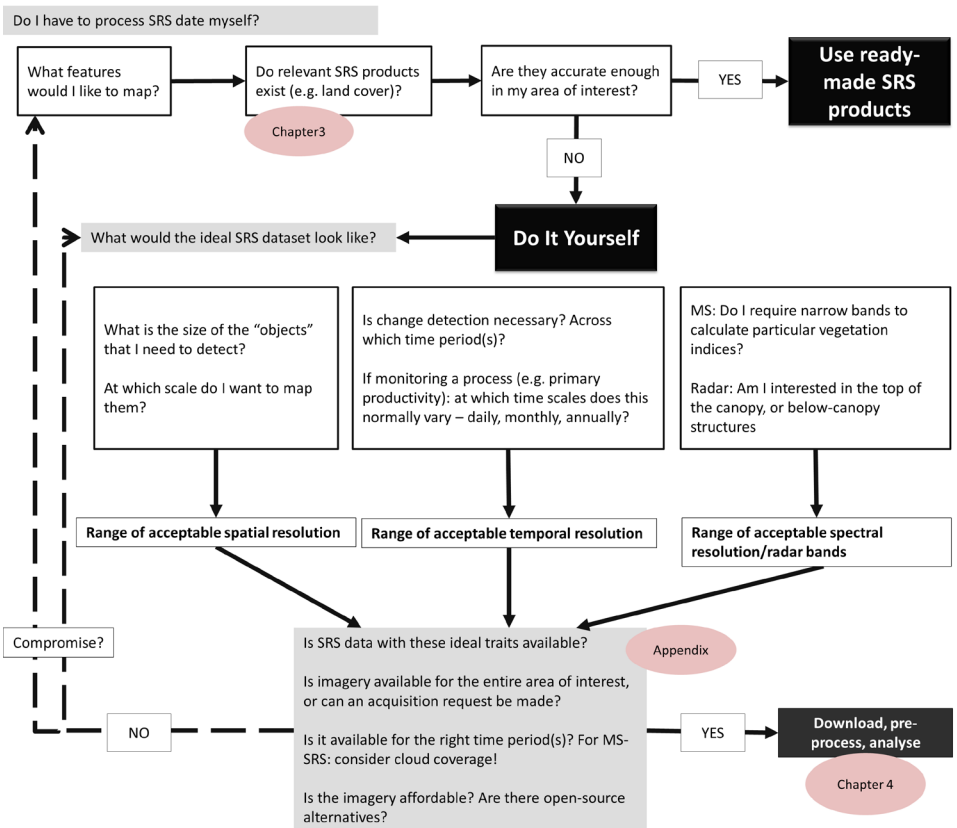


**Figure 4.1.** Decision flow chart to help choose appropriate SRS data. Given the large range of SRS data and SRS products that are now available, and the range of possible applications, choosing the right data can be tricky. This flowchart is intended to give an overview of important factors that will affect the choice of SRS imagery for most applications; it does however not address the issue of ground-truthing data.
MS-SRS: Multispectral satellite remote sensing.

## 4.1 Which resolution(s) are adequate?

It can be tempting to simply always choose the data with the highest spatial, temporal and spectral resolutions. However, even where financial constraints do not apply, data volume increases rapidly with spatial and/or temporal resolution. Larger areas cannot easily be covered by imagery with higher spatial resolution as they will require mosaicking of many smaller scenes. Pasher *et al.* (2014) estimates that complete coverage of the Canadian province of Ontario (ca. 1.1 million km$^2$) using WorldView-1 imagery (ca. 50 cm resolution) would require about 4,500 unique scenes, each 14 km x 17 km in size.

This corresponds to approximately 9 TB of data. In contrast, the corresponding area would be covered by about 80 Landsat 8 scenes (30 m spatial resolution), which would amount to approximately 130 GB. A SRS time series of the same area would obviously be a multiple of these respective data volumes. This means that to keep hardware and software requirements low and limit processing and analysis time, the spatial and temporal resolution should not be finer than needed. This then begs the question: what kind of resolution is really necessary?

*Spatial resolution*

As a rule of thumb, the feature of interest (ecosystem or habitat patch, or patch made up of a target plant species) should be at least as large as a single pixel, so that the spectral information contained in this pixel reflects primarily the feature of interest. Whereas coarse to medium spatial resolution (like that of the Landsat sensors) is appropriate to map large patches of forests, grasslands or wetlands, imagery with higher spatial resolution (i.e. < 10m) is necessary when the landscape of interest varies at a finer spatial scale, for instance to map hedgerows in an agricultural landscape (Betbeder *et al.* 2015). The spatial resolution of most satellite-borne sensors is too coarse to allow distinguishing individual plants for the most part, although plants which form large, relatively homogenous stands may be distinguished from surrounding vegetation. For instance, Everitt *et al.* (2008) mapped the distribution of Giant Reed *(Arundo donax)* with high accuracy when using QuickBird imagery, but had lower accuracy when using coarser SPOT 5 imagery. Conversely, Shapiro *et al.* (2015) found that mangroves could be mapped more accurately based on Landsat imagery than based on SRS imagery with higher spatial resolution (WordView-2) where “pure” classes may be more difficult to map due to noise. Using imagery with a very high spatial resolution for classification (compared to the size of the feature of interest) may require more effort, particularly when this imagery has more artefacts such as shadows, varied features such as roofs of houses, lawns and streets which make up an urban area, or individual trees or elements such as cars or tents, which can make the identification of consistent land cover classes and features more difficult (Sawaya *et al.* 2003). Put simply, SRS imagery has an appropriate spatial resolution when the smallest feature of interest is roughly the size of a single pixel.

Multispectral SRS data typically have a fixed spatial resolution, though sometimes thermal bands are collected at lower spatial resolution than the others. For instance, Landsat 7 and 8’s thermal bands are acquired at 60 m and 100 m spatial resolution respectively. Many sensors have a panchromatic band at higher resolution, which allows pansharpening of lower-resolution bands (see **Glossary**). However, this process may introduce some artefacts (i.e. features in the SRS imagery which are a result of the pansharpening process, and do not correspond to any real features on the ground), which can lead to errors in subsequent analysis (e.g. land cover classification). It is therefore typically used for visualisation rather than analysis (Leutner & Wegmann 2016). In most cases, it is safest to choose multispectral SRS data based on the spatial resolution of bands in the visible or near-infrared spectrum.

For radar SRS data, there often is a choice between different acquisition modes. These vary, broadly speaking, in swath width (i.e. the size of a single scene), and spatial resolution, with smaller swath width typically having higher spatial resolution. Along its orbit, a satellite might acquire imagery in different acquisition modes, depending on its intended use (see **Table 4.1**).

**Table 4.1.** Characteristics of different acquisition modes, illustrated using Sentinel 1. Reference: ESA (2013).

| NAME | SWATH WIDTH | SPATIAL RESOLUTION | COMMENTS |
|---|---|---|---|
| Stripmap | 80 km | 5 m x 5 m | Only in exceptional cases (emergencies) |
| Intereferometric Wide Swath | 250 km | 5 m x 20 m | Standard mode |
| Extra-Wide Swath | 400 km | 20 m x 40 m | Typically acquired over sea-ice, polar zones, marine areas |
| Wave | 20 km | 5 m x 5 m | Incomplete coverage: Acquired every 100km along the orbit |

*Temporal resolution*

In many cases, SRS data from a single point in time is sufficient to map the extent of an ecosystem (Giri *et al.* 2011) or the distribution of species habitat at a given point in time (Imam *et al.* 2009). In other instances, two or three time points are enough to monitor change in ecosystem extent over a long time period (Hansen *et al.* 2013). In some cases, however, denser time series are necessary, for instance, to characterise sub-annual vegetation phenology (Pettorelli *et al.* 2005) or monitor deforestation in near real time (Anderson *et al.* 2005).

*Spectral resolution*

The ability of multispectral SRS to distinguish between different classes of land cover or detect changes in continuous traits (e.g. woody vegetation cover) depends on whether these classes or traits have different spectral reflectance curves (**Figure 2.1**). If they do, the choice of multispectral sensor depends on whether its bands sample those parts of the spectrum where the features in question are different – which in most cases is difficult to know beforehand. However, there are a range of rules of thumb that can help choose the right spectral resolution.

Wider bands are generally more likely to be absorbed by water vapour. For instance, Landsat 7's NIR band is much wider (0.77 - 0.90 μm) than Landsat 8's (0.85 - 0.87 μm). In fact, Landsat 8's NIR band was chosen after it emerged that Landsat 7's NIR band was sensitive to water absorption at around 0.82 μm. This is important especially if the SRS data is intended for calculating vegetation indices such as the NDVI, which depend on accurate measurements of NIR reflectance, in which case sensors with narrow bands are often preferable (Elvidge & Chen 1995; Brown *et al.* 2006).

In areas where aerosol concentrations are expected to be high (e.g. because of smoke from wildfires or windblown dust), it can make sense to choose a sensor with a band towards the ultraviolet end of the spectrum (i.e. a blue band with very small wavelengths). These wavelengths are sensitive to very small aerosol particles in the atmosphere, and allow atmospheric correction of other spectral bands (Roy *et al.* 2014). In cases where precise cloud masking (identification and exclusion of imagery impacted by cloud cover) is important (e.g. for change detection), it is useful to choose a sensor with a short-wave infrared (SWIR) band. SWIR radiation is strongly absorbed by water, and thus sensitive to clouds (Zhu *et al.* 2015). Alternatively, thermal bands can help detect clouds accurately, because clouds are cooler than the Earth's surface (Zhu & Woodcock 2012).

Radar sensors typically only acquire information in a single, narrow microwave bandwidth (see **Chapter 2.2**); which band is appropriate in a given case depends on the feature of interest and the characteristics of the study area. Long-wave radar (i.e. L-band) is widely used to estimate forest extent and change (Almeida-Filho *et al.* 2009; Whittle *et al.* 2012; Thomas *et al.* 2014) aboveground biomass in areas where biomass is high, e.g. tropical forests (Morel *et al.* 2011), mangrove forests (Hamdan *et al.* 2014) or plantations (Baghdadi *et al.* 2015). However, it has also been employed in ecosystems with less dense vegetation, such as savannah (Mermoz *et al.* 2014). Radar with shorter wavelengths (i.e. C-band, X-band) does not penetrate the canopy as much as L-band radar (Sinha *et al.* 2015), thus its signal tends to saturate when biomass is high. As a result, L-band tends to be preferred for ecosystems with low biomass (Ghasemi *et al.* 2011). Because it is scattered by the top of the canopy, X-band radar is well-suited to derive canopy height (Karjalainen *et al.* 2012). In areas where canopy height is closely correlated to biomass (e.g. homogenous, continuous forests), X-band derived forest height has also been used to estimate biomass (Fatoyinbo & Simard 2013; Solberg *et al.* 2014). Sensors also vary with respect to polarization modes (see **Chapter 2.2**), providing single, dual or quad-polarization mode data. Different polarization modes can in some instances provide complimentary information about the Earth's surface (Almeida-Filho *et al.* 2009; Liesenberg & Gloaguen 2012).

## 4.2 Which level of pre-processing is adequate?

What type of processing is appropriate depends on the type of analysis that is planned. As a rule of thumb, there should be as few pre-processing steps as possible, to reduce the chance of introducing artefacts and errors (Young *et al.* 2017). Limiting pre-processing also saves time and computational resources, e.g. because fewer intermediate data have to be stored. Additionally, commercial data can be more expensive per image if more pre-processing options are ordered. This chapter provides an overview of common pre-processing steps for multispectral and radar SRS data. Typically, SRS data are available with different levels of pre-processing, and these products are detailed where applicable.

*Multispectral SRS data*

The radiation that is detected by a spaceborne multispectral sensor is not only affected by the type of land cover, but also by sensor characteristics, solar (such as differences in Earth-sun distance), atmospheric (such as haze or clouds), and topographic effects (such as differences in illumination between North and South facing slopes; Young *et al.* 2017). These effects can be attenuated by radiometric and geometric corrections (see **Figure 4.2**).

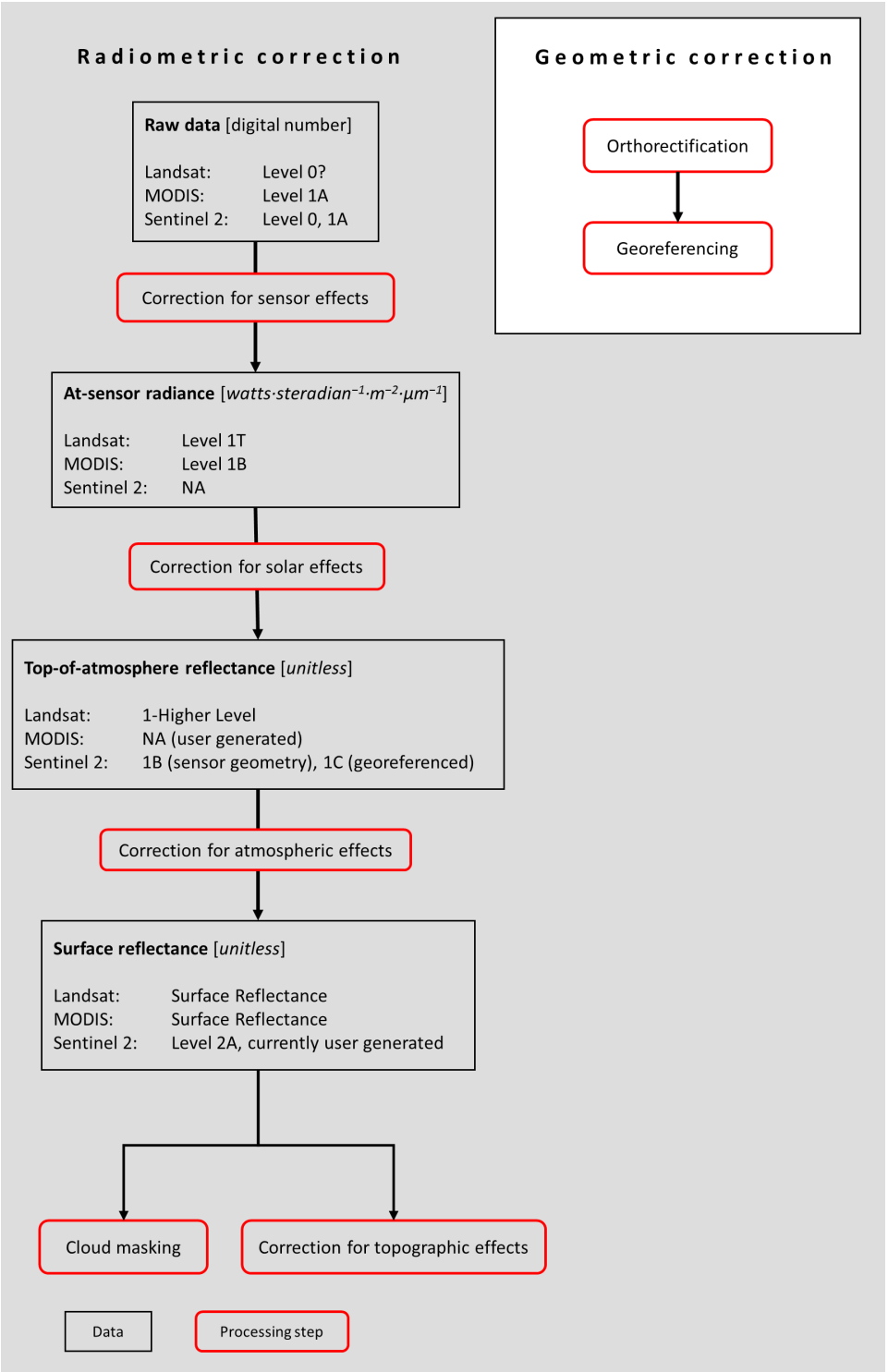


**Figure 4.2.** An overview of multispectral satellite imagery processing steps.

Raw sensor measurements are converted to radiance, i.e. the energy flux recorded by the sensor, using sensor-specific calibration coefficients that are part of SRS metadata. This at-sensor radiance is then corrected for solar effects, e.g. sun elevation angle, solar irradiance, and Earth-sun distance, which vary with date, time of day and latitude (Young *et al.* 2017). The resulting top-of-atmosphere (TOA) reflectance is a unitless ratio of radiation that is reflected by the Earth's surface relative to the incoming radiation. TOA reflectance is usually the least processed data level used for ecological applications, and can be appropriate for analyses that use a single image from a single point in time (Young *et al.* 2017). The new Landsat Level 1 collection provides such at-sensor radiance for TM, ETM+ and OLI/TIRS sensors with a formal data quality hierarchy (where Tier 1 refers to scenes with the highest data quality). TOA reflectance that has been corrected for atmospheric effects (such as haze) is called surface or bottom-of-atmosphere reflectance. Atmospheric correction methods include dark object subtraction (Chavez 1988), based on the assumption that in every image there are some pixels that do not reflect any light; any reflection measured over these dark objects is thus attributed to atmospheric scattering or absorption. Because it is difficult to carry out atmospheric correction without introducing artefacts, the use of surface reflectance products, such as Landsat Collection 1 Higher-Level products (see below) is recommended (Young *et al.* 2017; **Figure 4.3**).

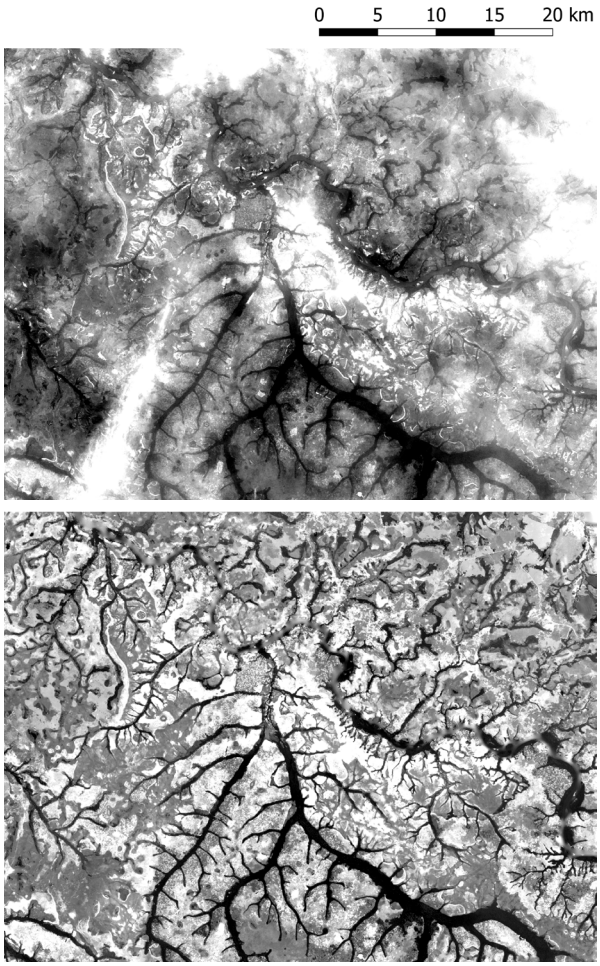


**Figure 4.3.** Comparing a multispectral satellite image before (top) and after (bottom) atmospheric correction. Shown is part of a Landsat 8 scene (band 3; path: 180, row: 63) acquired on August 10 2017. The bottom image shows the effect of the LaSRC algorithm which corrects for atmospheric effects.

Clouds can also be masked, if required, either by using a spectral index or by using cloud layers included in the SRS data (Zhu *et al.* 2015; Leutner & Wegmann 2016). For instance, all Landsat Level 1 products come with a Quality Assessment layer that flags cloud and cloud shadow pixel (USGS 2016) which allows a user to replace clouds with other data, such as from another less cloudy image. A cloud layer is part of Sentinel 2 Level 1C products, and is provided as a separate data product for MODIS (Platnick *et al.* 2014; ESA 2015).

When several images are being used in an analysis (e.g. a time series or several adjacent images), regardless of whether they represent at-sensor radiance, TOA or surface reflectance, it is useful to standardize the radiometric scale across all images (relative radiometric correction; Young *et al.* 2017), so that pixel values can be compared across images. Indeed, in cases where surface reflectance is not needed in the analysis, relative radiometric correction can be better at preserving relative reflectance values than applying atmospheric correction to each image separately (Schroeder *et al.* 2006). Common techniques for relative radiometric correction include histogram matching or methods based on pseudo-invariant features (Chen *et al.* 2005).

Both TOA and surface reflectance can be corrected for topographic effects of illumination, which can distort reflectance especially in rugged terrain (Shepherd & Dymond 2003; Vanonckelen *et al.* 2013; see Sola *et al.* 2016 for an overview of topographic correction methods). This is different from orthorectification, a type of geometric correction discussed below, which aims to correct topographic effects on pixel *location*.

Geometric corrections have the aim of aligning a given SRS image to an absolute or relative geographic location. SRS images are typically geolocated (i.e. contain information about the geographic location of each pixel). An important source of geometric error is local topography: large differences in elevation can lead to horizontal pixel displacement. This can be corrected via orthorectification, in which pixels are assigned locations based on a digital elevation model (Tucker *et al.* 2004). Furthermore, images can be co-registered (aligned with one another); though SRS data are often geolocated at sub-pixel accuracy (e.g. Landsat 8: Storey *et al.* 2014; Sentinel 2: ESA 2015), this may be necessary if images from different sensors or from different time periods are used. Landsat Level 1, and all higher levels, are both geolocated and orthorectified (with Level 1TP data having the highest geodetic precision, and Level 1GT or GS data having lower precision), whereas MODIS and Sentinel 2 Level 1B is only geolocated.

*Radar SRS data*

This section describes radiometric and geometric corrections of brightness information of radar SRS data (**Figure 4.4**). The phase information can be used to reconstruct a three-dimensional surface via interferometry (Zhou *et al.* 2009), e.g. to map forest biomass (Solberg *et al.* 2014). This requires advanced radar processing methods beyond the scope of this introduction.

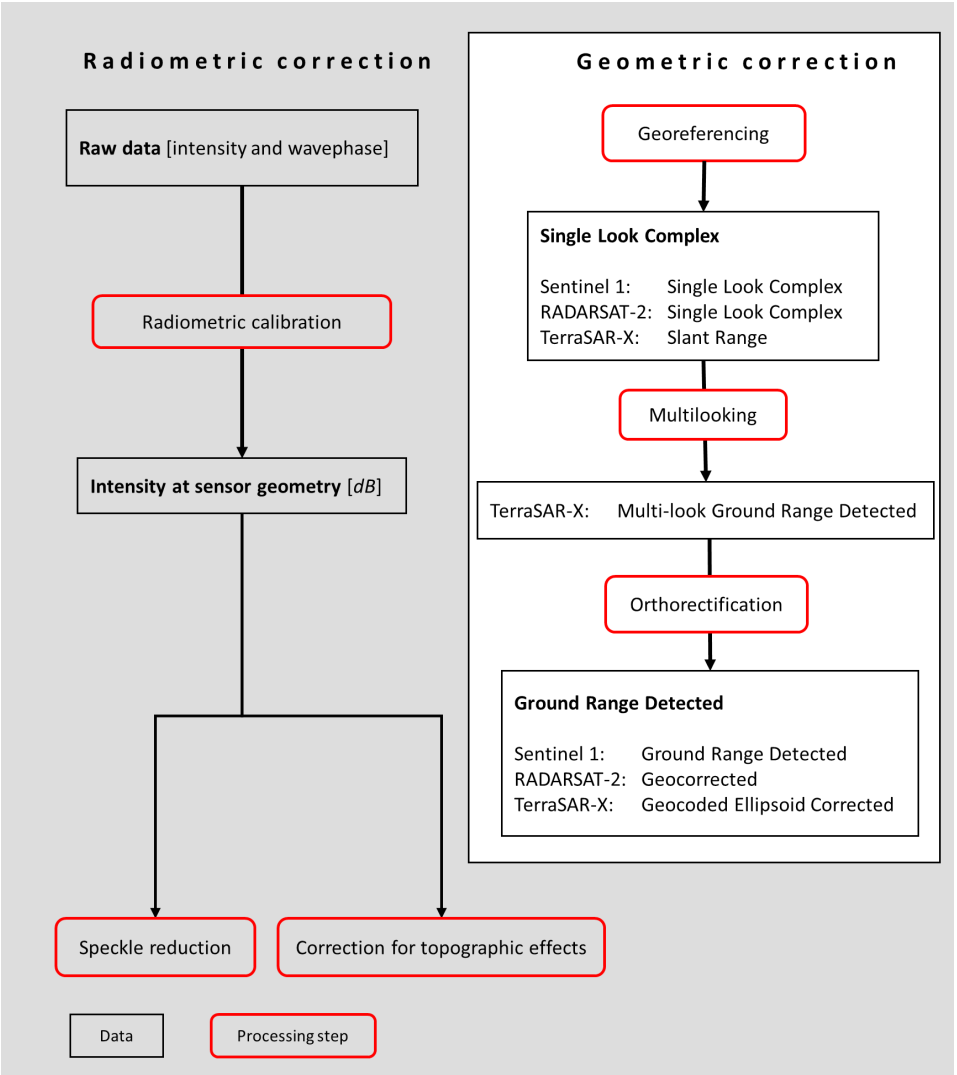


**Figure 4.4.** An overview of radar satellite imagery processing.

Raw data acquired by the radar sensor has to be converted to brightness, in a process called radiometric calibration, using sensor-specific coefficients contained in the metadata. The resulting brightness is called beta naught, and measures the reflectivity per unit area in slant range (i.e. in sensor geometry; expressed in dB), meaning that the pixels are not square. Consequently, multi-looking and geolocation are necessary steps after radiometric calibration.

A key radiometric correction for radar SRS data is speckle reduction. Radar speckle looks like noise ("salt-and-pepper effect"), but it is not random. Instead, it results from the deterministic interference of the backscatter of different objects in the same pixel. Depending on their arrangement, their backscatter phases may coincide (reinforcing each other) or be shifted relative to each other (cancelling each other out). Many despeckling techniques exist and their respective merit is actively debated (Di Martino *et al.* 2014). A simple despeckling technique is for instance passing a median filter over an image; additionally, speckle is reduced during multi-looking (see below).

Local topography not only introduces geometric effects (see below), but can also lead to radiometric errors because of small-scale variations in the incidence angle of the radar beam (Small 2011). These effects are corrected via radiometric terrain correction, which requires a digital elevation model (Small 2011). This correction is necessary to compare brightness values between images from different sensors, or between images acquired from different view angles.

Radar imagery has to undergo a series of geometric corrections before it can be used. Radar systems are side-looking, meaning that their view of the Earth's surface is stretched along the axis connecting the nadir to the furthest point that falls within the footprint, the range (see **Chapter 2**). As a result, pixels are not square, but instead elongated in range direction (**Figure 4.5**). To derive square pixels, radar images are multi-looked. This processing step essentially averages brightness values between several adjacent parts of the image (or "looks"). A positive side effect is speckle reduction (see below); however, the spatial resolution of multilooked imagery is always lower than single look imagery.

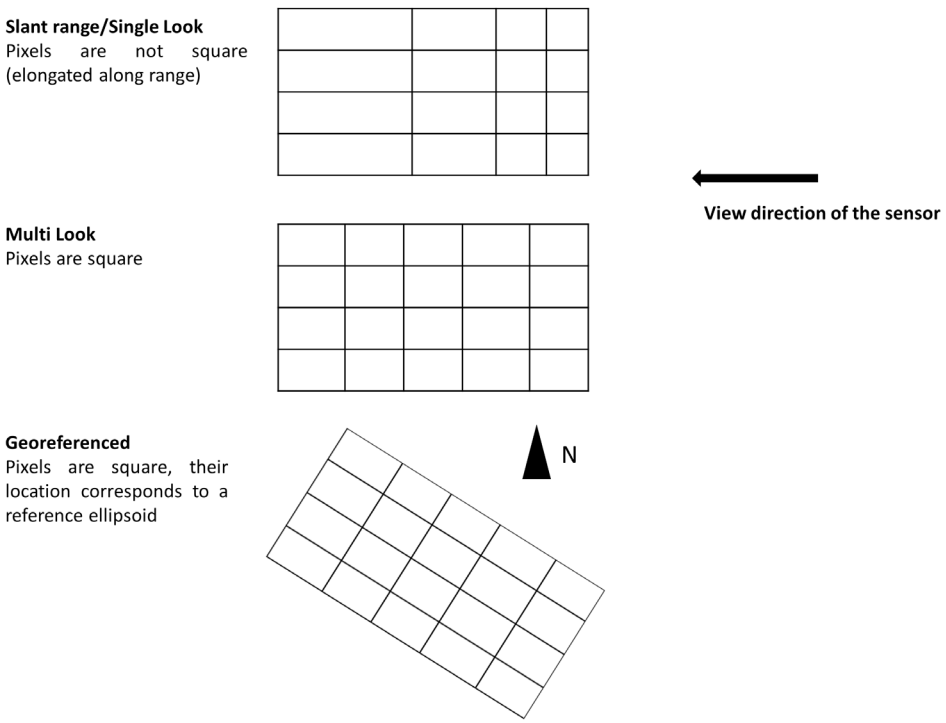


**Figure 4.5.** Difference between single look, multi look and georeferenced radar imagery. The top image shows a radar image in sensor geometry: areas which are further away from the sensor appear elongated (put differently, pixels further way from the sensor correspond to a larger area than pixels closer to the sensor). After multilooking, the image is in ground geometry: each pixel in the image corresponds to an area on the ground of the same size; areas further away from the sensor no longer appear "stretched". After the image has been georeferenced, each pixel now corresponds to a known location on the Earth's surface; such images are normally displayed with North up.

A key step for geometric corrections is geolocation, a process by which radar imagery is converted from sensor to ground geometry using a reference model of the Earth's surface (i.e. a reference ellipsoid, **Figure 4.5**). The resulting brightness values (called Sigma naught) measure the reflectivity per unit surface area in ground geometry, i.e. each pixel in the image corresponds to a pixel of the same area on the Earth's surface (Moreira *et al.* 2013). Multilooked and geolocated radar imagery is necessary for most applications because they ensure than the brightness information corresponds to a known location on the ground.

Though geolocation reduces some of the geometric distortions of radar images, local topography can introduce further artefacts, such as layover and foreshortening (**Figure 4.6**). Both effects result from the view geometry of radar satellites. In layover, the top of tall structures (mountains or buildings) appears to be closer in range than lower structures. This is because the signal from the top of tall structures arrives at the sensor sooner than a signal backscattered from a lower structure, which (in slant geometry) looks like the tall structure is closer to the sensor. *Foreshortening* refers to slopes which face the sensor appearing shorter than slopes that are tilted away. Again, this happens because backscatter from the latter reaches the sensor later than backscatter of the former (Campbell 1996). These topographic effects can be corrected via orthorectification, such as the Range Doppler method, which requires a precise digital elevation model (Sheng & Alsdorf 2005; **Figure 4.7**). However, if the terrain is flat, orthorectification may not be necessary.

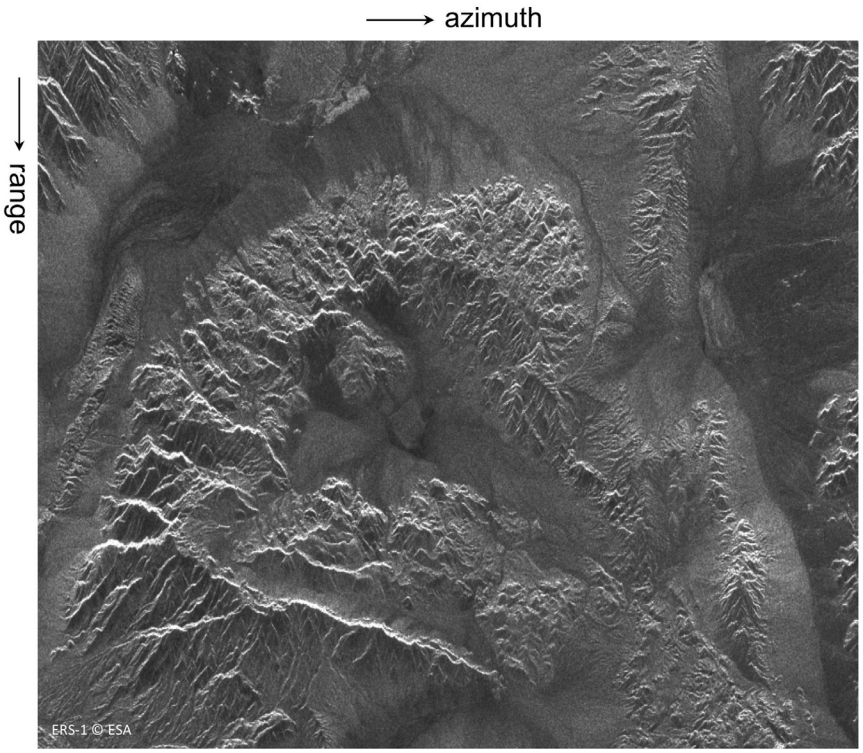


**Figure 4.6.** This SAR imagery from ERS-1 shows the effects of layover and foreshortening. The image was acquired over the Mojave Desert, and shows a mountain range. The top of each mountain seems to "lean" towards the SAR sensor (i.e. shifted across the range), and the slopes facing the satellite appear shorter than those facing away. © Michael Eineder, Richard Bamler (CC BY-SA 4.0).

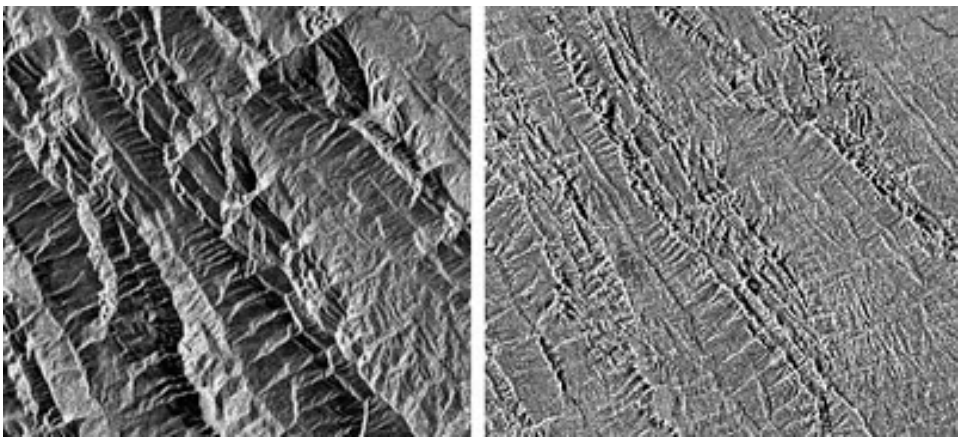

**Figure 4.7.** A Sentinel 1 image before (left) and after (right) terrain correction. Terrain correction involves adjusting pixel location as well as backscatter intensity to account for distortions such as foreshortening. Credit left: Copernicus Sentinel data 2015. Credit right: ASF DAAC 2016, contains modified Copernicus Sentinel data 2015.

## 4.3 Resources and software for accessing and processing satellite imagery

After SRS data has been acquired, there is a range of open-access and proprietary software available for visualisation; processing and analysis (see **Table 4.2**). Such programmes typically include a Geographic Information System (GIS) component, which can also deal with vector data (points, lines and polygons). For open source software there are useful extensions for SRS processing and analysis (e.g. 'RStoolbox'). QGIS and R have many tools for SRS imagery processing and analysis. R is a software environment that is used widely in ecology and conservation science to analyse and visualise data. Using it requires getting to know its syntax, but it has a lot of high-level SRS capability in packages such as 'raster', 'rgdal' and 'RStoolbox'. Google Earth Engine provides online cloud processing for many types of imagery in a simpler map interface as well as a coding platform. A popular commercial software package is ArcGIS from ESRI, which has a native image analysis window which provides fast processing, including clipping and classification tools. ESRI also provides image services which are streamed via the web and can be ingested directly into its GIS. For pre-processing Sentinel SRS data, ESA has developed dedicated, free software, called SNAP (which subsumes earlier, stand-alone toolboxes for Sentinel 1, 2 and 3).

QGIS
http://www.qgis.org/

R
https://www.r-project.org/

All of these packages allow (semi-)automated downloading of SRS imagery: MODIS SRS imagery and products can be downloaded through R, using the 'MODIS' package, whereas the Semi-Automatic Classification Plugin allows downloading Landsat 4-8, Sentinel 2 and ASTER data through QGIS.

There are online resources available to help carry out simple remote sensing projects, including forums (e.g. the Open Source Geospatial Foundation; Stack Exchange; or see Wegmann *et al*. 2016).

Open Source Geospatial Portal
http://www.osgeo.org/home

Stack Exchange
https://gis.stackexchange.com/

ESRI
https://community.esri.com

Google Earth Engine
https://developers.google.com/earth-engine/edu

Advanced users, who are interested in computational efficiency, flexibility and automatization, are likely going to prefer implementing GIS commands in a programming environment. GDAL, GRASS GIS and SAGA GIS all have a wide range of functions for SRS processing and analysis, and can be integrated into batch scripts (e.g. using Python).

**Table 4.2.** Software used for pre-processing, analysing and visualising SRS data.

| SOFTWARE | SHORT DESCRIPTION | OPEN-ACCESS? |
|---|---|---|
| ArcGIS | GIS environment for e.g. visualisation, map-making, pre-processing | No |
| eCognition | Software for object-based image analysis | No |
| ENVI | Image analysis software for SRS data, e.g. pre-processing, land cover classification, photogrammetry | No |
| ERDAS | Image analysis software for SRS data, e.g. pre-processing, land cover classification, photogrammetry | No |
| GDAL | Library for raster and vector data formats and utility programmes (commands which allow SRS data processing) | Yes |
| GRASS GIS | GIS environment for e.g. pre-processing, land cover classification, spatial modelling | Yes |
| IDRISI | GIS environment and image processing, including land cover classification | No |
| IMPACT | Portable GIS Toolbox for image processing and land cover mapping | Yes |
| QGIS | GIS environment; useful for visualisation, map making, downloading and land cover classification | Yes |
| R | Software environment for statistical computing, for e.g. pre-processing, land cover class, time series analysis | Yes |
| SAGA GIS | GIS environment for image processing and spatial modelling | Yes |
| SNAP | ESA toolbox for pre-processing Sentinel imagery | Yes |
| Python | Programming language; useful for batch processing large amounts of SRS data | Yes |

## 4.4 Common SRS analysis techniques

A simple way to use SRS imagery is to perform a visual inspection (often aided by composite images, such as RGB, Horning 2004). Often, this is enough to identify some features of interest, such as forests and water bodies. Additionally, visual inspection of layers can yield important information about which pre-processing steps might be necessary – is there visible haze, or topographic distortions? However, SRS imagery is rich in information that is not easily apparent to ad-hoc human interpretation. In the following, a short overview of three ways to use this information are presented: 1) generating new layers taking into account spatial context (textures), 2) extracting the most important information from many different bands (dimensionality reduction), and 3) image classification techniques.

*Textures*

SRS imagery provides not only information about the spectral or backscatter characteristics of each pixel, but also about their spatial context: what do the pixels around it look like? This spatial context is made evident in so-called texture layers. Texture layers are generated by moving a window across the image, calculating a particular statistic (such as mean or standard deviation) across all pixels in that window, and assigning this value to the focal pixel (Rocchini *et al.* 2016b). Texture layers can help discriminate between different types of land cover, both for multispectral (Wang *et al.* 2004) and radar imagery (Haack & Bechdol 2000).

*Dimensionality reduction*

A large number of layers can be generated from original SRS bands (e.g. texture variables, band ratios or vegetation indices). However, much of the information contained in these layers may be redundant, burdening further analysis with unnecessary amounts of data. In these instances, dimensionality reduction can be useful – essentially "collapsing" the information contained in many bands into a few. Principal Component Analysis (PCA) allows the generation of a reduced number of layers that contain most of the information from the original layers (Demšar *et al.* 2013). Tasselled cap algorithms, similar to PCAs, generate three new layers from linear combinations of the original layers, corresponding to brightness, wetness and greenness (Huang *et al.* 2002). Finally, spectral unmixing algorithms estimate the fraction, per pixel, of a number of predefined "pure" land cover classes (so-called spectral endmembers); for instance, the fraction of each pixel covered in vegetation, soil and shadow can be estimated (Asner 2014).

*Image classification*

Supervised or unsupervised land cover classification techniques are among the most widespread SRS image analysis techniques; they aim to assign similar pixels into classes or classes. Many machine learning land cover classification algorithms can assess pixel characteristics across a large number of bands, which can be a combination of original bands, band ratios, vegetation indices and/or texture variables. In supervised land cover classification the classification algorithm "learns" what each land cover class looks like by being given example locations of each class (training or calibration data), and then applies what it has learned to new areas. Common supervised classifiers include the Random Forest algorithm (Breiman 2001) or the maximum likelihood classifier (Xiuping Jia & Richards 1994). By contrast, unsupervised classification algorithms identify clusters of pixels that are similar by comparing their spectral and/or backscatter characteristics. These are assigned to unlabelled classes by the algorithm, and these classes are then then assigned to cover classes by the user. Another increasingly popular image classification technique is object-based image analysis (OBIA), where an image is segmented into groups of adjacent pixels that are more similar to each other than the surrounding pixels. These polygons are then be grouped into classes using spectral or pixel information like the classification described above, as well as texture and shape metrics of the objects (Blaschke 2010). Because OBIA takes into account the spectral information of each individual pixel, as well as its spatial context (i.e. its neighbouring pixel), it is a powerful technique for distinguishing discrete land cover classes. The accuracy of land cover maps can be assessed by comparing the predicted land cover against observed land cover, based on field observations or imagery with very high spatial resolution (see Olofsson *et al.* 2014) for good practice recommendations about accuracy assessments.

## BOX A: OBJECT-BASED LAND COVER CLASSIFICATION TO MAP PEAT SWAMP FORESTS IN SEBANGAU NATIONAL PARK

Sebangau National Park, Indonesia, covers ca. 5800 km² and has been affected by illegal logging. A land cover classification was carried out to distinguish forest from non-forest areas (i.e. potential sites of deforestation), and to map degraded and non-degraded areas of peat swamp within the remaining forest. There are two main reasons why such a land cover classification will benefit conservation in Sebangau National Park: first, it allows identifying candidate sites for afforestation, and second, mapping different forest types helps pinpoint key nesting sites for orangutans (*Pongo pygmaeus*).

To classify the land cover, an object-based image analysis was conducted. In the first step, adjacent pixels that were spectrally similar were clustered into discrete, contiguous objects (see **Chapter 4.4**). These objects were then labelled (e.g. forest, water, etc.) based on expert knowledge of the area and ancillary data such as topographic maps. The basis of the Sebangau National Park land cover classification was RapidEye imagery from 2009 and 2011. RapidEye is a multispectral sensor with 5 bands and a very high spatial resolution (6.5 m). The imagery was first atmospherically corrected using ATCOR-2, a type of software for atmospheric and topographic corrections of SRS imagery (Richter & Schläpfer 2016), and orthorectified using Erdas' Autosync algorithm. Then, a spectral mixture analysis was carried out, which produces three new layers, namely, the proportion of green vegetation, non-photosynthetically active vegetation and soil per pixel (per Asner *et al.* 2005).

These layers were then used to generate objects in eCognition. The land cover class of each object was identified via a rule set based on expert knowledge of the region as well as additional spectral information from Landsat. For instance, Landsat imagery helped discriminate between areas of palm swamp forest with different heights. Finally, visual post-processing of the maps was carried out to minimize errors, especially in the degradation classes. The resulting map (**Figure A**) shows relatively large areas of highly degraded palm swamp forest throughout the National Park, especially towards the West.

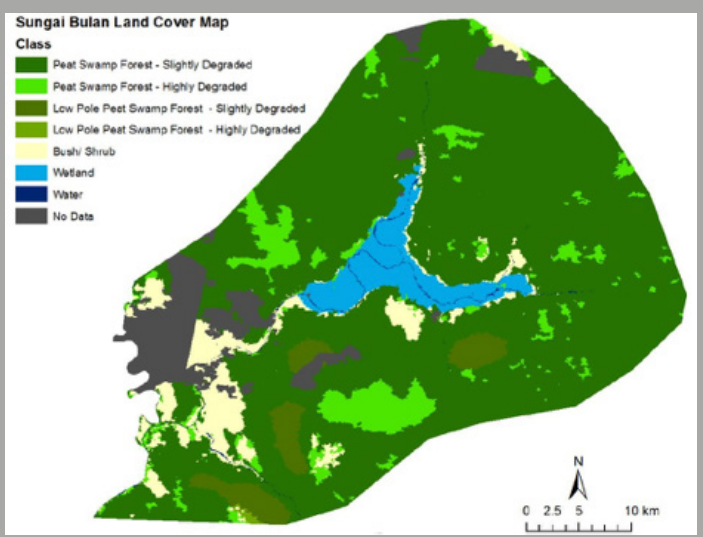


**Figure A.** Land cover classification based on object-based image analysis of high resolution, multispectral SRS imagery from RapidEye. The "no data" gaps are due to cloud cover.

## BOX B: SUPERVISED LAND COVER CLASSIFICATION TO MAP MOZAMBIQUE'S MANGROVES

Mangrove forests provide habitat for a diverse fauna and flora (Manson *et al.* 2005), and support essential ecosystem processes, functions and services such as carbon storage (Donato *et al.* 2011) and coastal protection (Dahdouh-Guebas *et al.* 2005). To support the conservation of Mozambique's mangroves, WWF-Germany and WWF-Mozambique estimated the extent of mangrove forests along the Indian Ocean coast in 2016. Satellite remote sensing data are well suited to national ecosystem mapping because they provide continuous wall-to-wall coverage. Multispectral satellite remote sensing data are widely used for forest mapping at large scales (Hansen & Loveland 2012) including mangrove forests (Giri *et al.* 2011). In this case, all analyses were carried out in Google Earth Engine, which provides free cloud computing services, as well as access to a large range of accessible satellite remote sensing data and products. The use of cloud computing facilitates processing of relatively large datasets without the need to invest in costly hardware or software.

The underlying satellite remote sensing data were provided by the Sentinel 2A satellite, launched by the European Space Agency in 2015, which carries a multispectral sensor that provides imagery with a spatial resolution of 10 m and overpass frequency of about once every two weeks, and is similar to Landsat 8, but with additional bands in the near-infrared spectrum. All Level-1C scenes covering the study area acquired in 2016 were accessed via Google Earth Engine. Level-1C data have been corrected for solar and sensor effects (i.e. it corresponds to top-of-atmosphere reflectance) and are georeferenced (ESA 2015)Scenes with a cloud cover of < 5% from 2016 were composited and mosaicked to produce a single cloud-free image; for the remaining scenes, all pixels that were flagged as clouds in the quality assessment band (which is distributed along with the spectral bands for each scene) were discarded and replaced with the median value of the remaining suitable observations in each spectral band.

This image was then masked to exclude areas that are unlikely to contain mangrove forests (see **Figure A1**) which reduced the volume of data that required processing, and increased the accuracy of the analysis by ensuring that no mangroves were mapped inland. This step included masking water using a Modified Normalized Difference Water Index, which is sensitive to water and moisture (Xu 2006). With this index, pixels with values below a particular threshold are classed as water and excluded from further analysis. Additionally, all land above 35 m elevation was masked using a digital elevation model to restrict the analysis to the coastal zone where mangroves occur. The remaining imagery was used to calculate a range of band ratios and indices, such as the NDVI, and the ratio between the SWIR /NIR, to aid land cover classification.

These indices and band ratios, together with the original spectral bands, were combined to map mangroves using a Random Forest supervised classification algorithm (Breiman 2001). A supervised classification algorithm is provided with samples of all land cover classes of interest, and "learns" their spectral characteristics, and then predicts land cover across a larger area (see **Chapter 4.4**). These samples are called training data (since they are used to train the algorithm to distinguish between different types of land cover) and they are typically provided in vector format (shapes or polygons). The source of training data, in this case, was existing mangrove maps and additional field observations of mangroves, and non-mangroves (**Figure A1**). The resulting map of mangrove and non-mangrove was filtered to remove erroneously identified single pixels. This map was then used to calculate mangrove extent for each province in Mozambique (**Figure A2**). A quantitative accuracy assessment was carried out using high resolution Google Earth and limited field data collected by partners. In areas where field data were collected, overall accuracy was estimated at 93%. Additional field data are being collected to extend the validation.

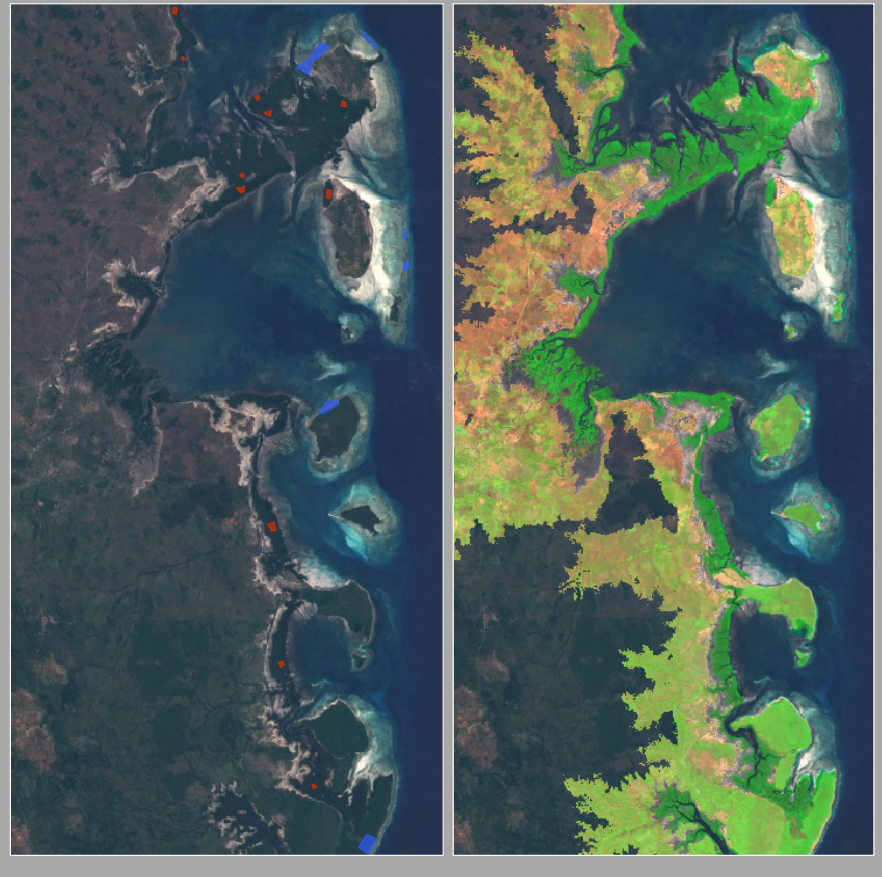

**Figure A1.** Both images show the cloud-free composite of Sentinel 2A scenes over Quirimbas National Park, rendered as an RGB image. The left image contains examples of mangrove (red) and non-mangrove (blue) training data. The right image was created following the masking of water and elevations above 35 m (remaining imagery is shown in bright colours).

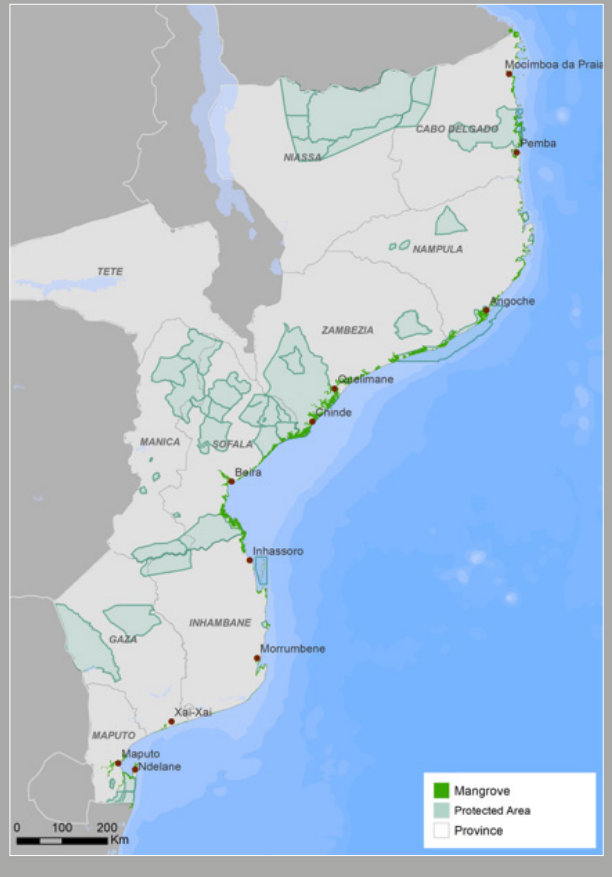


**Figure A2.** Map of mangrove extent in Mozambique in 2016 based on a supervised classification of Sentinel 2A imagery.

Image acquired at night above the Atlantic coast of South America by the VIIRS sensor onboard the Suomi NPP satellite. Its “day-night band” is sensitive to small amounts of light across a relatively large range of wavelengths (green to near-infrared), such as might be emitted by city lights.
Source: NASA Earth Observatory image by Jesse Allen and Robert Simmon, using VIIRS Day-Night Band data from the Suomi National Polar-orbiting Partnership.

# 5 APPLICATIONS OF SATELLITE REMOTE SENSING IMAGERY IN ECOLOGY AND CONSERVATION

## HIGHLIGHTS

- Remote sensing is regularly used to monitor vegetation and ecosystem structure, composition, and function, as well as threats such as deforestation and degradation, land cover change, pollution, and fire.
- Increasing spatial and temporal resolutions are now allowing the application of satellite remote sensing to monitor plant and animal populations.

During the last two decades, spaceborne sensors have become a routine source of information to track biodiversity, from the population to the ecosystem level – and crucially, the mounting anthropogenic pressures it is facing. Throughout this chapter, we focus on multispectral and radar SRS. Applications of hyperspectral imagery and LiDAR, which are currently primarily sourced from airborne missions, are reviewed in **Chapter 6**.

This chapter provides an overview of the most common applications of SRS in ecology and conservation, starting with ecosystem and habitat mapping (**Chapter 5.1**) and the use of SRS to monitor ecosystem condition (**Chapter 5.2**). **Chapter 5.3** highlights how SRS can contribute to monitoring some of the most common threats to biodiversity. This chapter concludes with an introduction to a relatively new, but promising, field of application, namely the direct detection of animal and plant species from space (**Chapter 5.4**). SRS can inform and support conservation management at a range of scales, from local (e.g. forest monitoring in a single protected area; **Box A**) to regional (e.g. vegetation monitoring across the entire Arctic; **Box E**). Importantly, SRS is the only source of biodiversity data with potentially global, continuous coverage and is expected to play an important role developing an operational global biodiversity monitoring scheme, focused around Essential Biodiversity Variables (**Box 1**).

## BOX 1: ESSENTIAL BIODIVERSITY VARIABLES AND SRS

Biodiversity has many dimensions – genes, species, and ecosystems – and structural, compositional and functional aspects. Answering the question "what is the state of biodiversity globally?" is thus challenging, and requires monitoring of many different variables. Essential Biodiversity Variables (EBVs) are being developed by the Group on Earth Observations Biodiversity Observation Network (GEO-BON, http://geobon.org/) to provide a comprehensive list of parameters which, together, will provide a synoptic picture of global biodiversity (Pereira *et al.* 2013). EBVs sit at an intermediate level between raw data (e.g. population counts) and indices which summarize a large variety of data to non-specialist policy makers and members of the public (e.g. the Living Planet Index, Loh *et al.* 2005). SRS data has a key role in the development of EBVs because it allows the standardized, repeated measurement of biodiversity-related parameters (SRS-EBVs) at global scales and with relatively high spatial resolution (**Chapter 5**, **Appendix**, **Figure A**). SRS data and analysis techniques are already capable of generating SRS-EBVs to monitor ecosystem structure and function (Pettorelli *et al.* 2016, 2017), and new satellite missions (**Chapter 6**) are expected to make species-level biodiversity monitoring possible.

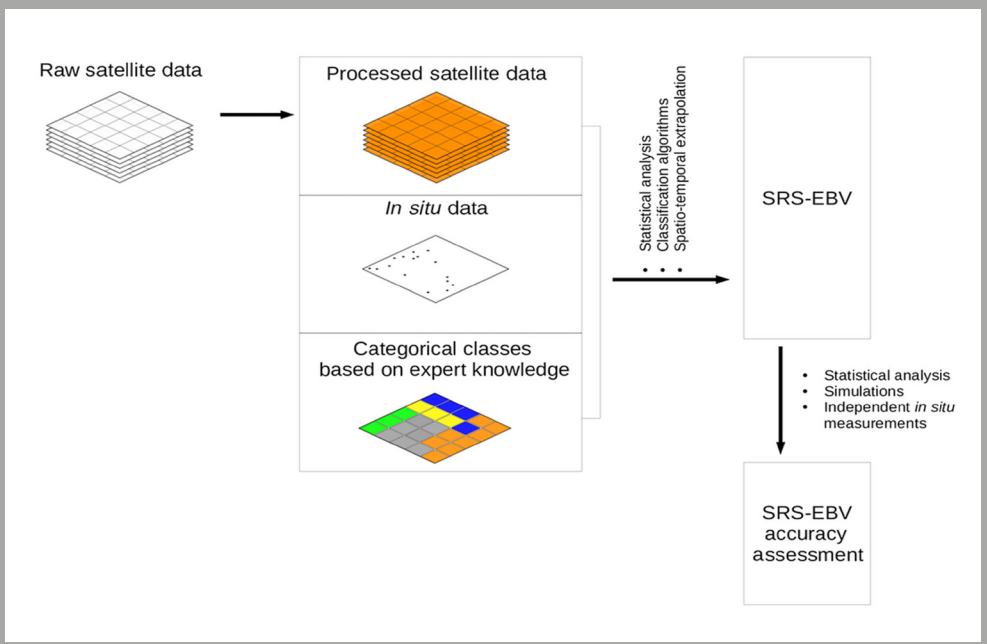


**Figure A.** Workflow for generating SRS-EBVs, integrating ground truth data and expert knowledge. Figure from Pettorelli *et al.* (2016), published under a CC-BY license.

### 5.1 Land cover mapping and vegetation monitoring

Before exploring how SRS can help track changes in ecosystem and habitat distributions, a few key concepts and definitions need to be introduced. The term "ecosystem" refers to an assemblage of species which are interacting with each other as well as their abiotic environment, and the physical space in which this occurs (Pickett & Cadenasso 2002). Ecosystems can be defined at many spatial scales. The entire Earth system can be thought of as a single ecosystem. In practice, however, ecosystems are often defined at the landscape scale. The term "habitat" refers to those resources and conditions in an area that produce occupancy, including survival and reproduction, by a given organism (Morrison *et al.* 2006). In contrast to ecosystem, habitat refers to areas home to particular species (or populations), meaning that the variables which are important in determining a habitat vary according to species, location, or which spatial or temporal scales are considered (Pettorelli 2013). SRS does not discern ecosystems and habitats. Instead, SRS provides information on land cover, or properties of vegetation such as rigor or health, which affect the physical properties of a given surface. These properties can be characterised by the radiation that remote sensors capture (Simard *et al.* 2011). To derive information about the spatio-temporal distribution of biodiversity from SRS imagery, land cover is then translated into ecosystems or habitats (**Figure 5.1**). The main conceptual challenge of ecosystem and habitat mapping is matching commonly mapped land cover classes to ecosystem or habitat types, which is not always straightforward (Nagendra *et al.* 2013). For instance, Hansen *et al.* (2013) defined "forest" (an ecosystem type) as "all vegetation taller than 5m in height" (a land cover class) to produce a SRS-derived global forest map. Tropek *et al.* (2014) however commented that this approach as being unable to distinguish between "natural" forests and monospecific plantations, which are identical in land cover, but are arguably different ecosystems (Braun *et al.* 2017)In the following chapter, we review applications of SRS to map the extent of ecosystems and habitats as defined above, but it is important to note that these terms are often used interchangeably, or conflated with land cover.

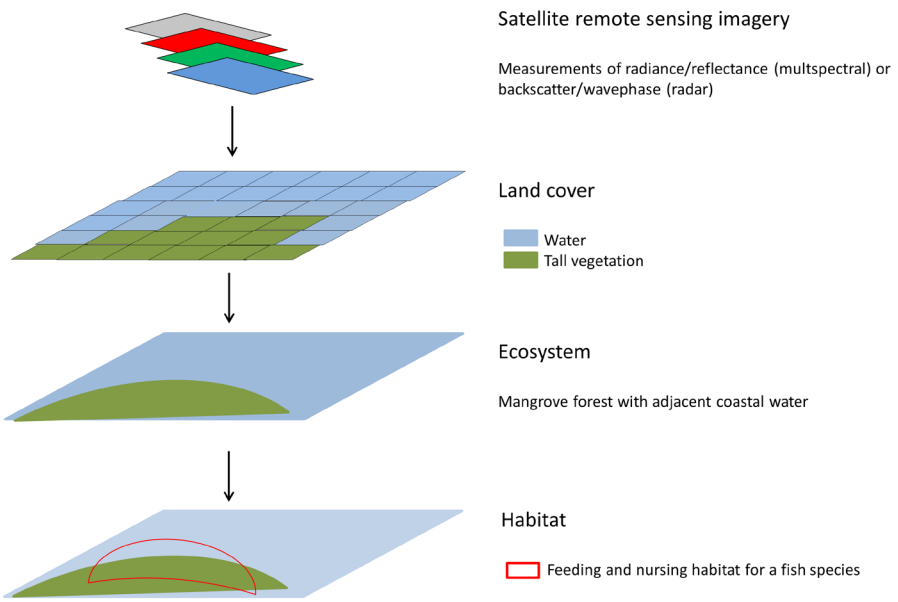


**Figure 5.1.** Satellite imagery can be used to derive information about land cover (such as type and structure of vegetation). This is then related to ecosystem distribution, or habitat use of particular species.

*Mapping ecosystem extent*

SRS has been used to map ecosystems at global (Verpoorter *et al.* 2012; Sayre *et al.* 2014), continental (McDonald *et al.* 2011), and local scales (Varela *et al.* 2008; Bargiel 2013; Buck *et al.* 2015, **Table 5.1**). Though many studies map ecosystem distribution at a single point in time, changes in extent over time can be tracked using satellite imagery (Cui & Li 2011; Hermas *et al.* 2012; Hansen *et al.* 2013; Chapman *et al.* 2015). In the terrestrial realm, examples of successful ecosystem classifications include mapping forests (Potapov *et al.* 2008; Achard & Hansen 2012), grasslands (Buck *et al.* 2015) wetlands (Klemas 2011; Evans *et al.* 2014) and mangroves (Fatoyinbo *et al.* 2008; Giri *et al.* 2011; Shapiro *et al.* 2015). Fine-grained mosaics of agriculture, semi-natural and natural ecosystems can be mapped accurately in many circumstances (Díaz Varela *et al.* 2008; Bargiel 2013), but require appropriate ground-truthing data to train machine learning algorithms. Compared to multispectral SRS, radar SRS has been applied to ecosystem mapping only relatively recently (Waske & Braun 2009), but it is already a key resource for monitoring forests in the tropics, since it is able to penetrate clouds (Whittle *et al.* 2012). Radar SRS has also been used to study wetland dynamics (Betbeder *et al.* 2015; Hess *et al.* 2015), because of its sensitivity to surface moisture, and consequent suitability for mapping the extent of surface water (Long *et al.* 2014), which can be used to characterise flooding frequency in a given area (Martinez & Le Toan 2007), even below the canopy (Lang *et al.* 2008).

**Table 5.1.** Overview of ecosystem distribution mapping of different ecosystem types.

| ECOSYSTEM TYPE | REFERENCE |
|---|---|
| Forests (including mangroves) | Giri *et al.* 2011; Fatoyinbo & Simard 2013; Hansen *et al.* 2013; Sexton *et al.* 2013 |
| Grassland/savannah | Bargiel 2013; Buck *et al.* 2015; Marston *et al.* 2017 |
| Tundra/bare ground | Hermas *et al.* 2012; Beck *et al.* 2015 |
| Wetlands | Klemas 2010; McDonald *et al.* 2011; Evans *et al.* 2014; Chapman *et al.* 2015 |
| Freshwater bodies | Cui & Li 2011; Verpoorter *et al.* 2012, 2014 |
| Seagrass meadows | Wabnitz *et al.* 2008; Roelfsema *et al.* 2009; Dierssen *et al.* 2010; Knudby *et al.* 2011; Lyons *et al.* 2012, |
| Coral reefs | Andréfouët 2008; Eakin *et al.* 2010; Knudby *et al.* 2011; Goodman *et al.* 2013 |

Since both optical and radar remote sensors typically do not penetrate deep water, applications in the marine realm have been limited to ecosystems at shallow depths less than 30 m, such as seagrass meadows and coral reefs (Roelfsema *et al.* 2009; Dierssen *et al.* 2010; Knudby *et al.* 2011). Dierssen *et al.* (2010) demonstrated that different types of shallow coastal benthic cover (such as sand, mud, seagrass and algae) have distinct optical spectra (especially around green light wavelengths), and so can be distinguished using optical SRS with medium or high spectral resolution. However, to derive benthic cover from spectral curves, the impact of water depth has to be taken into account. This is because the spectrum of a given benthic cover type is blue-shifted at greater depths: water attenuates green light more than blue light, so the deeper the water column, the less green light (relative to blue light) is reflected back to the remote sensor. There are a range of approaches to correct for this effect, ranging from using independent information about sea depth (Dierssen *et al.* 2010), to estimating sea depth from the satellite imagery itself

(Hedley & Mumby 2003). Alternatively, object-based segmentation can be used to divide SRS imagery into spectrally homogenous patches, which are then manually assigned to benthic cover classes (Knudby *et al.* 2011; Teixeira *et al.* 2016).

Mapping the extent of an ecosystem using SRS depends on dividing continuous spectral information into discrete classes and identifying those classes that characterise the ecosystem considered. Categorization of spectral information is fundamentally constrained by the differences in reflectance and backscatter properties – defining classes that "look" similar makes it hard to map them accurately. For instance, it is more difficult to accurately map different stages of forest regrowth using SRS information than to differentiate forest from grassland (Lu *et al.* 2011). It is also easier to accurately map classes with a relatively homogenous structure (such as forests with a closed canopy) than land cover classes characterised by high structural heterogeneity, such as open woodlands with scattered trees, shrubs and bare soil (Herold *et al.* 2008; Fritz *et al.* 2011; Tsendbazar *et al.* 2016). Certain ecosystems can be mapped based entirely on their distinct phenology as assessed by vegetation indices time series (Pettorelli 2013).

Where land cover varies on a relatively small spatial scale, and the spatial resolution of SRS imagery is relatively coarse, the signal in any given pixel may be a mixture of different classes. Some land cover classification schemes recognize this by allowing for explicitly mixed classes; for instance, the International Geosphere-Biosphere Programme (IGBP) land cover classification scheme includes as a mapping class "mosaic of croplands, forest, shrub lands, and grasslands". However, mixed classes tend to be more difficult to map accurately than more homogenous classes (Herold *et al.* 2008). If available, imagery with higher spatial resolution may resolve this issue (Betbeder *et al.* 2015). Alternatively, spectral unmixing allows estimating the proportions of different land cover classes in each pixel based on examples of reflectance signatures from "pure" pixels, or so-called endmembers (Cortés *et al.* 2014).

## BOX C: BENTHIC HABITAT CLASSIFICATION IN THE PRIMEIRAS AND SEGUNDAS ENVIRONMENTAL PROTECTED AREA

The Primeiras and Segundas Environmental Protected Area (PSEPA) encompass two atolls off Mozambique's coast, and is the largest African marine protected area, covering 10,000 km² (Teixeira *et al.* 2015). It comprises several types of ecosystems – mangroves, seagrass meadows and coral reefs – and supports substantial fisheries. To help support conservation management and planning efforts, WWF-Germany and ESA's G-ECO-MON (Geographic Ecosystem Monitoring & Assessment) mapped benthic habitat types across 12 islands within PSEPA, covering a total of 130 km². Sea cover classification occurred at three, nested levels, with increasing thematic resolution: Level 1 describes the geomorphology (e.g. shallow water, lagoon), level 2 the main sea bottom substrate (e.g. sand or coral), and level 3, termed benthic habitat, describes finer variation in sea bottom cover (such as rock alone or rock covered in brown macroalgae).

Multispectral satellite imagery with very high spatial resolution (WorldView-2, Quickbird 2 and GeoEye-1) was acquired for the study area. Pre-processing (carried out in IDRISI Selva) involved radiometric and atmospheric corrections. The latter used a Dark Object Subtraction to remove haze – this technique is based on the assumption that there are always some pixels in each image from which reflectance is close to zero. Any reflectance that is measured from them can be attributed to atmospheric scattering, and this information is used to correct the brightness values of all other pixels.

Two other pre-processing steps were necessary because benthic sea cover is covered by water: sun glint correction, and water column correction. Sun glint occurs when flat water reflects sunlight, appearing bright white, which occludes underlying benthic cover. In pixels with sun glint, the reflectance measured by the sensor is a combination of the signal from the water surface (due to glint) and the signal from the benthic cover (which is the feature of interest). The spectral signal associated with benthic cover can be recovered if the signal overall does not saturate the sensor. Brightness values for each glint-affected pixel are corrected based on the near-infrared band (Hedley *et al.* 2005). Water column correction aims to correct the reflectance for the attenuating effects of the water column, which vary with both water depth and the optical clarity of the water. This correction is based on the principle that, regardless of water depth, the ratio between two given spectral bands is constant if the benthic cover is the same. This can be used to derive depth-independent information about benthic cover, using water attenuation coefficients estimated for each bands (Lyzenga 1978, 1981).

An object-based image analysis technique called nearest neighbor (implemented in the eCognition software) was used to classify the pre-processed imagery. This algorithm has two main steps. First, the imagery is segmented into objects by grouping similar adjacent pixels into objects. Image segmentation (unlike other techniques such as k-means unsupervised classification) not only takes into account the spectral information of each pixel, but also considers its spatial context; the user can in fact define the types of shapes and size of objects, based on existing knowledge about the general "texture" of a landscape or seascape. Second, each object is assigned to a class. Classes are defined a priori, and field data is used to identify several objects belonging to each class. Then, several SRS-based statistics are calculated for each class (e.g. mean green reflectance, standard deviation of blue/green ratio, or similar). All objects are then assigned to a class based on whose statistics they most closely match (i.e. whose "nearest neighbor" they are). This process resulted in three maps (one per level) for each of the 12 islands.

After contextual editing to remove obvious errors, the resulting maps were validated using field data. Field observations of benthic habitat at 666 points were made in 2014. However, only six islands were safely accessible by boat, and so only those maps could be validated. For Level 3, overall mapping accuracy was 50%. This was likely due to a combination of high thematic resolution (between 13 and 24 benthic habitat classes were mapped per island) and the similarity between these classes (considering that "sand/rubble with rocks" and "rocks with sand and rubble" were considered separate classes for instance). At Level 2, overall accuracy was 70%, which is considered sufficient for marine mapping and planning purposes (Green & Edwards 2000).

**Figure C** displays the outcomes of this approach for one of the islands; these maps are commonly used in marine protected area management, e.g. to delineate fishing zones. The synoptic, wall-to-wall map of existing coral reefs helped characterize the environmental factors shaping their local distribution, such as water currents. This suggested there may be deeper coral reefs to the East of the archipelago (Teixeira *et al.* 2015).

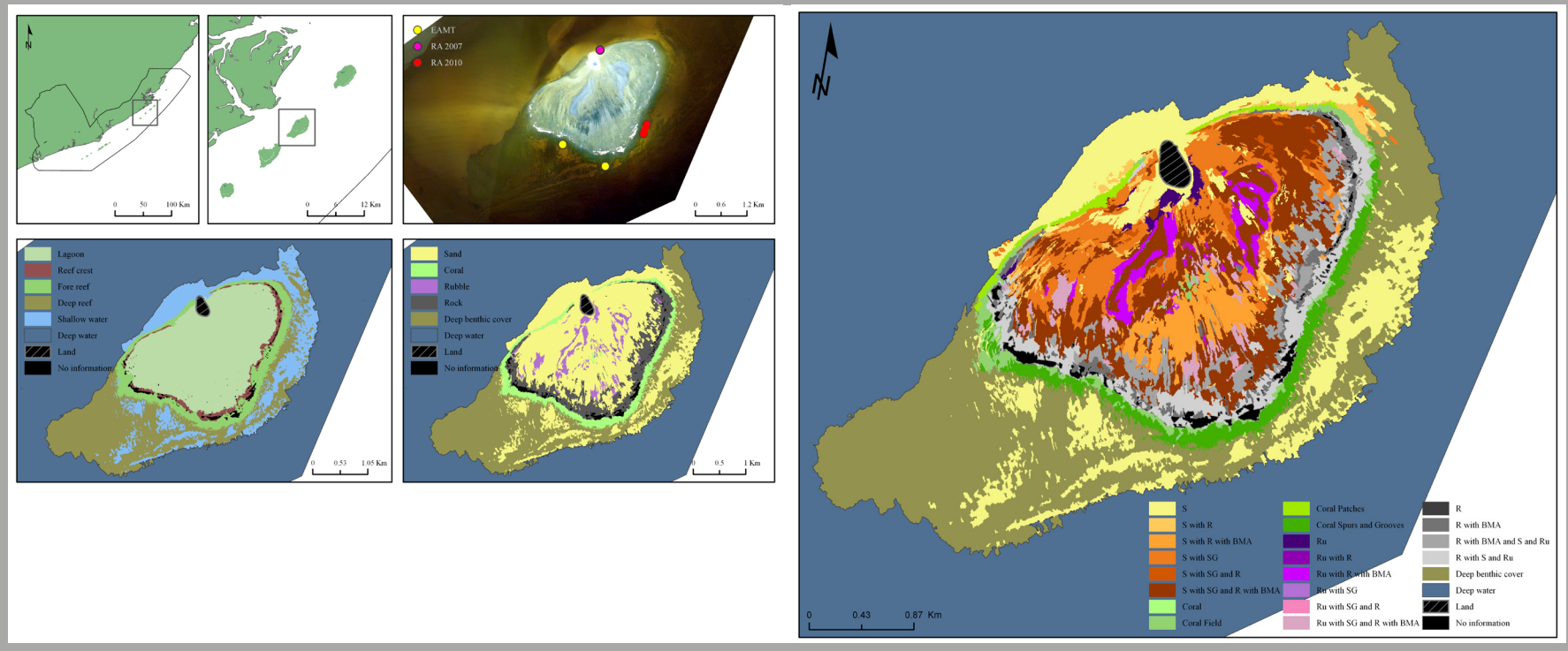


**Figure C.**
Classification results for Casuarina Island, at all three levels of classification.
S = Sand; R = Rock(s), Ru = Rubble; BMA = Brown Macroalgae; SG = Seagrass.

*Mapping habitat extent*

SRS can provide useful information to help map the habitat of particular species, via species distribution or habitat suitability modelling (Bradley *et al.* 2012; **Figure 5.2**). The general idea behind such models is to assess statistical relationships between a species' known occurrence (assessed through presence/absence data) and environmental variables that reflect crucial resources or conditions (such as vegetation productivity) to characterise suitable habitats for that species. SRS-derived variables have been widely used as predictor variables in habitat suitability models (He *et al.* 2015) and SRS-informed habitat maps have been used to identify priority areas such as wildlife corridors for migratory animal species such as elephants (Pittiglio *et al.* 2012); or pandas (Wang *et al.* 2014); areas for translocations (Freemantle *et al.* 2013); and for quantifying the impact of anthropogenic pressures on a species' distribution (Ramírez *et al.* 2014), such as climate change (Forrest *et al.* 2012).

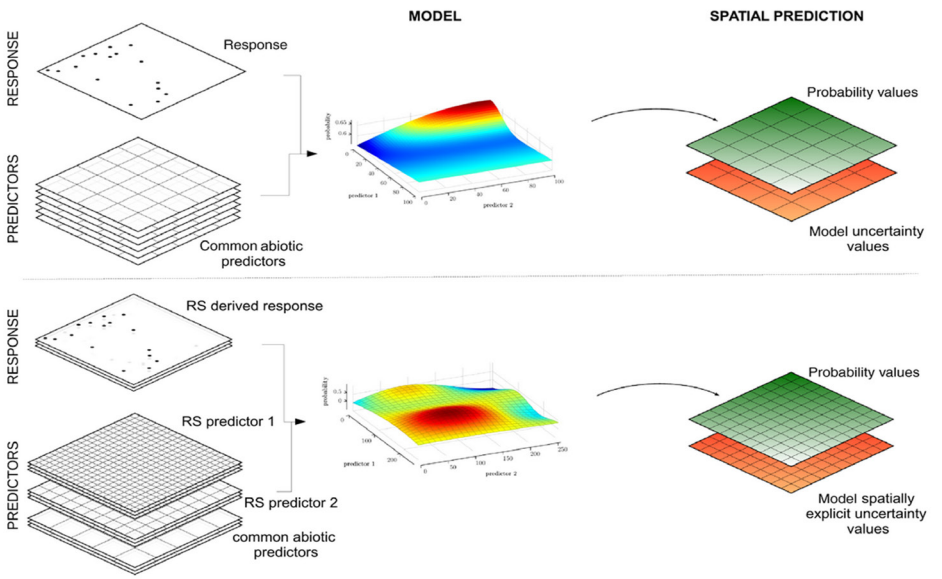


**Figure 5.2.** The concept behind all species distribution models (SDMs) is to use environmental information in the form of geospatial information (layers) to predict the probability of species occurrence (see first row). SRS can be used in two ways to inform SDMs: they can provide information about species occurrence (direct species detection; the response variable), or they can provide information about the environment (such as vegetation type; predictor variable). Habitat mapping using SRS refers to the latter. Direct species detection is discussed in **Chapter 5.4**. Figure from He *et al.* 2015, published under a CC-BY license.

The selection of meaningful SRS-derived variables to inform a given habitat suitability model depends on a robust understanding of the species ecology (Cord & Rödder 2011). For instance, Beck *et al.* (2005) used satellite-derived snow maps, in addition to other variables such as topography to predict suitable habitat for an Arctic dwarf shrub (*Dryas octopetala*) that is known to be absent from sites where it snows. In some cases it may be possible to map key habitat resources directly, such as food (Théau *et al.* 2005). More commonly, however, vegetation productivity, structure and phenology (as indexed, for instance, by the NDVI or the LAI), as well as land cover, are used to model both animal and plant habitat suitability (Kuemmerle *et al.* 2010, 2011; Nagendra *et al.* 2013; Pettorelli 2013; He *et al.* 2015). Imam *et al.* (2009) used NDVI as a proxy for forest density to map the habitat of Bengal tigers, whereas Louzao *et al.* (2011) demonstrated how wandering albatross habitat use could be partially explained by SRS-derived information relating to seascape structure, in this case bathymetric and sea surface temperature. Interestingly, including "raw" SRS data, such as surface reflectance, with no clear biological or ecological meaning has in some instances been shown to improve species distribution models, both for plants (Parviainen *et al.* 2013) and wildlife (St-Louis *et al.* 2014). Information about the three-dimensional structure of habitats as assessed from spaceborne radar sensors is currently rarely used in habitat modelling (airborne LiDAR is more widespread; Vogeler & Cohen 2016) but represents a clear opportunity to gain an even greater understanding of species' requirements in the future.

For both animal as well as plant species, SRS-based species distribution models are a key source of information to identify areas that are vulnerable to invasion, both now and in the future. For instance, Bisrat *et al.* (2012) modelled the habitat of an invasive frog (*Eleutherodactylus coqui*) in its native Puerto Rico, and used this information to predict its potential distribution in Hawaii (where it is invasive. Similarly, Roura-Pascual *et al.* (2004) used SRS-based habitat modelling to identify areas vulnerable to invasion by Argentine fire ants (*Linepithema humile*) worldwide, and Clark *et al.* (2014) used remotely sensed information about vegetation phenology to identify areas along the Appalachian trail (USA) which may be vulnerable to the spread of tree-of-heaven (*Ailanthus altissima*), an invasive shrub, as part of a natural resource management support system.

When modelling the habitat of plant species, there is a chance that SRS-derived environmental variables such as vegetation indices may not be independent from species distribution data. This is for example likely to be the case for overstorey species which are relatively common compared to the pixel size of the imagery used, and could therefore have a distinct impact on the vegetation indices. An example for this would be if the distribution of a forest tree in a fragmented landscape was predicted using the LAI; since forests have higher LAI than cropland, recently deforested areas might be predicted as unsuitable habitat (Bradley *et al.* 2012). However, in cases where a given plant species does not form homogenous stands large enough to impact vegetation indices directly, these indices can be valuable environmental predictors for plant distribution models. Examples include using the NDVI for habitat modelling of neotropical *Rubicae* (Amaral *et al.* 2007) and the LAI for five Amazonian tree species (Saatchi *et al.* 2008).

### 5.2 Ecosystem and habitat condition

Degradation can have negative impacts on biodiversity before conversion takes place (Keith *et al.* 2013), which is why many managers and scientists are interested in ways to monitor changes in ecosystem or habitat condition. Ecological condition can be defined as having three dimensions – structure, composition, and functioning – which can be captured via SRS, mainly using continuous variables such as biomass (a structural parameter), species diversity (a compositional parameter) or vegetation productivity (a functional parameter).

*Structure*

Ecosystem (or habitat) structure has two components: horizontal and vertical (Bergen *et al.* 2009). The horizontal component refers to the spatial configuration of ecosystem or habitat patches in a landscape, and can be quantified via a range of fragmentation indices, including the number of patches, edge length or patch cohesion (Saura 2004; McGarigal 2015). These can all be calculated based on appropriate SRS-derived information. For instance, (Armenteras *et al.* 2003) used maps of forest distribution derived from Landsat TM imagery to quantify forest fragmentation across Colombia. Similarly, Nagendra *et al.* (2008) investigated horizontal landscape structure of forest in Nepal to investigate forest fragmentation under different management regimes. Where SRS imagery with high spatial resolution is available, mapping small canopy gaps (e.g. as a result of selective logging) is possible (De Sy *et al.* 2012). Though long-term field experiments have been invaluable for investigating the outcomes of fragmentation on biodiversity, only SRS is able to provide wall-to-wall views on horizontal ecosystem and habitat structure at the landscape and even global scale (Haddad *et al.* 2015; Riitters *et al.* 2016).

By contrast, vertical structure refers to the vertical arrangement of landscape features, such as vegetation. Active satellite remote sensing (radar and LiDAR) is sensitive to the three-dimensional structure of land cover, and is thus often used to characterise vertical canopy structure. In closed forests, the focus is often on measuring vegetation height, mainly using airborne LiDAR (see Melin *et al.* 2017 for an overview). However, interferometry radar (InSAR) paired with a digital elevation model can also be used to map tree height in forest stands (Solberg *et al.* 2014). Longwave radar (P- and L-band) backscatter is affected by the presence and arrangement of tree trunks and branches (Imhoff 1995), and can be used to map fractional woody vegetation (Urbazaev *et al.* 2015). Radar SRS has emerged as a routine tool for investigating parameters such as aboveground biomass distribution (Sinha *et al.* 2015; Lu *et al.* 2016). Vertical structure can also be estimated from multispectral data; Lefsky (2010) combined MODIS imagery with height information from airborne LiDAR to produce a global forest height map. Finally, the LAI one-sided leaf area per unit ground area (Myneni 1997) is a key vertical structure parameter, sensitive to e.g. seasonal changes in canopy structures in broadleaf forests (Rautiainen *et al.* 2012). SRS imagery can be used to derive LAI at relatively coarse spatial resolution (see **Chapter 3.3**), whereas, for local scale investigations, airborne LiDAR allows estimating LAI at higher spatial resolution (Tang *et al.* 2014).

*Composition*

SRS data has been used to map plant species composition or richness by linking remotely sensed variables to field observations of species composition or richness using empirical models. For instance, Wolter & Townsend (2011) were able to estimate the relative basal area of several tree species in a given pixel by combining multispectral and radar data, essentially mapping forest composition. SRS data has also been used to extrapolate local measurements of tree species richness across the entire Amazon (Saatchi *et al.* 2008) by combining multispectral and radar SRS-derived variables.

*Functioning*

Satellite remote sensing data has large potential to inform large scale, repeated monitoring of a range of ecosystem functions (Pettorelli *et al.* 2017). To date, the focus has been on characterising vegetation productivity as a key ecosystem process. Often, a vegetation index such as the NDVI is used directly as a proxy for productivity, e.g. to characterise changes in phenology over time or differences in productivity in space (Fensholt *et al.* 2015). For instance, NDVI time series are used widely to characterise

degradation of drylands, under the assumption that NDVI declines in areas where vegetation recedes (Higginbottom & Symeonakis 2014). Alternatively, gross and net primary productivity of terrestrial vegetation can be estimated from multispectral SRS data combined with the fraction of photosynthetically active vegetation and vegetation respiration rates (Running *et al.* 2004). Insights into characteristic patterns of productivity (e.g. seasonal phenology) and changes therein can be used to elucidate the environmental drivers behind changes in productivity (Pettorelli *et al.* 2005). In the marine realm, ocean colour (i.e. surface reflectance over the oceans) is a standard tool for monitoring algal blooms, via estimates of chlorophyll-α concentrations (Blondeau-Patissier *et al.* 2014), both in pelagic and the optically more complex coastal waters (Kratzer & Vinterhav 2010; González Taboada & Anadón 2014; Palmer *et al.* 2015). SRS-derived chlorophyll-α concentration also allows modelling marine primary productivity at large spatial scales (Chassot *et al.* 2010).

SRS has moreover become a useful tool for characterizing disturbance regimes at the landscape or even continental scale. For instance, thanks to the sensitivity of mid-infrared wavelengths to water (Frazier *et al.* 2000) it is possible to create flood risk maps by repeatedly mapping surface water extent, e.g. using Landsat imagery (Skakun *et al.* 2014). Floods can also be detected by radar (Gan *et al.* 2012. Long *et al.* 2014) mapped flooding frequency in a remote area in Southern Africa based on a time series of radar images. At a global scale, radar imagery is being used to construct a global record of inundation frequencies (McDonald *et al.* 2011) and a global record of changes in global surface water dynamics was generated from Landsat imagery (Mayaux *et al.* 2013).

Herbivory shapes ecosystem functioning through its effects on primary and secondary productivity (Duffy *et al.* 2003) and nutrient regulation (Piñeiro *et al.* 2010); it is also a mechanism of biological control (Stiling & Cornelissen 2005) and seed dispersal (Nathan *et al.* 2008). The ecosystem-level effects of wild and domesticated herbivores on vegetation can be quantified using vegetation indices such as the NDVI (Blanco *et al.* 2009; Rickbeil *et al.* 2015). To attribute changes in NDVI to herbivores, their effect needs to be separated from the effect of season, precipitation and vegetation type, which is possible if variation in herbivory pressure is known. In large forest stands with continuous canopy cover, the impact of short bursts of defoliating insects can also be tracked, even when using satellite imagery with relatively coarse spatial resolution (Bradley *et al.* 2012). The impact of insects can be distinguished from other disturbances such as fire or logging (Senf *et al.* 2015), although, it can be difficult to reliably quantify outbreak intensity (as opposed to simply distinguishing affected and non-affected area) if intensity varies at small spatial scales compared to the spatial resolution of the imagery used (Eklundh *et al.* 2009).

## BOX D: USING VEGETATION INDICES FOR MONITORING AND UNDERSTANDING ECOSYSTEM FUNCTIONING IN THE ARCTIC

The two previous case studies have illustrated how satellite remote sensing can be used to map ecosystem distribution or changes in ecosystem structure as a result of degradation. SRS data also provide information about ecosystem processes and functions (Pettorelli *et al.* 2017). Vegetation index products (see **Chapter 2.3** and **3.3**) are widely used as proxies for primary productivity and a key resource for large-scale mapping of ecosystem functioning.In this case study, areas of high terrestrial primary productivity were mapped across the Arctic, based on a MODIS NDVI product. This effort is part of WWF's Rapid Assessment of Circum-Arctic Ecosystem Resilience (RACER). The idea underpinning this approach is to map areas of high habitat diversity and productivity, identify the drivers behind them, and estimate the effects of future climate change on these drivers with the aim of appraising present and predicting future ecosystem resilience. Using SRS products is necessary for the "Rapid" aspect of RACER: the routine production of high-level SRS products such as NDVI enables fast assessments of ecosystem condition across large areas. The basis for the ecosystem productivity assessment was the MODIS Global Monthly NDVI, which is distributed as part of the MOD13A3 product. This NDVI product has a spatial resolution of 1km, and is a composite of 16-day NDVI product which is derived from MODIS surface reflectance (Huete *et al.* 2002). All available scenes covering the study area between 2000 and 2010 were downloaded. For each summer (June-August) the maximum NDVI value was calculated in each pixel and the median of these values from 2000 to 2010 was calculated. For each of the five Arctic bioclimatic zones, which are determined based on mean July temperatures and Summer warmth index, as well as distinct vegetation structure (Walker *et al.* 2005), the distribution of NDVI values was generated, and each pixel assigned into a percentile. Lastly, pixels in high percentiles (> 75%) were mapped (see **Figure D**). These maps can then be compared to areas of conservation significance, e.g. Key Bird Habitat Areas, Protected Areas and caribou calving grounds, or used to quantify which types of vegetation contribute the most to overall arctic ecosystem productivity.Mapping current hotspots of ecosystem productivity allows identification of the factors driving productivity in this part of the world. Climate change effects can then be modelled to gauge how productivity may change with varying climatic conditions. This can help identify areas which are at a high risk of losing their ecological resilience, and which should thus be prioritized for conservation.

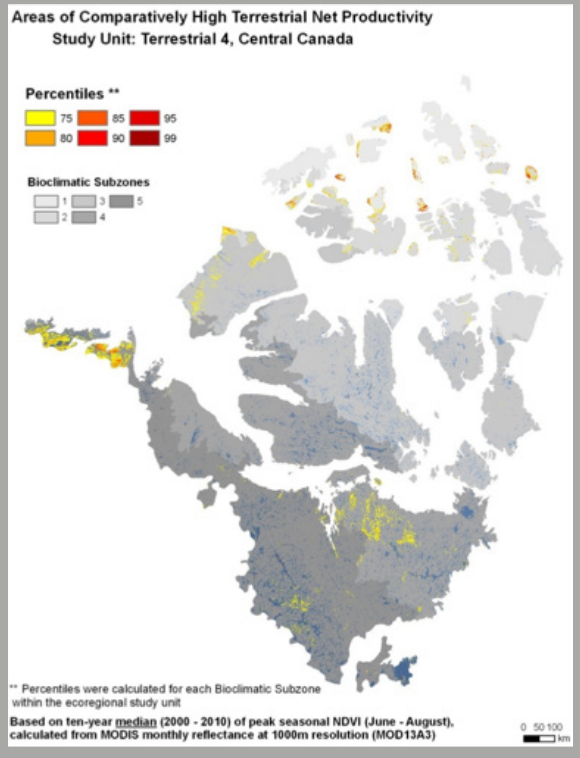


**Figure D.** Results of ecosystem productivity mapping for central Canada. Areas in yellow, orange and red have exceptionally high median NDVI values (2000-2010), which were derived from MODIS Global NDVI. These areas are important hubs of ecosystem productivity in the Arctic.

### 5.3 Threats to biodiversity

As pressures on biodiversity increase (Butchart *et al.* 2010; Venter *et al.* 2016), information about the type, magnitude, and spatio-temporal distribution of threats to biodiversity are necessary to inform management responses (Tulloch *et al.* 2015). SRS has been employed to monitor a wide range of anthropogenic threats which affect species and ecosystems, from climate change to resource extraction, in both terrestrial and marine systems. It provides a means to monitor biodiversity threats at the global scale, and detect changes in threat over time; two aspects which are crucial for informing policy response, yet are often missing from existing datasets on biodiversity threats (Joppa *et al.* 2016).

*Deforestation and forest degradation*

SRS is a routine tool for monitoring deforestation and forest degradation, especially in the tropics, and is expected to be an important data source for an operationalised REDD+ mechanism (Herold & Johns 2007; Romijn *et al.* 2015). Multispectral SRS imagery such as Landsat or MODIS is the most commonly used data source for monitoring deforestation (De Sy *et al.* 2012) at both global (Hansen *et al.* 2013) and regional scales (Potapov *et al.* 2012). Indeed, a range of operational deforestation monitoring programmes are based on multispectral SRS (FORMA in Asia, Africa and South America, PRODES and DETER for the Brazilian Amazon; Wheeler *et al.* 2014; i-Terra for South America and global tropical regions; Leisher *et al.* 2013). Cloud cover can significantly reduce data availability from multispectral sensors in tropical regions, especially during the wet season (Garonna *et al.* 2009). For instance, there is very little chance of acquiring a Landsat image with less than 30% clouds over the Brazilian Amazon during the wet season (Asner 2001). However, Image compositing, which is the creation of a cloud-free image by choosing cloud-free pixels from images acquired at different times, can overcome this problem, at the expense of temporal resolution. Radar data are therefore sometimes used as an alternative to map deforestation (Rahman & Sumantyo 2010), since it is sensitive to differences in canopy volume and vertical structure, and can provide data even under cloudy conditions. Combining multispectral and radar data has been shown to be particularly powerful, increasing both the spatial accuracy and reducing detection lags (Reiche *et al.* 2015a), thereby allowing near real-time detection of deforestation events (Reiche *et al.* 2015b).

SRS is also a key resource to detect subtler forest degradation (De Sy *et al.* 2012), which refers to changes in forest structure, functioning, biomass or composition e.g. as a result of selective logging or disturbance from wildfire. In the context of REDD+, forest degradation generally refers to the loss of carbon stock in forests in the absence of significant forest cover change (Herold *et al.* 2011a). SRS is useful especially for mapping degradation that affects the canopy structure (e.g. forest fragmentation, large fires), rather than subtler changes which may for instance result from firewood collection, understorey thinning or extraction of non-timber products (Herold *et al.* 2011a, b). Examples for SRS-based degradation monitoring include mapping per-pixel canopy gap fractions using Landsat imagery (Asner *et al.* 2004), and using the spatial signature of logging activities (log landings and roads) to distinguish anthropogenic from natural forest degradation (Souza & Roberts 2005; Souza *et al.* 2005). Mapping burn scars and active fires allows monitoring changes in fire dynamics, which is associated with forest degradation e.g. in the Amazon (Miettinen *et al.* 2016; see below). There have also been successful examples of using SRS imagery to monitor the impact of defoliating insects (Gleeson *et al.* 2000; Pasquarella *et al.* 2017). Additionally, some studies have used proxy methods to assess degradation from Landsat or MODIS (Chaplin-Kramer *et al.* 2015; Riitters *et al.* 2016; Shapiro *et al.* 2016; Brinck *et al.* 2017).

*Fire*

Though fire is an important disturbance process in many ecosystems, e.g. savannahs (Lehmann *et al.* 2014; Caillault *et al.* 2015), fire frequency and intensity is altered by humans in many areas as a result of land use change (Bucini & Lambin 2002), with harmful effects on biodiversity. Multispectral as well as SAR have been used to monitor active fires, map burned area, or quantify fuel availability and flammability (see Herawati *et al.* 2015 for a review; see **Appendix** for routinely produced active fire and burned area maps; **Figure 5.3**) sometimes as part of operational fire products, including the MODIS Active Fire products (Giglio *et al.* 2016). These products can be used to characterise fire disturbance at large spatial scales (Hempson *et al.* 2017), to understand their drivers (Mollicone *et al.* 2006; Hantson *et al.* 2015).

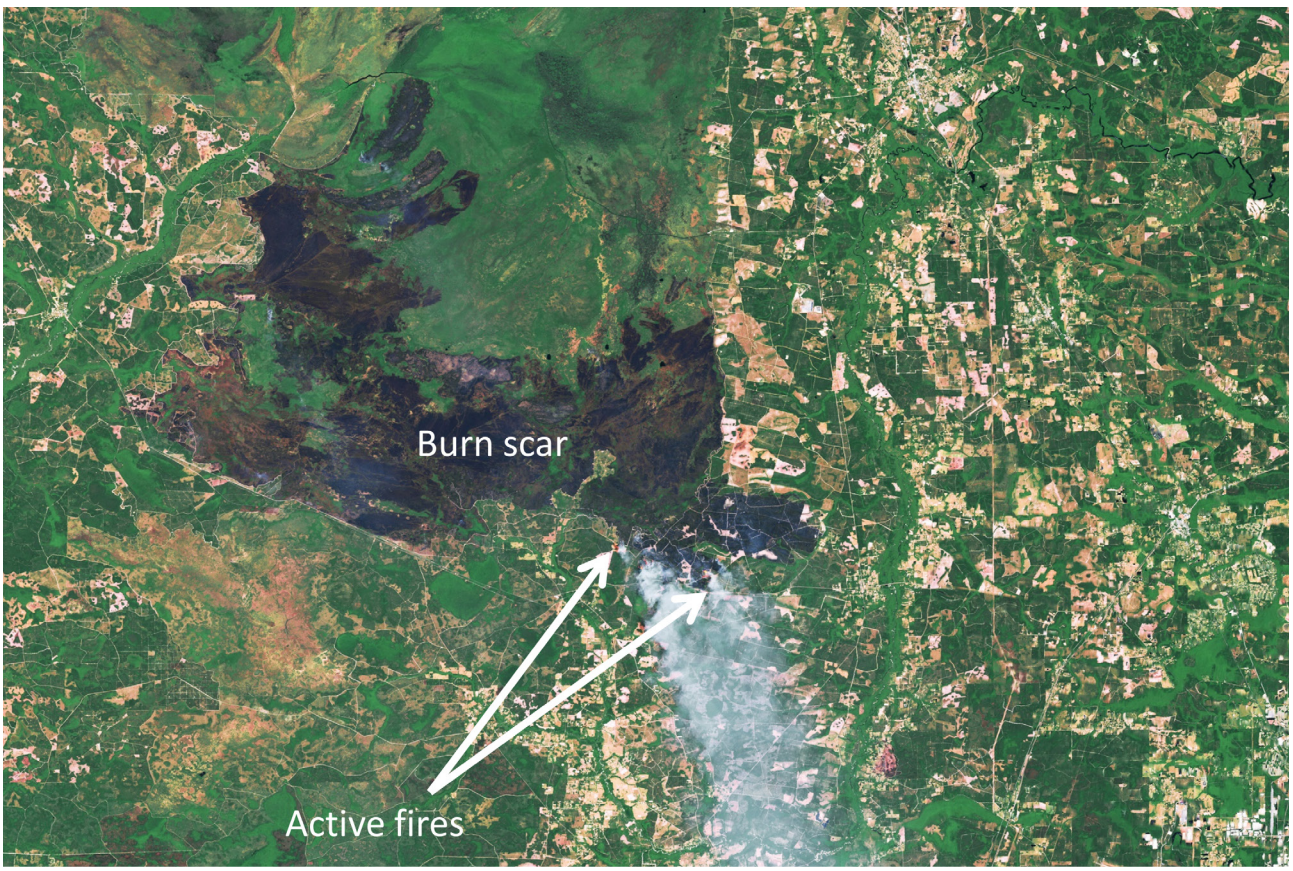


**Figure 5.3.** Active fire and burn scars in the Okefenokee National Wildlife Refuge in the United States. Active fires can be detected from space from their high temperature using thermal bands of multispectral sensors. Burn scars can be detected by multispectral sensor as well as radar sensors from the change in surface structure (e.g. loss of vegetation), and their darker colour (multispectral sensors only). Image credits: NASA Earth Observatory image by Joshua Stevens, using Landsat data from the U.S. Geological Survey.

*Climate change*

SRS data have provided independent records of the effects of global climate change, from increasing sea and tropospheric temperatures, retreating snow cover as well as land and sea ice cover, to global sea level rise (Shirley *et al.* 2013). SRS has also informed models of temperatures in permafrost soil (Langer *et al.* 2013), an important reservoir of carbon susceptible to release with increasing temperatures (Schuur *et al.* 2009). In the context of biodiversity conservation, SRS allows monitoring and predicting the impact of climate change on species and ecosystems. Shifts in species' phenology and distribution, as well as extinction, in response to climate change have been observed globally (Parmesan 2006). Information from SRS can help predict the effects of climate change on a given species via SRS-based projections of future habitat change (Singh & Milner-Gulland 2011). At the ecosystem level, climate change can be expected to affect structural, compositional and functional aspects, and SRS can provide insight into the impact of climate change on these aspects. For instance, radar SRS imagery can be used to map coastal retreat to gauge threats from sea level rise to low–lying ecosystems, such as marshes and mangrove forests (Cornforth *et al.* 2013; Kirwan & Megonigal 2013). Vegetation indices enable large-scale monitoring of primary productivity, making it possible to track the impact of climate change on this key ecosystem process, e.g. the use of NDVI to monitor large-scale changes in vegetation productivity and phenology in response to changing precipitation regimes (de Jong *et al.* 2011; Pettorelli *et al.* 2012).

Apart from gradual changes, climate change is likely to affect the frequency and intensity of extreme events such as heat waves, heavy rains, droughts, extreme coastal high water (Intergovernmental Panel on Climate Change (IPCC) 2012), and fires. Such extreme events can impact biodiversity (Ameca y Juárez *et al.* 2012), since their intensities and frequencies are (by definition) different from common disturbance processes in a given ecosystem, exhausting adaptive capacity (Jentsch & Beierkuhnlein 2008). In the marine realm, SRS imagery is a key tool for monitoring coral reef bleaching events (Liu *et al.* 2003); the United States National Oceanic and Atmospheric Administration's Coral Reef Watch integrates SRS data from different sensors to detect extreme thermal conditions (Liu *et al.* 2014). In the terrestrial realm, droughts can be detected using SRS-derived information on precipitation, soil moisture and evapotranspiration, and their effect on vegetation can be monitored via the NDVI (or NDWI) and derived indices, and land surface temperature (AghaKouchak *et al.* 2015), which has also been used to derive a continental map of drought probability for Africa (Rojas *et al.* 2011).

NOAA Coral Reef Watch
https://coralreefwatch.noaa.gov/satellite/index.php

*Atmospheric and water pollution*

Atmospheric nitrogen deposition can have negative consequences for plant biodiversity, both via direct toxic effects (Pearson & Stewart 1993) or via indirect effects such as increasing susceptibility to pathogens and herbivores (Nordin *et al.* 2005). The source of this pollution – nitrous oxides – can be detected by multispectral and UV SRS imagery, for example from the Ozone Monitoring Instrument (Beirle *et al.* 2011; Schaap *et al.* 2013). There is evidence that cloud cover tends to be higher when there is more nitrous oxide in the air, potentially resulting in underestimation of this pollutant when measured by multispectral SRS (Geddes *et al.* 2012).

In the marine realm, SRS provides timely information about the extent, type and movement of oil spills, which can have significant negative consequences for affected ecosystems (Beyer *et al.* 2016). Thin layers of oil produce glint, whereas thick layers emit radiation at high wavelengths, both of which can be detected by optical SRS. In addition, the oil layer dampens waves, reducing sea roughness, which can be picked up by radar (Klemas 2011). Both types of SRS were important to informing the response to the British

Petroleum Deepwater Horizon spill (Leifer *et al.* 2012): MODIS and MERIS imagery were used to map the oil field's extent and its change over time, and AVIRIS was useful in characterizing the thickness of the oil field.

In both freshwater and marine ecosystems, SRS data have been used to monitor eutrophication of coastal waters via a range of indices, including chlorophyll-α, Secchi Disk Depth and/or coloured dissolved organic matter mapped based on ocean colour imagery (Matthews *et al.* 2010; Zhu *et al.* 2014; Harvey *et al.* 2015). Additionally, blooms of certain toxic algae can be detected from space, such as *Karena brevis*, which causes harmful "red tides" along the West Coast of Florida (Carvalho *et al.* 2010).

*Urbanisation and agricultural expansion*

Urban and agricultural areas are often easily distinguishable in SRS imagery because of their distinct land cover composition, including bare soil, short vegetation and impervious surfaces. Impervious surfaces in particular have a strong effect on surface reflectance (compared to water, vegetation or bare soil), allowing them to be accurately mapped using vegetation indices (Sawaya *et al.* 2003), or their reflectance in the visible spectrum (Taubenböck *et al.* 2012). Urban areas can also be monitored via artificial night light emissions, which can be detected by optical sensors that are very sensitive in the visible spectrum. For instance, the VIIRS/DNB sensor can detect light emitted from a single street lamp (Miller *et al.* 2013). Night time light has been used to investigate patterns of urban expansion and population growth (Álvarez-Berríos *et al.* 2013).

Multispectral imagery with high and medium spatial resolution is commonly used to map agricultural areas at local or regional scales (Schulte to Bühne *et al.* 2017; **Figure 5.4**). To distinguish between similar types of agricultural land use (such as different crop or management types), a combination of optical and radar SRS data is often useful (Joshi *et al.* 2016). Especially in tropical forests, ecosystems are often not replaced by cropland or settlements, but rather by plantations, such as oil palm (in Southeast Asia and Africa) and rubber. Plantations are structurally more similar to forests than other anthropogenic land use types (e.g. they have tall canopies), but they have characteristics that enable them to be distinguished via SRS (such as regular spacing of trees and homogenous canopy height). For instance, L-band radar imagery (e.g. ALOS PALSAR), which interacts with branches and foliage below the canopy, has been used to distinguish oil palm from primary or logged forest (Koh *et al.* 2011; Morel *et al.* 2011). In cases where cloud cover is low enough, multispectral imagery has been used instead, mapping phenological differences between plantations and primary forest (Dong *et al.* 2013; Li *et al.* 2015). Human land use not only causes immediate changes to vegetation structure and composition – such as a shift from a multi-layered, multispecies forest canopy to single-layer, monospecific cropland – but can also lead to long-term changes in processes such as desertification and soil degradation. Here, too, SRS offers monitoring opportunities: the NDVI has for example been widely used to assess desertification, although validation of this approach has been limited (Higginbottom & Symeonakis 2014), and soil parameters (e.g. pH or grain size) have been mapped at continental scales based on MODIS imagery and a network of in situ measurements (Vågen *et al.* 2016).

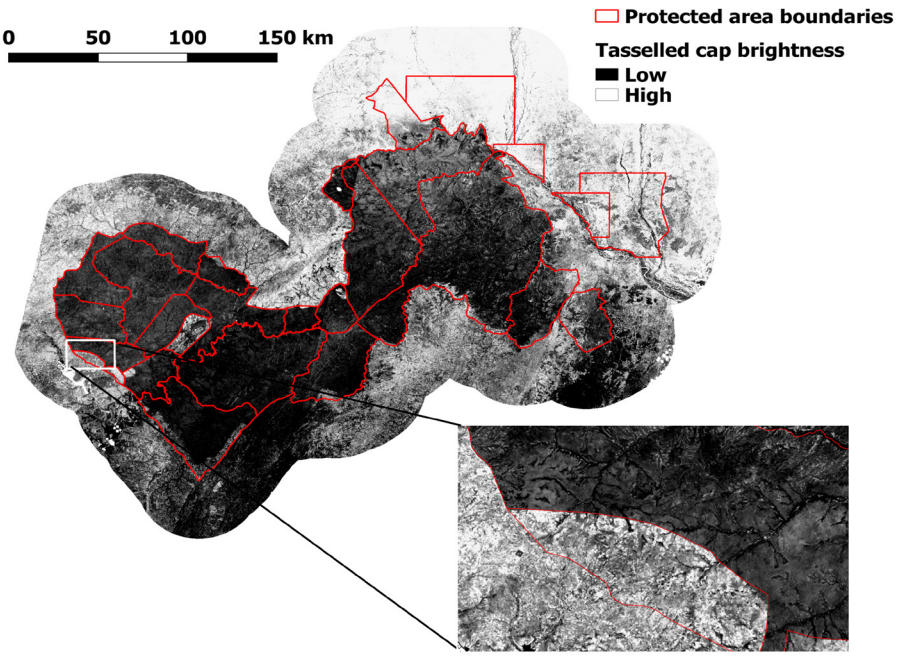


**Figure 5.4.** Contrasting tasselled cap brightness between cropland (light) and savannah vegetation (dark) across the entire W-Arly-Pendjari transboundary protected area complex (West Africa). The zoomed in area shows how the Tindangou-Nadiagou Enclave in Burkina Faso has been cleared for agriculture, while the Pama Centre Sud hunting zone (also in Burkina Faso) was not. Imagery: Landsat 8 from USGS, September-October 2013.

*Oil exploration and mining activities*

Oil exploration and mining can have harmful effects on biodiversity, resulting in habitat and ecosystem loss (Simmons *et al.* 2008; Deikumah *et al.* 2014; Stabach *et al.* 2017), increased human-wildlife conflict and poaching (Suárez *et al.* 2009), as well as pollution (Dudka & Adriano 1997; Akani *et al.* 2004). Surface mining for minerals or coal results in drastic land cover change (e.g. deforestation), which is detected by SRS imagery (Townsend *et al.* 2009; Swenson *et al.* 2011; Álvarez-Berrios & Mitchell Aide 2015). Importantly, clandestine, small-scale mining operations can be detected using SRS imagery with high spatial resolution (30 m) by mapping sub-pixel vegetation cover (Asner *et al.* 2013). Oil plants are much less spatially extensive, but they can be detected by finding oil flares, which have high infrared reflectance (Casadio *et al.* 2012). For instance, burning oil fields in the Persian Gulf region can be identified by their high infrared reflectance as detected by the AVHRR sensor (Matson & Dozier 1981). The MODIS active fire product was built to monitor vegetation fires, but can also detect these flares (Oom & Pereira 2012). Alternatively, Landsat imagery has been used to identify previously unknown oil plants on a regional scale (Duncan *et al.* 2014) and detect plumes from oil fires (Cahalan 1992). It might also be possible to identify oil exploration activities by mapping associated infrastructure, especially in desert ecosystems, using radar SRS (Felbier *et al.* 2012); however, this approach would requires an additional processing step to distinguish oil extraction from other infrastructure, e.g. settlements (Duncan *et al.* 2014).

*Illegal fishing*

Both optical and radar imagery have been used for decades to detect ships (Corbane *et al.* 2010; Brusch *et al.* 2011), which can aid MPA management by detecting potential fishing vessels (Kachelriess *et al.* 2014). The size of the smallest ship that can be distinguished is constrained by the spatial resolution of the SRS imagery (ca. 100 m for Landsat, ca. 5 m for SPOT-5). Corbane *et al.* (2010) identified ships from SPOT-5 imagery by first screening the imagery for very bright but small objects (potential ships), and then reducing the number of false positives by taking into account context (e.g. discarding high wave crests that are erroneously identified as ships), using a completely unsupervised image analysis process. However, even though true ships were reliably detected, the false positive rate was several orders of magnitude higher than true positives. Interestingly, Trujillo *et al.* (2012) demonstrated that imagery with very high spatial resolution from Google Earth can be used to detect fish cages across large spatial scales. This does not systematically constitute illegal fishing, but it is necessary to accurately estimate farmed fish production for good resource use.

### 5.4 Monitoring individual species

In contrast to ecosystem and habitat mapping for a particular species (He *et al.* 2015; **Chapter 5.1**), or threat detection, SRS data are also sometimes used to detect individual species (**Table 5.2**), and a growing number of cases studies are determining whether it is possible to count individual animals or map homogenous stands or species richness (for plants and phytoplankton) from space. In this chapter, we give an overview of examples where SRS data have been used to detect or map species directly.

**Table 5.2.** Overview of ecosystem distribution mapping of different ecosystem types.

| REFERENCE | FOCAL SPECIES | SRS DATA USED | SPATIAL RESOLUTION | DETECTION METHOD | VALIDATION DATA |
|---|---|---|---|---|---|
| ANIMALS | | | | | |
| Laliberte & Ripple (2003) | Domestic cattle (*Bos taurus*) | IKONOS | 1 m | Thresholding | Manual screening of imagery |
| LaRue *et al.* (2011). | Weddle Seals (*Leptonychotes weddellii*) | QuickBird2, WorldView-1 | 0.6 m | Manual screening of imagery | Ground counts |
| Fretwell *et al.* (2012) | Emperor penguins (*Aptenodytes fosteri*) | QuickBird2 | 0.6 m | Supervised classification | None |
| Platonov *et al.* (2013) | Polar bears (*Ursus maritimus*) | Geo-Eye | 0.5 m | Manual screening of imagery | None |
| Fretwell *et al.* (2014) | Southern Right Whale (*Eubalaena australis*) | WorldView-2 | 0.5 m | Thresholding | Manual screening of imagery |
| Stapleton *et al.* (2014) | Polar bears (*Ursus maritimus*) | WorldView-2, QuickBird | 0.5 – 0.65 m | Manual screening of imagery | Aerial survey |
| Yang *et al.* 2014 | Wildebeest (*Connochaetes spp.*), Burchell's zebras (*Equus quagga burchelli*) | GeoEye-1 | 0.5 m | Supervised classification and thresholding | Manual screening of imagery |

| REFERENCE | FOCAL SPECIES | SRS DATA USED | SPATIAL RESOLUTION | DETECTION METHOD | VALIDATION DATA |
|---|---|---|---|---|---|
| PLANTS (TERRESTRIAL) AND PHYTOPLANKTON (MARINE) | | | | | |
| Alvain *et al.* (2005) | Phytoplankton (haptophytes, Prochlorococcus, Synechococcus-like cyanobacteria, diatoms) | SeaWiFs | 9 km | Look-up table of spectral characteristics of pigments | Qualitative comparison with in situ sampling |
| Bradley & Mustard (2006) | Cheatgrass (*Bromus tectorum*) | Landsat | 30 m | Thresholding | In situ observations |
| Raitsos *et al.* (2008) | Phytoplankton (diatoms, dinoflagellates, coccolithophores, silicoflagellates) | SeaWiFS, AVHRR, QuickSCAT, ERS-2 | 4 – 50 km | Machine learning algorithm | In situ observations |
| Tuanmu *et al.* (2010) | Arrow bamboo (*Bashania faberi*), umbrella bamboo (*Fargesia robusta*) | MODIS | 250 m | Maxent model based on NDVI | In situ observations |
| Hoyos *et al.* (2010) | Glossy Privet (*Ligustrum lucidum*) | Landsat | 30 m | Machine learning algorithm | In situ observations |
| Gavier-Pizarro *et al.* (2012) | Glossy Privet (*Ligustrum lucidum*) | Landsat | 30 m | Machine learning algorithm | In situ observations; observations from SRS imagery with very high spatial resolution |
| Ghulam *et al.* (2014) | Guava (*Psidium cattleianum*), Madagascar cardamom (*Aframomum angustifolium*), Molucca raspberry (*Rubus moluccanus*) | Landsat, Hyperion, Geoeye-1, IKONOS; RADARSAT-2; ALOS PALSAR | 0.5 – 30 m | Machine learning algorithm | In situ observations |

*Wildlife*

Counting wildlife via SRS can be a valuable alternative or complement to field-based approaches, especially where a population of interest is distributed across a large and/or inaccessible area, there is limited vegetation and clouds that hamper the view, and animals stand out clearly against the background (for example snow or dark, short vegetation; Fretwell *et al.* 2012; Yang *et al.* 2014). Indeed, there are many successful examples from the Arctic or Antarctica (LaRue *et al.* 2011; Fretwell *et al.* 2012; Stapleton *et al.* 2014) where these kinds of conditions prevail. Whereas SRS is mainly used to count terrestrial animals, mapping marine animals is possible when they come close enough to the surface to be visible (e.g. for breathing or hunting), since SRS sensors normally do not penetrate the water column very deeply. For instance, Fretwell *et al.* (2014) were able to detect Southern Right Whales (ca. 16 m in length) in Golfo Nuevo Bay using multispectral imagery.

SRS data with very high spatial resolution (typically < 1 m) is necessary to be able to distinguish individuals with a length of at least 1-2 m from their background (**Figure 5.5**; He *et al.* 2015). Despite the growing availability of imagery with very high spatial resolution,

most of these data are only available from commercial providers (which means costs can be considerable), and data coverage may be limited or only available for small footprints (see **Chapter 3.1**). As a result, the area across which animals are counted is typically limited, with notable exceptions from the Antarctic coastline (Fretwell *et al.* 2012) and one exploiting imagery from different years to monitor changes in animal numbers (LaRue *et al.* 2011).

There are two main approaches to counting animal individuals using SRS imagery with very high spatial resolution. Imagery can either be screened manually in a GIS environment (LaRue *et al.* 2011; Stapleton *et al.* 2014), which is useful if the population of interest is small and/or individuals occur in clusters. Manual methods however, can be time-consuming (Platonov *et al.* 2013). Alternatively, individuals can be detected automatically, either by setting manual thresholds to distinguish (bright) individuals from the (darker) background (Press & Laliberte 2003; Fretwell *et al.* 2014) or via supervised classification algorithms or machine learning techniques (Fretwell *et al.* 2012; Yang *et al.* 2014).

Counts from such automated approaches should be validated where possible, for instance using aerial imagery (Fretwell *et al.* 2012; Stapleton *et al.* 2014) or ground counts (LaRue *et al.* 2011). However, especially for highly mobile species, validation imagery must be acquired very close in time the counts, which can be difficult. As a result, many case studies use manual counts on the same imagery used for automated methods for validation instead (Fretwell *et al.* 2014; Yang *et al.* 2014). As the availability of SRS data with very high spatial resolution will increase with the new SmallSats/CubeSats and other missions (see **Chapter 6**), data cost and availability of appropriate validation data will remain among the main challenges to monitoring animal species using SRS at large spatial and temporal scales.

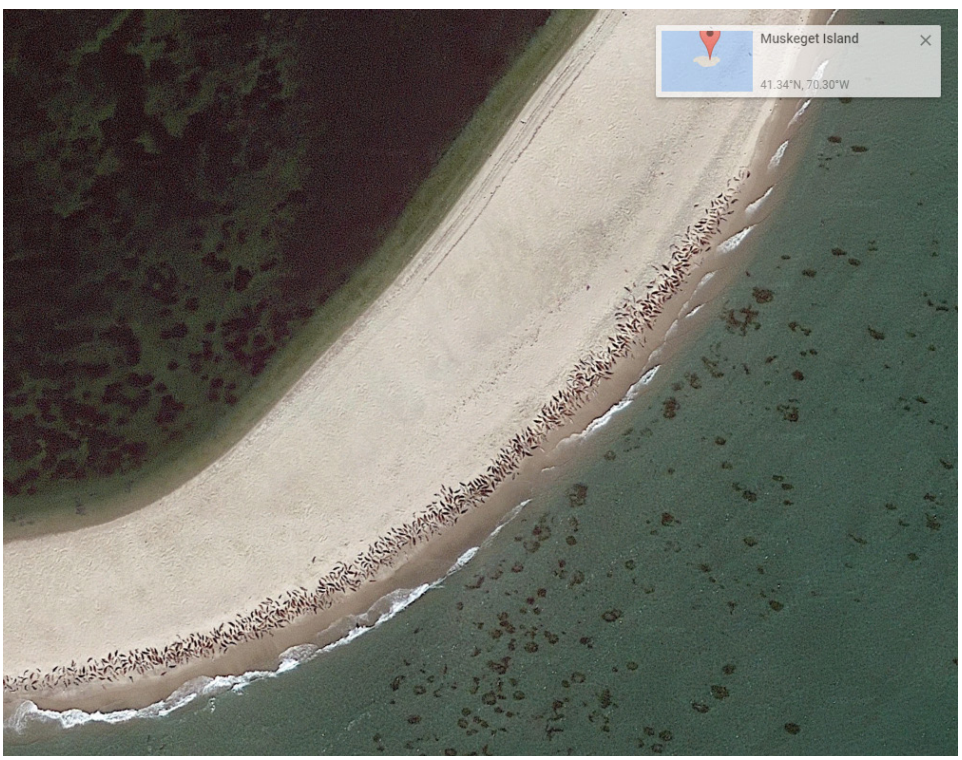


**Figure 5.5.** Google Earth imagery (with very high spatial resolution) depicting seals resting on a beach.

*Plants and phytoplankton*

Multispectral SRS imagery is able to directly detect plant species that form large, spectrally or structurally distinct stands compared to surrounding species, as indicated by vegetation indices (Pettorelli 2013; **Figure 5.6**). A common application of plant species detection from space is the detection of invasive species, which often form such stands. For instance, Glossy Privet (*Ligustrum lucidum*), an invasive tree in Latin American forests, has been mapped with > 80% accuracy using Landsat, making it possible to assess its impact on forest structure and biodiversity (Hoyos *et al.* 2010; Gavier-Pizarro *et al.* 2012).

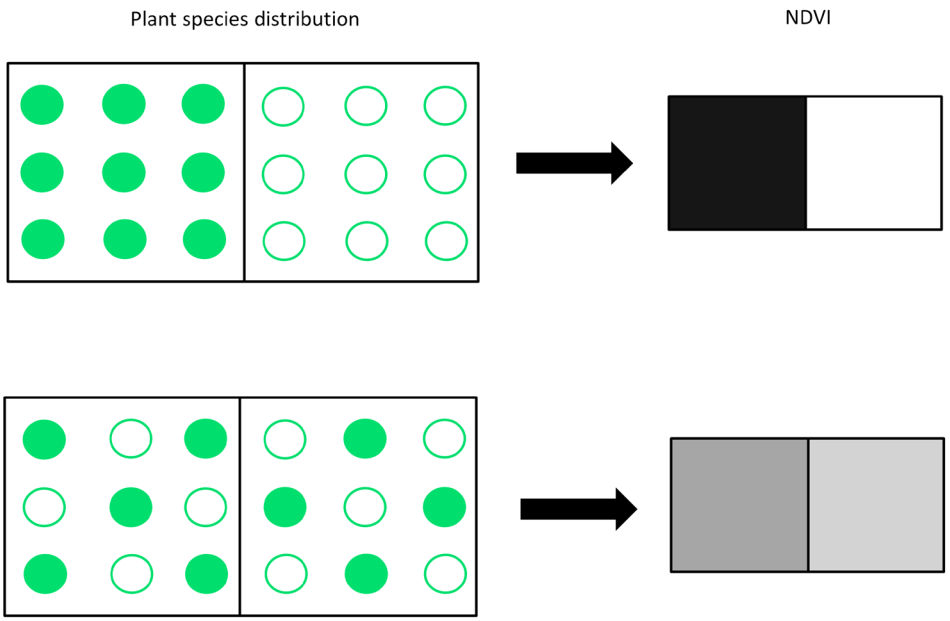


**Figure 5.6.** Plant species can be detected if they dominate the phenological or spectral signal of different pixels (A). In a mixed canopy, the phenological or spectral signal will be a mixture of different species, making detection more difficult (B).

A distinct phenological "signature" compared to the surrounding vegetation is required to be able to map single plant species. For instance Bradley & Mustard (2006) took advantage of the fact that invasive cheatgrass (*Bromus tectorum*) (1) reaches peak greenness earlier during the growing season, and declines earlier and faster, than native species, and (2) that during wet years, cheatgrass greenness is much higher than in dry years, whereas native species show little response. By comparing NDVI derived from Landsat imagery from early and late in the same growing season, and between dry and wet years, they mapped its spread through the Great Basin (USA). Plant species can even be detected in the understory of forests if their phenology stands out. For instance, Tuanmu *et al.* (2010) were able to map two bamboo species in the understory of a forest using a vegetation index similar to NDVI, largely because, compared to other understorey species, bamboo had quite high biomass (which resulted in overall higher NDVI values) and distinct phenology (which resulted in a larger amplitude in NDVI changes over time). Similarly, Wilfong *et al.* (2009) used NDVI to map the invasive Amur honeysuckle (*Lonicera maackii*) underneath deciduous trees, based on the observation that

honeysuckle still had green leaves (i.e. higher NDVI) late in the growing season, when the overstory vegetation had largely senesced. By contrast, Ghulam *et al.* (2014) capitalised on the ability of longwave radar to penetrate the canopy to map several invasive understory species in a tropical rainforest.

In the marine realm, ocean colour (i.e. ocean surface reflectance) has been used to map phytoplankton groups based on in situ information about the spectral properties of different phytoplankton pigments (Alvain *et al.* 2005). Alternatively, ocean colour has been combined with other SRS-derived information (such as sea surface temperature and wind stress) to distinguish between functional types of phytoplankton with an accuracy of 80-93% (Raitsos *et al.* 2008).

Mapping single plant species from space is an active research field, which is likely going to benefit from the growing availability of open-access radar imagery, which can help distinguish different growth forms (Hong *et al.* 2014). Additionally, the advent of hyperspectral spaceborne sensors (e.g. EnMAP, HyspIRI, PRISMA) should facilitate the identification of single species in mixed canopies, because these sensors are able to resolve subtle spectral differences resulting from differences in leaf chemistry and physiology (He *et al.* 2011; see also **Chapter 6**).

A mixed agricultural landscape and newly planted trees comprise this landscape in the Philippines as seen by DigitalGlobe's Worldview-02 satellite on August 1, 2012.

# 6 ADVANCED SATELLITE REMOTE SENSING DATA AND APPLICATIONS

## HIGHLIGHTS

- Recent developments in Light detection and ranging (LiDAR), hyperspectral satellite remote sensing, smaller and cheaper satellite platforms, and Big Data analytical ability have greatly expanded remote sensing horizons.
- Space-borne LiDAR has been used to estimate aboveground biomass and ecosystem structure, and two new missions will soon be providing opportunities to support ecological research and environmental management.
- The higher spectral resolution of hyperspectral remote sensing data, relative to multispectral, provides opportunities for monitoring ecosystem functions such as resilience to disturbances by defoliating insects and fire, and the mapping of plant species from space.
- The new CubeSats and SmallSats are small (< 10 and < 250 kg respectively), relatively inexpensive satellites. They are released in large fleets rather than singly, enabling the daily collection of imagery of the entire Earth's surface.
- Improvements in hardware processing power enable increasingly sophisticated and complex analyses of and integrations of remotely sensed datasets.

To this point, the focus of this guide has been on summarizing applications of multispectral and radar SRS, which are well-established tools in ecology and conservation, each associated with open-access, global data sets such NASA's Landsat and MODIS and ESA's Sentinel suite of satellites. To provide a more complete picture of SRS capabilities, this chapter provides an overview of data types and applications that represent more recent opportunities for SRS to inform biodiversity monitoring and conservation, including LiDAR and hyperspectral remote sensing (**Chapter 6.1**), CubeSats and SmallSats (**Chapter 6.2**) and Big Data analysis (**Chapter 6.3**).

### 6.1 LiDAR and hyperspectral remote sensing

In an ecological context, LiDAR has been mainly used to map aspects of vertical vegetation structure, such as vegetation height (Wulder *et al.* 2012b), with applications that include estimating aboveground biomass (Asner *et al.* 2012; Xu *et al.* 2017), and investigating terrestrial (Vierling *et al.* 2008) and coastal (Pe'eri *et al.* 2011) ecosystem structure. Whereas the ICESat satellite did collect global LiDAR data between 2003 and 2009 (data was only acquired during 6 months of each year: February, March, May, June, October and November; Lee *et al.* 2011), there is currently no active spaceborne platform collecting such data. However, two new missions are being planned – namely GEDI (Patterson & Healey 2015) and ICESat-2 (Brown *et al.* 2016) – which would increase our capability to map aboveground biomass, vegetation height as well as ice dynamics at global scales. Interested readers are referred to (Melin *et al.* 2017) who have reviewed the LiDAR technology and applications in more detail.

Hyperspectral remote sensing gives a more nuanced view of surface structure and chemical composition than multispectral remote sensing because it has a much higher spectral resolution (Chambers *et al.* 2007). It provides novel avenues for monitoring ecosystem

functions (Pettorelli *et al.* 2017), such as disturbance by defoliating insects (Fassnacht *et al.* 2014) and net primary productivity (Ollinger & Smith 2005). There is currently no spaceborne hyperspectral sensor (after Hyperion was deactivated in 2017), but there are three upcoming missions – Environmental Mapping and Analysis Program (EnMAP), the Hyperspectral Infrared Imager (HyspIRI), and the Hyperspectral Precursor of the Application Mission (PRISMA) – which are aimed at expanding our ability to monitor terrestrial and aquatic ecosystem condition and dynamics from space (Guanter *et al.* 2015). Airborne hyperspectral remote sensing has been demonstrated to be sensitive to subtle, species-specific variation in canopy spectra, and can be used to map plant species directly (He *et al.* 2011; Prospere *et al.* 2014), thereby likely allowing the mapping of individual plant species from space. A particularly exciting consequence of the increased spectral resolution could be the ability to capture genetic diversity of plant species from space (Madritch *et al.* 2014).

### 6.2 Novel platforms: CubeSats and SmallSats

CubeSats and SmallSats are both types of small, relatively inexpensive satellites (**Figure 6.1**) – SmallSats typically weigh below 250 kg (Richardson *et al.* 2015), whereas CubeSats weigh less, and even sometimes much less than 10 kg (Marvin *et al.* 2016). For reference, Landsat 8 and Sentinel 1 weigh ca. 1500 kg and 2,200 kg respectively. The know-how of putting all the technology necessary for a functioning satellite in such a small a space is relatively new, with the first CubeSat design dating from 1999 (Richardson *et al.* 2015). They typically carry multispectral sensors with a limited number of bands, but high spatial resolutions, which allows true colour imaging at sub-meter resolution, as well as generating vegetation indices such as NDVI (Marvin *et al.* 2016). Because these mini-satellites are much cheaper to produce than their larger cousins, releasing a large fleet is more economically feasible. As a consequence, some companies have launched constellations of small satellites with the aim to provide daily imagery of the entire Earth's surface (e.g. Planet's SkySat; Marvin *et al.* 2016). Such SRS imagery might contribute to mapping patchy or highly dynamic ecosystems and habitats, as well as large animal species, due to their very high spatial and temporal resolution (Traganos *et al.* 2017).

**Figure 6.1.** Three CubeSats in orbit as seen from the International Space Station.

## BOX E: USING BIG DATA FOR CHANGE DETECTION FOR MONITORING LAND DEGRADATION IN KAZA

Land cover change, from conversion (e.g. clearing all vegetation for human settlements) to more subtle degradation (removal of large trees), is a major driver of species habitat loss and fragmentation (Green *et al.* 1998b) and threatens biodiversity worldwide (Sala *et al.* 2000; Fahrig 2003). This case study, carried out by Wageningen University, in collaboration with WWF and Peace Parks Foundation, used a time series analysis of SRS data to map anthropogenic land degradation in a dynamic savannah ecosystem, specifically the Kavango Zambezi Transfrontier Conservation Area (KAZA TFCA). A dedicated cloud computing platform was implemented to process the required amount of SRS data, owing to 1) the size of KAZA TFCA (covering portions of five different Southern African countries) and 2) the length of the time series (ca. 30 years, with several images per year).

Anthropogenic land cover conversion and degradation was detected based on the principle that such changes result in a sudden and persistent reduction in green vegetation. This contrasts with seasonal changes in vegetation, which are not persistent, or longer term changes due to altered climate, which are more gradual. Sudden and persistent shifts in vegetation were detected via the Breaks For Additive Seasonal and Trend (BFAST) Monitor algorithm. This algorithm detects linear trends and seasonal changes in a time series, and separates them from residual changes, and is available in the R package "bfast" (Verbesselt *et al.* 2010). The magnitude and timing of the residual changes can then be used to detect sudden, persistent changes in land cover that are associated with degradation.

To map land degradation across the KAZA TFCA, all available Landsat 4/5 TM, 7 ETM+ and 8 OLI/TIRS available from EarthExplorer (http://earthexplorer.usgs.gov/) were identified. This corresponds to imagery across 40 adjacent scenes between 1982, the date when Landsat 4 TM was launched, and 2016. Only Level-1T scenes were chosen because they have the highest possible geodetic accuracy, having been georeferenced and terrain corrected using Ground Control Points and a digital elevation model. As a result, a majority of scenes have sub-pixel geometric accuracy. This is crucial for time series analysis, to ensure any detected change is a result of change on the ground, and not changes in sensor view. Other geometric processing levels (1GT and 1GS) are frequently not precise enough for time series analysis without aligning the imagery manually (i.e. additional co-registration). There were, on average, 304 images per scenes available at Level-1T between 1982 and 2016, though this varied across the study site.

The scenes were atmospherically corrected using the Landsat Ecosystem Disturbance Adaptive Processing System LEDAPS (Schmidt *et al.* 2013; USGS 2017a) for Landsat 4-7 and the Landsat Surface Reflectance Code (LaSRC) for Landsat 8 (USGS 2017b). This correction is carried out on demand whenever atmospherically corrected scenes ("Collection 1 Higher-Level") are ordered through EarthExplorer. The data are made available when processing is complete, and were downloaded to a cloud server via USGS' Bulk Download Application. Further processing and analysis was carried out on this server because of the large amount of data using the programming language IDL (Interactive Data language) which is widely used for remote sensing data processing. However, the land degradation detection process was implemented later in R.

First, clouds and cloud shadows were removed using a quality layer that is distributed as part of the surface reflectance product. The quality layer is generated by the CFmask algorithm (USGS 2017a), and flags pixels which contain clouds, cloud shadows, water and snow. To minimize the amount of cloud contamination, a three-pixel buffer was removed around any cloud or cloud shadow pixel. This approach does not remove all atmospheric noise, but is sufficient to ensure that the BFAST algorithm can work. Based on the original spectral bands, the Normalized Difference Fraction Index (NDFI) was calculated for each scene. This index is based on the fraction of green vegetation, non-

photosynthetically active vegetation, soil, and shade for each pixel, which is generated from a spectral unmixing algorithm (Souza *et al.* 2005). The benefit of this approach is that, unlike the NDVI or other vegetation indices, the NDFI is based on information from all spectral bands.

The NDFI time series was then partitioned into a historic baseline period (1985-2005) and a monitoring period (2006-2016). The BFAST algorithm was applied to the baseline period. This resulted in a model describing a linear trend and seasonal changes in NDFI. This model was used to predict NDFI values until 2016. The generated predictions were then compared to the observed data (i.e. the time series from 2006-2016) to see where they diverge. The principle behind the change detection is that if the observed time series has much lower NDFI values than the predicted time series, this indicates land degradation. These changes were aggregated by year and mapped per minimum mapping unit of 0.5 ha (or 5,000 $m^2$, ca. 5.5 Landsat pixels) to reduce noise (see **Figure E**).The result of the analysis is a map of disturbance, where every pixel is assigned a year of disturbance (or a value of 0 where no disturbance was observed). This provided the first analysis of land use or land cover change at this scale in dynamic seasonal forest ecosystem. The outputs are being used to determine the impacts of anthropogenic land use change in wildlife corridors, protected areas, important bird areas to assess the success and impacts of transboundary conservation efforts, and to support improved spatial planning for sustainable development.

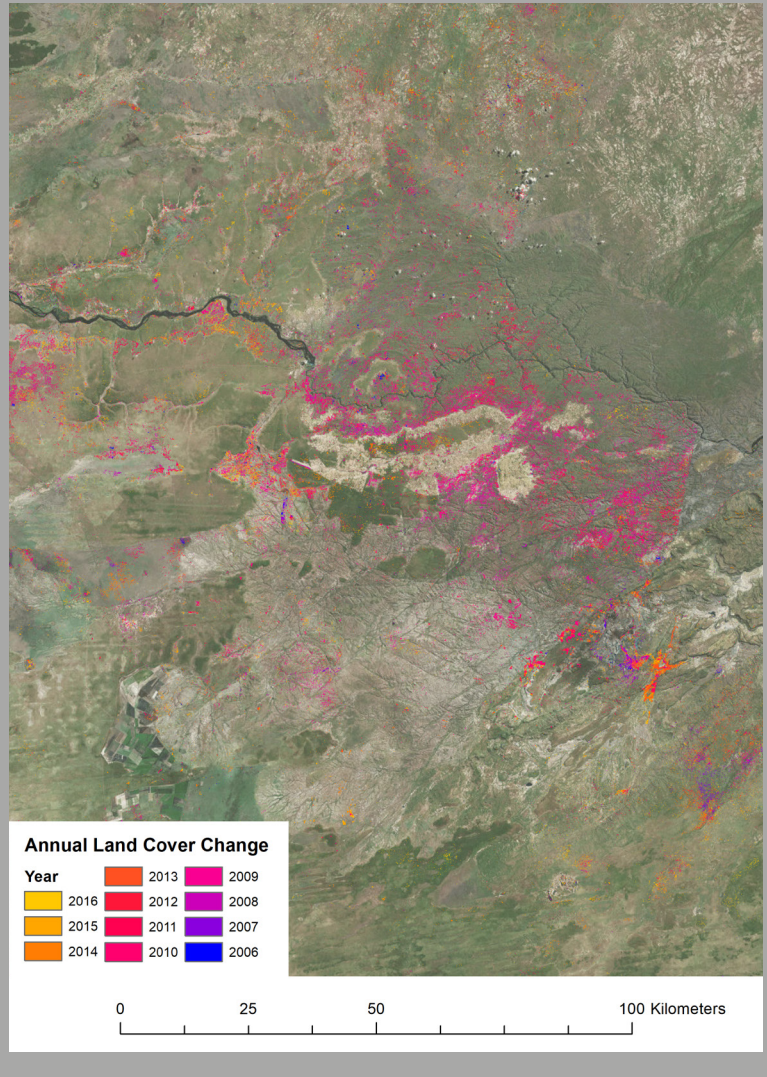


**Figure E.** Map of land cover change in the KAZA Transfrontier Conservation Area, with the year of detected disturbance. Land degradation was detected via time series analysis of Landsat imagery.

### 6.3 Advanced processing paradigms: Big Data analysis

Improvements in hardware capacity and the increasing accessibility of SRS data have driven a trend towards processing and analyzing large numbers of images at once. One example for this Big Data approach is time series analysis. Rather than comparing two or three SRS scenes to detect change across a landscape, this approach reconstructs time series of SRS data for each pixel based on dozens or hundreds of pictures. Dense time series can characterize Earth surface dynamics with high temporal (often sub-annual) resolution (Roy *et al.* 2014), and have been used to map historic forest disturbance (Senf *et al.* 2017) and detection of deforestation in near-real time (Hansen *et al.* 2016). There is a large range of methodological approaches to SRS time series analysis (Roy *et al.* 2014), including LandTrendr, which divides time series into segments to detect both abrupt and gradual changes such as deforestation and subsequent forest recovery (Kennedy *et al.* 2010), and Breaks For Additive Season and Trend (BFAST), which decomposes time series into trend, seasonal component and noise (Verbesselt *et al.* 2010). Apart from analysing many SRS scenes from the same sensor, a second Big Data approach to SRS analysis is integrating data from different types of sensors to take advantage of complimentary spatial, temporal or spectral resolutions. This integration includes using SRS imagery from multiple sensors as input into the same supervised classification algorithm to map land cover or ecosystem structure more accurately (Pouteau *et al.* 2010; Attarchi & Gloaguen 2013) or to combine imagery from different sources into a new, derived image via so-called image fusion (Lucas *et al.* 2014; Schulte to Bühne & Pettorelli 2017).

Regardless of its application, Big Data requires appropriate hardware and software that supports effective storage and processing of large quantities of data. Widely known high-level programming languages such as R have some Big Data capabilities, even though they were not built for that purpose. For instance, R has dedicated packages to aid parallel processing ("parallel"), handling big data volumes ("big memory") and efficient code compilation ("Riposte"). Python (combined with geoprocessing commands from SAGA and GDAL) can be even more efficient (Marvin *et al.* 2016). For intense processing requirements, there are dedicated software packages for setting up parallel processing (e.g. Hadoop). Alternatively, cloud computing services can be purchased from commercial providers (e.g. Amazon Web Services, Microsoft Azure). Google Earth Engine is an open-access option for cloud-based Big Data analysis, and has been used to produce large scale SRS products, such as the Global Forest Change map (Hansen *et al.* 2013), and the Global Surface Water product (Pekel *et al.* 2016), to support the Map of Life platform (Jetz & Thau 2018).

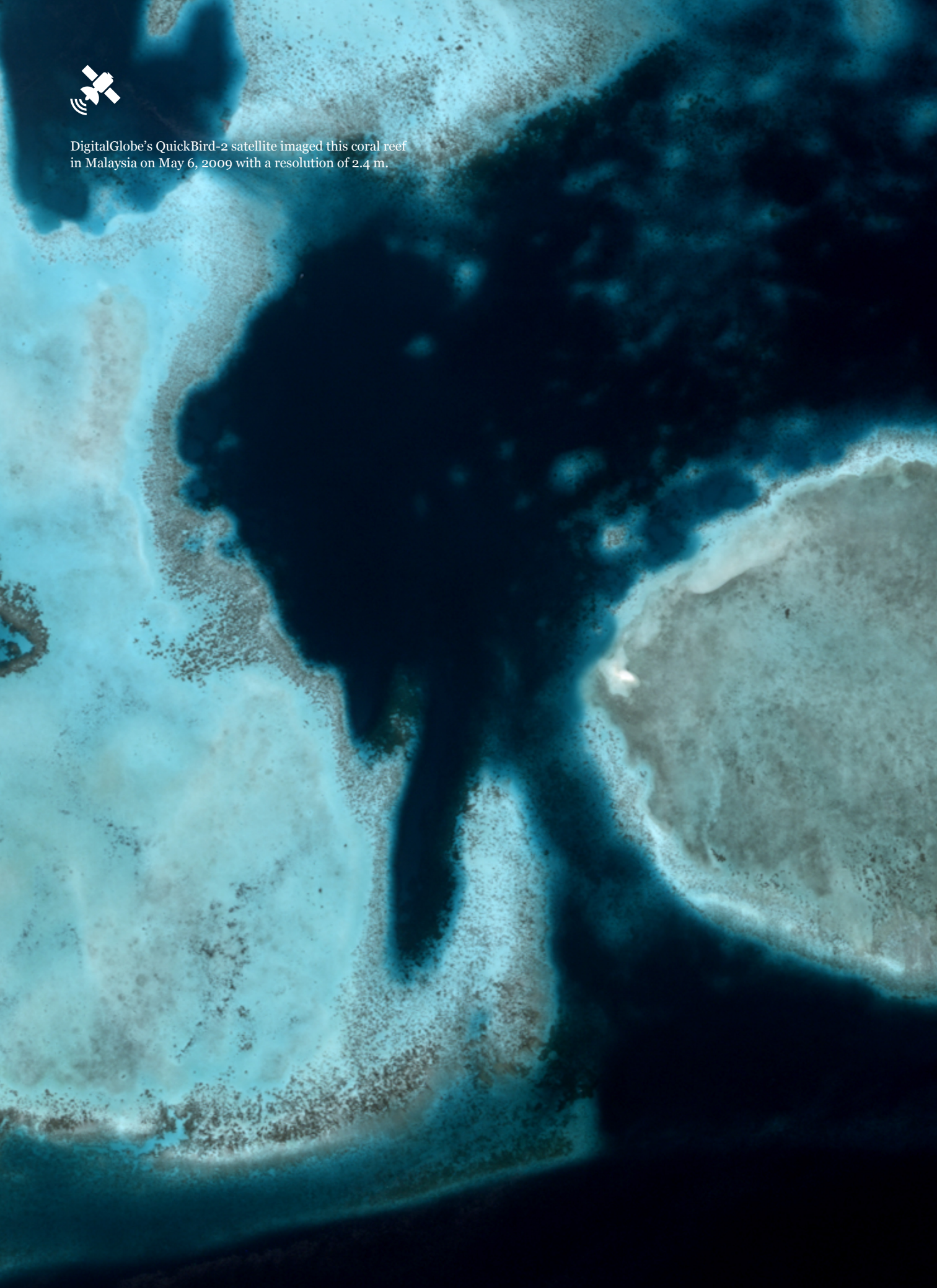

DigitalGlobe's QuickBird-2 satellite imaged this coral reef in Malaysia on May 6, 2009 with a resolution of 2.4 m.

# 7 CAVEATS AND LIMITATIONS WHEN USING SATELLITE REMOTE SENSING DATA

## HIGHLIGHTS

- Although satellite remotely sensed data have been applied widely in both conservation science and practice, there remain limitations to the information it can provide.
- Although species are increasingly being mapped using satellite remote sensing, the spatial resolution of satellite remote sensing data remains insufficient for locating many species of plant and animal species, and the temporal resolution of the data may be inadequate for detecting the dynamics of events that occur daily, especially where cloud cover produces long temporal gaps in datasets.
- Data coverage can vary geographically, and globally derived products should be treated with caution for local assessments.
- Although many remotely sensed datasets are now open-access, much remains hidden behind paywalls, especially data with very high spatial resolution, or from hyperspectral and radar sensors.
- The need for ground-truthing data to evaluate satellite remote sensing analyses and interpret results should not be underestimated. Relevant ground observations are increasingly being aggregated from online data platforms, and citizen science approaches provide additional opportunities to generate such data at large scales.

SRS data have been applied widely in both conservation science and practice, but there are limitations to the information they can provide. This chapter outlines three areas of potential constraints on the utility of satellite-derived imagery: 1) spatial and temporal resolution of SRS data, 2) data and product availability, 3) SRS data accessibility and literacy.

### 7.1 Spatial and temporal resolution of SRS data

SRS is only capable of capturing spatial patterns that can be resolved by its spatial resolution. SRS data with global coverage (see **Appendix**) typically have spatial resolutions of tens or hundreds of meters, limiting their application for detecting very small objects (see **Chapter 5.4**). Whereas SRS data with medium spatial resolution (like that of the Landsat sensors) are appropriate for mapping land cover classes forming relatively large contiguous patches, imagery with higher spatial resolution (i.e. < 10 m) is necessary when the landscape of interest varies at a finer spatial scale (for instance to map hedgerows in an agricultural landscape, Betbeder *et al.* 2015). Additionally, the spatial resolution of most satellite-borne sensors is generally too coarse to allow distinguishing individual plants, although plants which form large, relatively homogenous stands may be distinguished from surrounding vegetation (Huang & Asner 2009; Nagendra *et al.* 2013).

The temporal resolution of multispectral SRS is not only constrained by the mission design, but can also be reduced by cloud cover. Over the tropics and the subtropics, any given point on the Earth's surface might be imaged less than once annually by satellites with low repeat frequencies (e.g. Landsat; **Figure 7.1**) because of continuous cloud cover. This is a problem in cases where dynamics of the earth's surface vary at higher temporal frequencies than the revisit time (e.g. for near real time deforestation detection). One

solution is to use imagery from satellites with higher overpass frequency, such as MODIS, to increase the chance of obtaining cloud free images. However, it is possible that data gaps persist under very cloudy conditions. For instance, Garonna *et al.* (2009) found gaps in an NDVI time series over a tropical forest despite using 16-day composites and interpolating missing values using the previous and following values. Another alternative is to integrate different imagery types. For instance, Xin *et al.* (2013) combined MODIS and Landsat imagery to construct high-resolution time series, whereas Reiche *et al.* (2015) integrated Landsat and cloud-independent radar data from ALOS PALSAR to monitor deforestation at high temporal resolution.

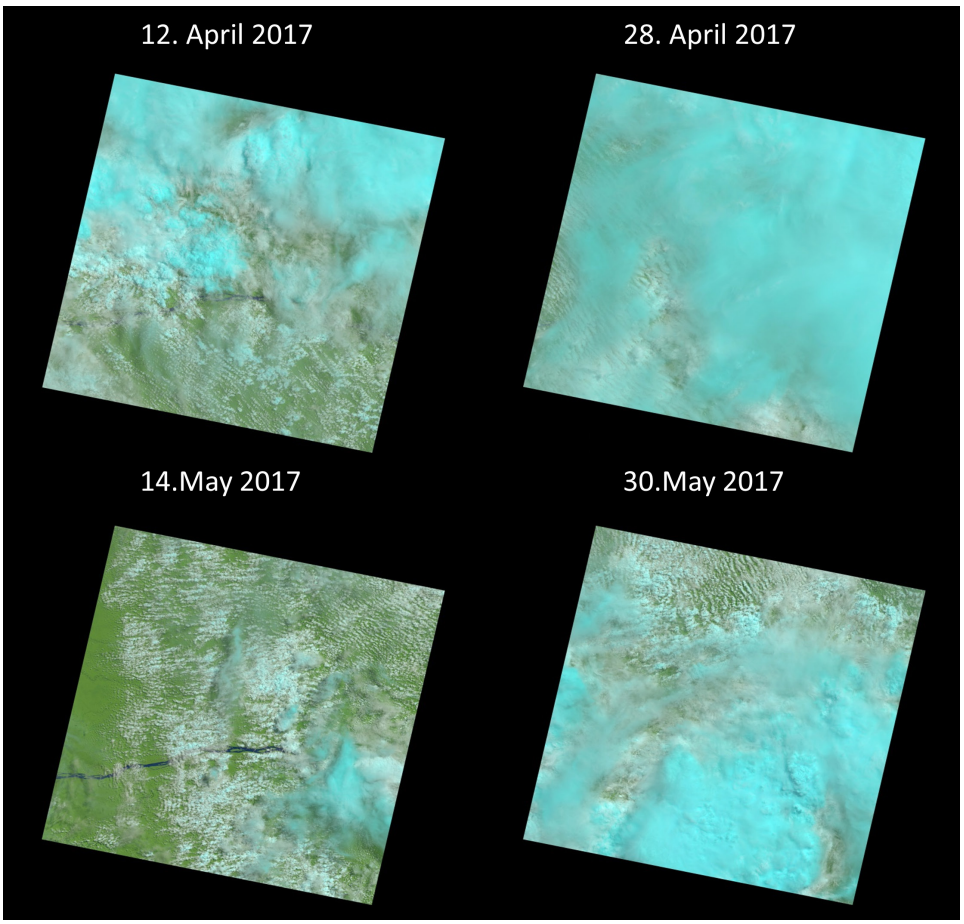


**Figure 7.1.** Cloud coverage can severely reduce the amount of multispectral SRS data available, especially over tropical areas. This figure shows cloud cover in a Landsat scene over the Amazon, taken in April and May 2017. ©USGS, NASA.

### 7.2 Data and product availability

Though the number of satellites that provide repeated coverage of the entire earth's surface is increasing, such missions are relatively new. As a result, long-term spatiotemporal availability of SRS data reflects historical acquisition priorities of different countries, or available infrastructure. For instance, there are noticeable gaps in the Landsat archive over Northern and Central Africa, and Western Europe before 2000, whereas the United States are well covered (Wulder *et al.* 2016). SRS imagery with very high spatial resolution has so far only been available from commercial satellites, whose acquisition programme is determined by the areas which users requested (though global coverage has more recently been provided by commercial fleets of smaller satellites, e.g. Planet's SkySat fleet). Hyperspectral and LiDAR satellite imagery has patchy coverage, especially over biodiverse regions (Pettorelli *et al.* 2014a). As a consequence, establishing which type of SRS data exists over a given area of interest is an important first step in processing and analysis design. It might be appropriate to combine SRS data from different sensors, for instance to increase the number of observations in a SRS time series. This requires that the imagery is precisely aligned (co-registered), and resampling may be necessary if the pixel sizes are initially different. Integrating SRS data from different sensors during analysis is referred to as data fusion, and can increase the quality of information. For instance, integrating multispectral and radar SRS data has been shown to increase land cover classification accuracy (Joshi *et al.* 2016).

Apart from the availability of SRS data, more widespread uptake of SRS approaches in conservation science and management is currently hampered by an absence of operational SRS products optimized at a national scale (Pettorelli *et al.* 2014b). Processing SRS data requires appropriate hardware, software and expertise, which can be a considerable obstacle for some users. Open-access SRS products such as land cover, vegetation and fire indices have been primarily produced at the global scale (**Appendix**), and their local accuracy can be limited (Congalton *et al.* 2014; Giglio *et al.* 2016), limiting their usefulness for mapping and monitoring at smaller, management-relevant scales.

Ground-truthing information is a key element when using SRS data, and is necessary for training supervised classifications, quantifying the validity and reliability of the results, and helping to interpret the results in their proper context (Congalton *et al.* 2014; Wohlfahrt *et al.* 2016). Collecting ground-truthing data – should it be on land cover distribution or tree cover, or collecting in situ spectral measurements – requires significant labour, time and money. Where adequate ground-truthing data are too expensive to obtain, open-access imagery with very high spatial resolution, such as Google Earth, is an alternative (Connette *et al.* 2016). Crowd sourcing ground truth data is a relatively recent approach that aims to leverage the land cover classification skills of human brains at large scales (Fritz *et al.* 2017). The largest potential opportunity for ground-truthing SRS data is making already existing ground-truth data available and accessible through online data platforms (such as Movebank, Smithsonian Wild, Map of Life; Pettorelli *et al.* 2014b).

**Movebank**
https://www.movebank.org/

**Smithsonian Wild**
http://emammal.si.edu/siwild

**Map of Life**
https://mol.org/

### 7.3 SRS data accessibility and literacy constraints

Using SRS imagery requires reasonably fast internet speeds for downloading raw data, high processing power, and sufficient data storage for raw imagery and intermediate and final data products. Hardware and software requirements typically increase with study area size, resolution and the complexity of analysis. To put this into perspective, an average Landsat scene (ca. 180 km x 190 km) has a file size of between 500 MB (Landsat 4-5) and 1.62 GB (Landsat 8), whereas a single Sentinel-1 scene has a size of 1 GB. Whilst an average laptop provides sufficient storage space and processing power to conduct a land cover classification based on a single-date Landsat image, processing large time

series of multi-scene mosaics requires more processing power, and in some cases may require the use of cloud computing services (e.g. Google Earth Engine).

More open-source SRS imagery is now available than ever before, but a considerable amount of useful data remains behind paywalls (Turner *et al.* 2015), especially SRS data with very high spatial resolution, or from hyperspectral and radar sensors. Additionally, appropriate hardware can be expensive, especially when large amounts of data have to be processed. Fortunately, although software used for image processing and analysis used to be a limitation to SRS uptake due to their cost (Pettorelli *et al.* 2014b), the increasing availability of open-access alternatives (e.g. R, QGIS or SAGA) commercial software donations, and relevant documentation and accessible training resources have largely removed this barrier to the application of SRS (Wegmann & Leutner 2016; Bernd *et al.* 2017).

**Group on Earth Observations**
http://geobon.org/

**Remote Sensing for Biodiversity**
http://remote-sensing-biodiversity.org/networks/ceos-biodiversity/

**GitHub**
https://github.com/

SRS can be a valuable tool in ecology and conservation, yet interdisciplinary collaboration has been limited because the remote sensing and ecology/conservation communities remain segregated (Pettorelli *et al.* 2014b). Platforms such as the Group on Earth Observations Biodiversity Observation Network or the group on Remote Sensing for Biodiversity within the Committee on Earth Observation Satellites (CEOS) provide important shared spaces to reduce communication problems (e.g. by encouraging the use of shared terminology) and transfer of data products, tools and knowledge between the groups. Additionally, platforms enabling data and code sharing (e.g. GitHub), provide an opportunity for making SRS workflows more transparent and repeatable which are promising a better future for remote sensing collaboration (Rocchini & Neteler 2012).

Tandem-X image of Christmas Island. Tandem X provides synthetic-aperture radar imagery using relatively short microwaves. As a result, the signal is scattered by small objects in its path, such as leaves, or small wave crests. This makes the texture of the sea and land surface visible in high detail. Photo: DLR (CC-BY 3.0)

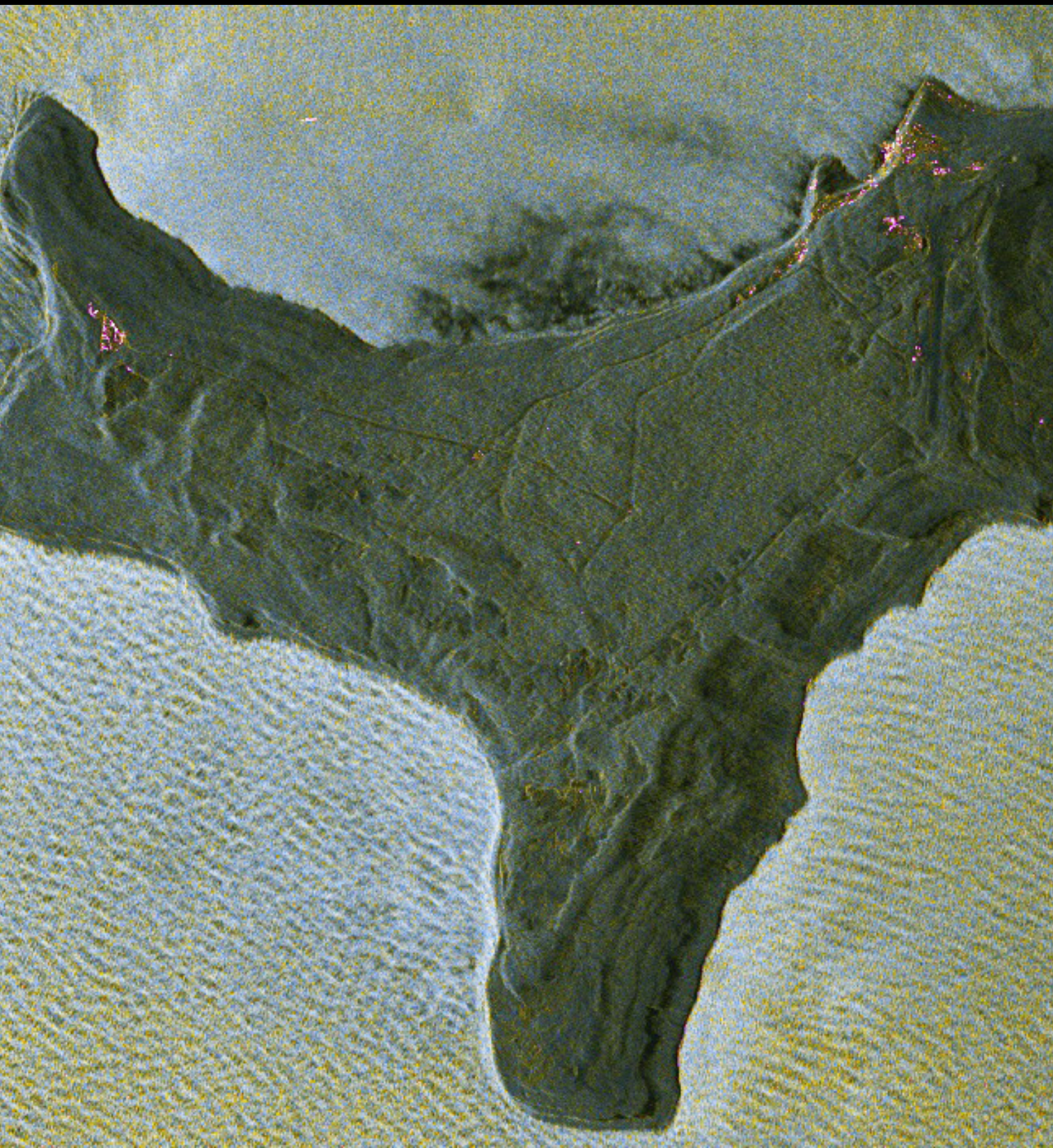

# 8 GLOSSARY

**Active sensor:** Sensors which emit radiation themselves, and then measure the returning signal.

**Acquisition mode:** Refers to the different modes in which spaceborne radar sensors can acquire imagery; they vary in swath width and spatial resolution.

**Artefact:** Features in SRS imagery which are a result of processing steps (such as pansharpening or atmospheric correction), but do not correspond to any real features on the ground. They can lead to errors in subsequent analysis (e.g. during land cover classification).

**Band:** A defined section of the electromagnetic spectrum in which a sensor measures electromagnetic radiation (Wegmann & Leutner 2016).

**Bottom-of-atmosphere reflectance:** See Surface Reflectance.

**Brightness:** Amount of energy measured by a sensor in a given pixel; mostly used in reference to multispectral sensors.

**C-band:** See Radar.

**Coverage**

- **spatial**: The surface area over which a remote sensor has provided imagery
- **temporal**: The time period during which a remote sensor has provided imagery.

**Cubesat:** Small satellite which weighs less (sometimes much less) than 10 kg (Marvin *et al.* 2016).

**Earth observation:** Gathering information about the atmosphere, the biosphere, land surface, the oceans, and solid Earth observations, often via satellite remote sensing.

**Electromagnetic radiation**: Radiation consisting of electromagnetic waves (i.e. waves that describe periodic variation in both electric and magnetic field intensity), including radio waves, microwaves, infrared, visible light and ultraviolet.

**Footprint:** Image extent or coverage. See scene.

**Foreshortening:** Geometric distortion of radar imagery which causes slopes which face the sensor to appear shorter than slopes that are tilted away.

**Geometric correction:** Correcting remote sensing imagery to correctly align it to an absolute or relative geographic location. E.g. georectification, orthorectification.

**Geolocation:** See georectification.

**Georectification:** Assigning each pixel in a remote sensing imagery the correct position with respect to a reference coordinate system.

**Geostationary orbit:** Orbit in which a satellite appears to remain fixed over a single point on the Earth's surface.

**GIS:** Geographic Information System; an environment for processing and analysing geospatial data.

**Grain:** Used synonymously with “spatial resolution”.

**Ground geometry:** With respect to radar imagery, an image in which each pixel corresponds to a pixel of the same area on the Earth’s surface as every other pixel.

**Ground truthing:** Validating remote sensing measurements or analysis results with observations derived from field observation.

**Hyperspectral sensors:** Multispectral sensors with hundreds of bands.

**Image:** Collection of measurements (i.e., bands) captured in the scene at a given time point; an image can be thought of as a particular instance of measurement of electromagnetic radiation from a certain scene.

**Inferometry:** Reconstructing the three-dimensional position of an object based on the phaseshift of the radar signal.

**Intensity**: See brightness.

**LAI:** Leaf Area Index, a structural canopy parameter that can be derived from satellite remote sensing.

**Land cover:** Physical properties of a given surface that can be characterised by the radiation that remote sensors capture (Simard *et al.* 2011).

**L-band:** See Radar.

**Layer:** Data file in raster format containing measurement of a scene in a single band (multispectral sensors) or a single polarization mode (radar sensor).

**Layover:** Geometric distortion of radar imagery which causes the top of tall structures (mountains or buildings) to appear to be closer in range than lower structures.

**LiDAR:** Sensors which emit a laser beam, and measure the returning signal to measure the distance between the sensor and the object.

**Multilooking:** Averaging brightness values between several adjacent parts of a radar image (“looks”) to reduce speckle and adjust pixel size to ground geometry.

**Multispectral:** Passive remote sensors which measure electromagnetic radiation in a limited number of narrow sections of the electromagnetic spectrum (“bands”).

**NDVI:** A widely used vegetation index, calculated from the red (R) and the near-infrared (NIR) band as NDVI = (NIR-R)/(NIR+R) (Rouse *et al.* 1974).

**Orthorectification**: Correcting remote sensing imagery for errors in geolocation as a result of differences in elevation (topographic errors).

**Overpass frequency:** Frequency with which a satellite passes over a given location on the Earth’s surface. Constrains temporal resolution of the imagery.

**Panchromatic:** A band in a multispectral sensor with a much higher spatial resolution covering a much larger range of wavelengths than the other band. This band can be used to pansharpen the other bands.

**Pansharpening:** A process in which the brightness values of coarser-grain multispectral bands are substituted for those of the panchromatic band of the same sensor, resulting in an image with higher spatial resolution.

**Passive sensors:** Sensors which do not emit radiation themselves, and measure radiation which is reflected, emitted or scattered by an object.

**P-band:** See Radar.

**Polarization:** Orientation of the wavelengths of electromagnetic radiation. Radar sensors can transmit and receive radiation in horizontal and/or vertical polarization.

**Polar orbit:** An orbit in which a satellite passes over, or near the poles.

**Radar:** Active remote sensing based on the principle of transmitting a signal (radiation in the microwave or radiowave part of the electromagnetic spectrum) and deriving information about the Earth's surface from the returning signal. Radar can be categorised according to the wavelength of the transmitted and received signal (e.g. X, C, L or P-band in order of increasing wavelength).

**Radiance:** The amount of radiation reflected from a unit surface area, measured by a remote sensor as Watt per solid angle and unit area [$W \cdot sr^{-1} \cdot m^{-2}$].

**Radiometric resolution:** Ability of a remote sensor to distinguish differences in the intensity of electromagnetic radiation.

**Raster**: Rectangular grid of pixels, each of which has an associated measurement (such as radiance) and geographic location. Satellite imagery is distributed in different raster formats, e.g. GeoTIFFs.

**Reflectance:** The proportion of radiation that is reflected back by an object (instead of being absorbed or transmitted), i.e. the ratio of incident and reflected radiation.

**Repeat frequency:** See overpass frequency.

**Resolution**

- **spatial:** The smallest object that can be identified by a given sensor; corresponds to the size of an individual pixel.
- **temporal:** Time between two successive images of the same location, and is given by the repeat frequency of a satellite.
- **spectral:** Sensitivity of a remote sensor to differences in wavelength of electromagnetic radiation.
- **radiometric:** Sensitivity of a remote sensor to differences in the intensity of electromagnetic radiation.

**SAR:** See Synthetic Aperture Radar.

**Satellite:** Spaceborne carrier of remote sensors and ancillary technology.

**Satellite Remote Sensing (SRS):** Identifying, observing and measuring objects on the Earth's surface via a spaceborne sensor.

**Scene:** The area across which a remote sensor makes measurements. SRS data are normally available as different scenes, whose size vary between sensors but are normally in the 100s or 1,000s of km$^2$. This means that, to make an image covering a large area (such as a country), many adjacent scenes have to be mosaicked together.

**Sensor:** Device that measures the intensity of electromagnetic radiation.

**Signal:** The electromagnetic radiation detected and (for active sensors) emitted by a remote sensor.

**Smallsat:** A small satellite which typically weighs below 250 kg (Richardson *et al.* 2015).

**Speckle**: "Salt-and-pepper" effects common in radar/SAR images; can be corrected e.g. via multilooking.

**Spectral resolution:** Ability of a remote sensor to detect differences in wavelength of electromagnetic radiation.

**Sun-synchronous orbit:** Orbit in which a satellite flies over a given location at the same solar time during each pass.

**Surface Reflectance:** Radiance measured by a multispectral sensor which has been corrected for sensor, solar and atmospheric effects.

**Synthetic Aperture Radar:** Artificially increasing the antenna length of a radar sensor to increase its spatial resolution; technology underlying all spaceborne radar sensors.

**Tile:** See Scene.

**Top-of-atmosphere reflectance:** Radiance measured by a multispectral sensor which has been corrected for sensor and solar, but not atmospheric effects.

**Vegetation Index:** Linear combinations of different multispectral bands which are sensitive to variations in vegetation "greeness" and provide synoptic views of vegetation dynamics.

**X-band:** See Radar.

A well trained eye might see the large herd of elephants crossing this wetland savanna in the Zambezi region of Namibia. Data collected by Digital Globe's Worldview-02 satellite can detect anything smaller than a meter with a pan-sharpening resolution of less than 50cm.

# 9 APPENDIX

Widely used multispectral remote sensing (A) and radar (B) SRS data, as well as derived SRS products (C) with global, or close to global, coverage. This is not a complete list of all available data or derived data products. MS = multispectral bands. PAN = panchromatic band. T = Thermal bands.

**(A) Multispectral SRS data**

| SATELLITE | SENSOR | SPATIAL RESOLUTION | COLLECTION FREQUENCY | SPATIAL COVERAGE | TEMPORAL COVERAGE | COST? | AVAILABLE FROM | REFERENCES |
|---|---|---|---|---|---|---|---|---|
| Envisat MERIS | 15 MS | Ocean: 1040 m x 1200 m, Land & coast: 260 m x 300 m | 3 days | Global | 2002 | Open-access | ESA Free data sets (see https://earth.esa.int/web/guest/pi-community/apply-for-data) | https://earth.esa.int/web/guest/missions/esa-operational-eo-missions/envisat/instruments/meris |
| AVHRR | 4 MS, 2 T | 1090 m | Daily | Global | 1978 -present | Open-access | EarthExplorer(https://earthexplorer.usgs.gov/) | NOAA/NESDIS 2014 |
| OrbView-2 SeaWiFS | 8 MS | 1 km | Daily | Global | 1997 - 2010 | Open-access | https://oceandata.sci.gsfc.nasa.gov/SeaWiFS/Mapped/Monthly/9km/chlor_a | https://oceancolor.gsfc.nasa.gov/SeaWiFS/ ; https://directory.eoportal.org/web/eoportal/satellite-missions/o/orbview-2 |
| MODIS Terra/Aqua | 30 MS, 6 T | 250 m, 500 m, 1,000 m, 5,600 m | Daily (8 day composite available) | Global | Feb 2000 - present/ July 2002 -present | Open-access | EarthExplorer(https://earthexplorer.usgs.gov/, under NASA LPDAAC Collections) | Vermote S.Y. Kotchenova and J.P. Ray 2011https://modis.gsfc.nasa.gov/data/dataprod/ |
| Landsat 4/5 TM | 6 MS, 1 T | MS/T: 30 m | 16 days | Global | July 1982 -May 2012 | Open-access | EarthExplorer(https://earthexplorer.usgs.gov/) | https://landsat.usgs.gov/what-are-band-designations-landsat-satellites, USGS 2017; Young *et al.* 2017 |
| Landsat 7 ETM+ | 6 MS, 1 T, 1 PAN | MS/T: 30 mPAN: 15 m | 16 days | Global | April 1999 - present | Open-access | EarthExplorer(https://earthexplorer.usgs.gov/) | USGS 2010; Young *et al.* 2017 |
| Landsat 8 OLI/TIRS | 8 MS, 2 T, 1 PAN | MS/T: 30 mPAN: 15 m | 16 days | Global | April 2013 -present | Open-access | EarthExplorer(https://earthexplorer.usgs.gov/) | USGS 2016; Young *et al.* 2017 |
| Terra ASTER | 10 MS, 5 T | 15 m (VNIR), 30 m (SWIR), 90 m (TIR) | Variable, but minimum 16 days | Variable, but potentially global (tasked) | 2000 -present | Open-access | Access options at https://asterweb.jpl.nasa.gov/data.asp, including USGS EarthExplorer | Abrams 2000; Abrams *et al.* 2015; USGS 2015 https://lpdaac.usgs.gov/node/1091 |
| Sentinel 2 MSI | 12 MS | 10 m, 20 m or 60 m, depending on the band | A & B: 5 days (at equator); A or B: 10 days (at equator) | Global | June 2015 (A) -present/ March 2017 (B) - present | Open-access | Copernicus Open Access Hub (https://scihub.copernicus.eu/dhus/#/home) | Drusch *et al.* 2012; ESA 2015 https://sentinel.esa.int/web/sentinel/user-guides/sentinel-2-msi/processing-levels |

| SATELLITE | SENSOR | SPATIAL RESOLUTION | COLLECTION FREQUENCY | SPATIAL COVERAGE | TEMPORAL COVERAGE | COST? | AVAILABLE FROM | REFERENCES |
|---|---|---|---|---|---|---|---|---|
| SPOT 1-3 (HRV) | 3 MS, 1 PAN | MS: 20 m, PAN:10 m | 1 to 3 days | Global coverage | 1986 - 2013 | Free on request (https://earth.esa.int/web/guest/data-access/how-to-access-esa-data) | NA | https://earth.esa.int/web/guest/data-access/browse-data-products/-/article/spot-1-to-4-hrv-ir-archive |
| SPOT 4 (HRVIR, VEGETATION) | 4 MS, 1 PAN | MS: 20 m, PAN: 10 m | Nearly daily | Global | 1998 - 2013 | Free on request (https://earth.esa.int/web/guest/data-access/how-to-access-esa-data) | NA | https://directory.eoportal.org/web/eoportal/satellite-missions/s/spot-4 |
| SPOT 5 (HRG) | 4 MS, 1PAN | MS: 10 - 20 m, PAN: 2.5 m | 2 - 3 days; 5 days since 2015 | Not global; above sites of interest | 2002 -present | Free on request (ESA 2015b) | NA | https://directory.eoportal.org/web/eoportal/satellite-missions/s/spot-5 |
| SPOT 6-7 | 4 MS, 1 PAN | 6 m (MS), 1.5 m (PAN) | Variable; daily possible | Variable, but potentially global (tasked) | 2012/2014 | Commercial | Airbus GeoStore (http://www.intelligence-airbusds.com/geostore/) | http://www.intelligence-airbusds.com/en/4388-spot-1-to-spot-5-satellite-images, https://directory.eoportal.org/web/eoportal/satellite-missions/s/spot-6-7 |
| RapidEye 1-5 | 5 MS | 6.5 m | 1 - 5.5 days | Global | 2008 -present | Commercial | https://www.planet.com | Toth & Jóźków 2016 |
| IKONOS | 4 MS, 1 PAN | 0.8 m - 3.2 m | 3 days | Global | 1999 - 2015 | Commercial | https://www.digitalglobe.com/ | https://www.digitalglobe.com/resources/satellite-information |
| Pléiades 1/2 | 4 MS, 1 PAN | 2.8 m (MS), 0.7 m (PAN) | Daily | Global | 2011/2012 | Commercial | http://www.intelligence-airbusds.com/pleiades/ | Gleyzes *et al.* 2012 |
| QuickBird | 4 MS, 1 PAN | 0.60 m-2.4 m | 1 - 3.5 days (at equator) | Global | 2002 - 2015 | Commercial | Digital Globe (https://www.digitalglobe.com/) | http://glcf.umd.edu/data/quickbird/; Digital Ata 2001 |
| WorldView 2/3 | 8 MS, 1 PAN | PAN: 0.46 m/0.31 mMS: 1.84 m/1.24 m | 1 - 2 days | Variable, but potentially global (tasked) | 2009/2014 -present | Commercial | Digital Globe (https://www.digitalglobe.com/) | DigitalGlobe 2017b |
| GeoEye | 4 MS, 1 PAN | PAN: 0.41 mMS: 1.65 m | 11 days | Variable, but potentially global (tasked) | 2008 -present | Commercial | https://www.digitalglobe.com/ | DigitalGlobe 2017a |

**(B) Radar SRS data**

| NAME | SENSOR | SPATIAL RESOLUTION | COLLECTION FREQUENCY | SPATIAL COVERAGE | TEMPORAL COVERAGE | COST? | AVAILABLE FROM | REFERENCES |
|---|---|---|---|---|---|---|---|---|
| JERS-1 | L-band SAR | 18 m | 44 days | Global | 1992 - 1998 | Open-access | ESA Free data sets (see https://earth.esa.int/web/guest/pi-community/apply-for-data) | https://directory.eoportal.org/web/eoportal/satellite-missions/j/jers-1 |
| ALOS PALSAR | L-band SAR | 10 m – 100 m | 46 days | Global | 2006 - 2011 | Open-access | Alaska Satellite Facility (https://vertex.daac.asf.alaska.edu/) ESA Free data sets (see https://earth.esa.int/web/guest/pi-community/apply-for-data) | JAXA 2008 |
| ALOS-2 | L-band SAR | 3 m – 100 m | 14 days | Global | 2014 -present | Commercial | http://en.alos-pasco.com/ | http://en.alos-pasco.com/new/2017/02.html |
| Envisat ASAR | C-band SAR | 30 – 1,000 m, depending on acquisition mode | 35 days | Variable, but potentially global (tasked) | 2002 - 2012 | Open-access | ESA Free data sets (see https://earth.esa.int/web/guest/pi-community/apply-for-data) | Toth & Jóźków 2016 https://earth.esa.int/web/sppa/mission-performance/esa-missions/envisat/asar/sensor-description |
| ERS-1/2 | C-band SAR | 30 m – 50 km, depending on acquisition mode | 35 days | Global | 1991 - 2000 (ERS-1), -1995 - 2011 (ERS-2) | Open-access | ESA Free data sets (see https://earth.esa.int/web/guest/pi-community/apply-for-data) | https://directory.eoportal.org/web/eoportal/satellite-missions/e/ers-1 |
| Sentinel 1 SAR | C-band SAR | 5 – 40 m, depending on acquisition mode | A & B: 3 days (at equator); A or B: 6 days (at equator) | Global | 2014 (April), 2016 (B) | Open-access | Copernicus Open Access Hub (https://scihub.copernicus.eu/dhus/#/home) | Potin 2013 |
| RADARSAT-1/2 | C-band SAR | 3 – 100 m | 24 days | Variable, but potentially global (tasked) | 1995/2007 -present | Commercial | MDA (http://mdacorporation.com/corporate) | Sinha *et al.* 2015 |
| TerraSAR-X | X-band SAR | 0.25 – 18 m | 2.5 days | Global | 2007 -present | Free (requires project proposal) | https://terrasar-x-archive.terrasar.com/ | https://tandemx-science.dlr.de/; https://earth.esa.int/web/guest/pi-community/apply-for-data/3rd-party |
| TanDEM-X | X-band SAR | 1 – 18 m | 2.5 days | Global | 2010 -present | The derived DEM is free; other data requires project proposal | https://tandemx-science.dlr.de/ | https://tandemx-science.dlr.de/pdfs/TD-GS-PS-0021_DEM-Product-Specification_v3.1.pdf |

| SATELLITE | DESCRIPTION | SPATIAL RESOLUTION | COLLECTION FREQUENCY | SPATIAL COVERAGE | TEMPORAL COVERAGE | COST? | AVAILABLE FROM | REFERENCES |
|---|---|---|---|---|---|---|---|---|
| **VEGETATION INDICES AND BIOPHYSICAL PARAMETERS (MONITORING VEGETATION PHENOLOGY, STRUCTURE, PRIMARY PRODUCTIVITY; USED IN ECOSYSTEM MAPPING, SPECIES DISTRIBUTION MODELLING)** | | | | | | | | |
| MODIS Vegetation Index Products | NDVI & EVI, based on MODIS Surface Reflectance | 250 m, 500 m, 1,000 m or ca. 5,600 m | 16 days, monthly | Global (terrestrial) | Feb 2000 - present/ July 2002-present | Open-access | USGS EarthExplorer https://earthexplorer.usgs.gov/ (under NASA LPDAAC Collections) | Solano *et al.* 2010 |
| MODIS LAI | Leaf Area Index, based on MODIS Surface Reflectance & NDVI | 500 m | 4 or 8 days | Global | February 2000 – present/ July 2002-present | Open-access | USGS EarthExplorer https://earthexplorer.usgs.gov/ (under NASA LPDAAC Collections) | LP DAAC 2015 |
| MODIS chlorophyll-α concentration | Chlorophyll-α in surface water, based on MODIS Surface Reflectance | 4.6 km | Daily | Global | 2002 - present | Open-access | NASA Ocean Color (https://oceancolor.gsfc.nasa.gov/cgi/browse.pl) | Hu *et al.* 2012 |
| MODIS Land Cover Dynamics | Phenology dynamics, based on MODIS Surface Reflectance | 500 m | Annually | Global (terrestrial) | 2001 - 2012 | Open-access | USGS EarthExplorer https://earthexplorer.usgs.gov/ (under NASA LPDAAC Collections) | https://lpdaac.usgs.gov/dataset_discovery/modis/modis_products_table/mcd12q2 |
| **FIRE PRODUCTS (MONITORING ANTHROPOGENIC AND WILDFIRE; DETECTING CHANGES IN FIRE REGIME)** | | | | | | | | |
| MODIS Thermal anomalies/Fire | Location of active fires | 1 km | Daily, or 8 day composite | Global | February 2000 – present/ July 2002-present | Open-access | USGS EarthExplorer https://earthexplorer.usgs.gov/ (under NASA LPDAAC Collections) | Oom & Pereira 2012; Giglio 2015 |
| MODIS Burned area product | Date of burning | 500 km | Monthly | Global | 2000 - present | Open-access | LP DAAC (http://reverb.echo.nasa.gov/) | Boschetti *et al.* 2008; Mouillot *et al.* 2014 |
| VIIRS Active Fire Product | Location of active fires | 375 m | Daily | Global | 2012 - present | Open-access | NASA Earth Data (https://earthdata.nasa.gov/earth-observation-data/near-real-time/firms/active-fire-data) | Schroeder 2015 |

### (C) Derived SRS products

| SATELLITE | DESCRIPTION | SPATIAL RESOLUTION | COLLECTION FREQUENCY | SPATIAL COVERAGE | TEMPORAL COVERAGE | COST? | AVAILABLE FROM | REFERENCES |
|---|---|---|---|---|---|---|---|---|
| LAND COVER PRODUCTS, ECOSYSTEM AND HABITAT MAPPING AND CHANGE DETECTION | | | | | | | | |
| MODIS Vegetation continuous fields | Proportional cover of vegetative covers (woody, herbaceous, bare ground), based on MODIS Terra & Landsat | 250 m | Annually | Global (terrestrial) | 2000 - 2013 | Open-access | USGS EarthExplorer https://earthexplorer.usgs.gov/ (under NASA LPDAAC Collections) | Townshend *et al.* 2011 |
| MODIS Land cover type | 17 land cover classes | 500 m | Annually | Global (terrestrial) | 2001 - 2012/13 | Open-access | https://lpdaac.usgs.gov/data_access/data_pool | Friedl *et al.* 2010 |
| MODIS Vegetative Cover Conversion | 16 land cover change classes | 250 m | Annually | Global (terrestrial) | 2000 - present | Open-access | https://e4ftl01.cr.usgs.gov/MOLT/ | Zhan *et al.* 2002 |
| Landsat Global Forest Change | Forest cover in 2000, forest loss, gain cf. 2015 & year of loss/gain | 30 m | Change between two years | Global (terrestrial) | 2000 - 2015 | Open-access | https://earthenginepartners.appspot.com/science-2013-global-forest | Hansen *et al.* 2013 |
| Global 30m Tree Cover | Proportion of peak growing-season tree canopy cover | 30 m | NA | Global (terrestrial) | 2010 | Open-access | https://landcover.usgs.gov/glc/TreeCoverDescriptionAndDownloads.php | Hansen *et al.* 2013 |
| Landsat Tree Cover Continuous Fields | Per-pixel cover of vegetation >5m | 30 m | NA | Global | 2000 & 2005 | Open-access | http://glcf.umd.edu/data/landsatTreecover/ | Sexton *et al.* 2013 |
| Global 30m Bare Ground | Proportion of peak growing-season bare ground cover | 30 m | NA | Global (terrestrial) | 2010 | Open-access | https://landcover.usgs.gov/glc/BareGroundDescriptionAndDownloads.php | Hansen *et al.* 2013 |
| IGBP DISCover | 17 land cover categories, based on AVHRR | 1 km | NA | Global (terrestrial) | 1992/1993 | Open-access | ORNL DAAC (https://daac.ornl.gov/cgi-bin/dsviewer.pl?ds_id=930&nav=OGC) | Loveland *et al.* 2000; Congalton *et al.* 2014 |
| University of Maryland Land Cover | 14 land cover categories, based on AVHRR | 1 km, 8 km or ca. 110 km | NA | Global (terrestrial) | 1992/1993 | Open-access | http://glcf.umd.edu/data/landcover/ | Hansen *et al.* 2000; Congalton *et al.* 2014 |
| Global Land Cover 2000 | 22 land cover categories, based on SPOT VEGETATION-1 | 1 km | NA | Global (terrestrial) | 1999/2000 | Open-access | http://forobs.jrc.ec.europa.eu/products/glc2000/products.php | Congalton *et al.* 2014 |
| GlobCover 2005/2009 | 22 land cover classes, based on Envisat MERIS | 300 m | NA | Global (terrestrial) | 2005 & 2009 | Open-access | http://due.esrin.esa.int/page_globcover.php | Arino *et al.* 2012 |
| CCI Land cover | 22 land cover classes, based on AVHRR, MERIS & PROBA-V | 300 m | Annual | Global (terrestrial) | 1992 - 2015 | Open-access | http://maps.elie.ucl.ac.be/CCI/viewer/ | https://www.esa-landcover-cci.org/?q=node/175 |

| SATELLITE | DESCRIPTION | SPATIAL RESOLUTION | COLLECTION FREQUENCY | TEMPORAL COVERAGE | COST? | AVAILABLE FROM | REFERENCES |
|---|---|---|---|---|---|---|---|
| | | | OTHER | | | | |
| NOAA Coral Reef Watch products | Sea Surface Temperature (SST), 7-day SST trend, SST Anomaly, Coral Bleaching HotSpots, Degree Heating Weeks & 7-day maximum Bleaching Alert Area | 5 km | Daily | 2013 - present | Open-access | NOAA Coral Reef Watch (https://coralreefwatch.noaa.gov/satellite/bleaching5km/index.php) | Liu *et al.* 2014 |
| Global Surface Water Change | Surface water occurrence, change, seasonality, recurrence, transition & extent based on Landsat satellite data | 30 m | Change between two epochs (1984-1999; 2000-2015); monthly (extent & recurrence); yearly (seasonality) | 1984 - 2015 | Open-access | Browse: https://global-surface-water.appspot.com/ Download: https://global-surface-water.appspot.com/download | JRC 2016; Pekel *et al.* 2016 |

Africa as seen from space by the Terra MODIS sensor. Satellite remote sensing is a key source of information in for a range of scientific disciplines – from meteorology and geography to ecology – as providing wall-to-wall coverage of the state of the Earth's surface.
Source: NASA (Reto Stöckli and Robert Simmon).

# 10 BIBLIOGRAPHY

Abrams, M. (2000). The Advanced Spaceborne Thermal Emission and Reflection Radiometer (ASTER): Data products for the high spatial resolution imager on NASA's Terra platform. *Int. J. Remote Sens.*, 21, 847–859.

Abrams, M., Hook, S. & Ramachandran, B. (2015). ASTER User Handbook Version 2.

Achard, F. & Hansen, M.C. (2012). *Global forest monitoring from earth observation*. CRC Press.

AghaKouchak, A., Farahmand, A., Melton, F.S., Teixeira, J., Anderson, M.C., Wardlow, B.D., *et al.* (2015). Remote sensing of drought: Progress, challenges and opportunities. *Rev. Geophys.*, 53, 452–480.

Akani, G., Politano, E. & Luiselli, L. (2004). Amphibians recorded in forest swamp areas of the River Niger Delta (southeastern Nigeria), and the effects of habitat alteration from oil industry development on species richness and diversity. *Appl. Herpetol.*, 2, 1–22.

Almeida-Filho, R., Shimabukuro, Y.E., Rosenqvist, A. & Sánchez, G.A. (2009). Using dual-polarized ALOS PALSAR data for detecting new fronts of deforestation in the Brazilian Amazônia. *Int. J. Remote Sens.*, 30, 3735–3743.

Alvain, S., Moulin, C., Dandonneau, Y. & Bréon, F.M. (2005). Remote sensing of phytoplankton groups in case 1 waters from global SeaWiFS imagery. *Deep Sea Res. Part I Oceanogr. Res. Pap.*, 52, 1989–2004.

Álvarez-Berríos, N.L., Parés-Ramos, I.K. & Aide, T.M. (2013). Contrasting Patterns of Urban Expansion in Colombia, Ecuador, Peru, and Bolivia Between 1992 and 2009. *Ambio*, 42, 29–40.

Álvarez-Berrios, N.L. & Mitchell Aide, T. (2015). Global demand for gold is another threat for tropical forests. *Environ. Res. Lett.*, 10, 14006.

Amaral, S., Bestetti, C., Camilo, C. & Rennó, D. (2007). Normalized Difference Vegetation Index (NDVI) improving species distribution models: an example with the neotropical genus Coccocypselum (Rubiaceae). In: *Anais XIII Simpósio Brasileiro de Sensioramento Remoto*. pp. 2275–2282.

Ameca y Juárez, E.I., Mace, G.M., Cowlishaw, G. & Pettorelli, N. (2012). Natural population die-offs: Causes and consequences for terrestrial mammals. *Trends Ecol. Evol.*

Anderson, L.O., Shimabukuro, Y.E., Defries, R.S. & Morton, D. (2005). Assessment of deforestation in near real time over the Brazilian amazon using multitemporal fraction images derived from terra MODIS. *IEEE Geosci. Remote Sens. Lett.*, 2, 315–318.

Armenteras, D., Gast, F. & Villareal, H. (2003). Andean forest fragmentation and the representativeness of protected natural areas in the eastern Andes, Colombia. *Biol. Conserv.*, 113, 245–256.

Asner, G.P. (2001). Cloud cover in Landsat observations of the Brazilian Amazon. *Int. J. Remote Sens.*, 22, 3855–3862.

Asner, G.P., Scurlock, J.M.O. & A. Hicke, J. (2003). Global synthesis of leaf area index observations: implications for ecological and remote sensing studies. *Glob. Ecol. Biogeogr.*, 12, 191–205.

Asner, G.P., Knapp, D.E., Cooper, A.N., Bustamante, M.M.C., Olander, L.P., Asner, G.P., *et al.* (2005). Ecosystem Structure throughout the Brazilian Amazon from Landsat Observations and Automated Spectral Unmixing. *Earth Interact.*, 9, 1–31.

Asner, G.P., Mascaro, J., Muller-Landau, H.C., Vieilledent, G., Vaudry, R., Rasamoelina, M., *et al.* (2012). A universal airborne LiDAR approach for tropical forest carbon mapping. *Oecologia*, 168, 1147–1160.

Asner, G.P., Llactayo, W., Tupayachi, R. & Luna, E.R. (2013). Elevated rates of gold mining in the Amazon revealed through high-resolution monitoring. *Proc. Natl. Acad. Sci. U. S. A.*, 110, 18454–9.

Asner, G.P. (2014). Satellites and psychology for improved forest monitoring. *Proc. Natl. Acad. Sci. U. S. A.*, 111, 567–8.

Attarchi, S. & Gloaguen, R. (2013). Joint processing of Landsat ETM+ and ALOS-PALSAR data for species richness and forest biodiversity monitoring. In: *Proceedings of SPIE - The International Society for Optical Engineering*.

Baghdadi, N., Le Maire, G., Bailly, J.S., Osé, K., Nouvellon, Y., Zribi, M., *et al.* (2015). Evaluation of ALOS/PALSAR L-Band Data for the Estimation of Eucalyptus Plantations Aboveground Biomass in Brazil. *IEEE J. Sel. Top. Appl. Earth Obs. Remote Sens.*, 8, 3802–3811.

Baig, M.H.A., Zhang, L., Shuai, T. & Tong, Q. (2014). Derivation of a tasselled cap transformation based on Landsat 8 at-satellite reflectance. *Remote Sens. Lett.*, 5, 423–431.

Bargiel, D. (2013). Capabilities of high resolution satellite radar for the detection of semi-natural habitat structures and grasslands in agricultural landscapes. *Ecol. Inform.*, 13, 9–16.

Beck, H.E., McVicar, T.R., van Dijk, A.I.J.M., Schellekens, J., de Jeu, R.A.M. & Bruijnzeel, L.A. (2011). Global evaluation of four AVHRR–NDVI data sets: Intercomparison and assessment against Landsat imagery. *Remote Sens. Environ.*, 115, 2547–2563.

Beck, P.S.A., Kalmbach, E., Joly, D., Stien, A. & Nilsen, L. (2005). Modelling local distribution of an Arctic dwarf shrub indicates an important role for remote sensing of snow cover. *Remote Sens. Environ.*, 98, 110–121.

Beirle, S., Boersma, K.F., Platt, U., Lawrence, M.G. & Wagner, T. (2011). Megacity emissions and lifetimes of nitrogen oxides probed from space. *Science (80-. ).*, 333, 1737–1739.

Bergen, K.M., Goetz, S.J., Dubayah, R.O., Henebry, G.M., Hunsaker, C.T., Imhoff, M.L., *et al.* (2009). Remote sensing of vegetation 3-D structure for biodiversity and habitat: Review and implications for lidar and radar spaceborne missions. *J. Geophys. Res. Biogeosciences*, 114, n/a-n/a.

Bernd, A., Braun, D., Ortmann, A., Ulloa-Torrealba, Y.Z., Wohlfart, C. & Bell, A. (2017). More than counting pixels - perspectives on the importance of remote sensing training in ecology and conservation. *Remote Sens. Ecol. Conserv.*, 3, 38–47.

Betbeder, J., Hubert-Moy, L., Burel, F., Corgne, S. & Baudry, J. (2015). Assessing ecological habitat structure from local to landscape scales using synthetic aperture radar. *Ecol. Indic.*, 52, 545–557.

Beyer, J., Trannum, H.C., Bakke, T., Hodson, P. V. & Collier, T.K. (2016). Environmental effects of the Deepwater Horizon oil spill: A review. *Mar. Pollut. Bull.*, 110, 28–51.

Bisrat, S.A., White, M.A., Beard, K.H. & Richard Cutler, D. (2012). Predicting the distribution potential of an invasive frog using remotely sensed data in Hawaii. *Divers. Distrib.*, 18, 648–660.

Blanco, L.J., Ferrando, C.A. & Biurrun, F.N. (2009). Remote Sensing of Spatial and Temporal Vegetation Patterns in Two Grazing Systems. *Rangel. Ecol. Manag.*, 62, 445–451.

Blaschke, T. (2010). Object based image analysis for remote sensing. *ISPRS J. Photogramm. Remote Sens.*

Blondeau-Patissier, D., Gower, J.F.R., Dekker, A.G., Phinn, S.R. & Brando, V.E. (2014). A review of ocean color remote sensing methods and statistical techniques for the detection, mapping and analysis of phytoplankton blooms in coastal and open oceans. *Prog. Oceanogr.*, 123, 123–144.

Blumstein, D.T., Mennill, D.J., Clemins, P., Girod, L., Yao, K., Patricelli, G., *et al.* (2011). Acoustic monitoring in terrestrial environments using microphone arrays: applications, technological considerations and prospectus. *J. Appl. Ecol.*, 48, 758–767.

Bontemps, S., Defourny, P., Bogaert, E. Van, Kalogirou, V. & Perez, J.R. (2011). GLOBCOVER 2009 Products Description and Validation Report. *ESA Bull.*, 136, 53.

Bradley, B.A. & Mustard, J.F. (2006). Characterizing The Landscape Dynamics Of An Invasive Plant And Risk Of Invasion Using Remote Sensing. *Ecol. Appl.*, 16, 1132–1147.

Bradley, B.A., Olsson, A.D., Wang, O., Dickson, B.G., Pelech, L., Sesnie, S.E., *et al.* (2012). Species detection vs. habitat suitability: Are we biasing habitat suitability models with remotely sensed data? *Ecol. Modell.*, 244, 57–64.

Braun, A.C., Troeger, D., Garcia, R., Aguayo, M., Barra, R. & Vogt, J. (2017). Assessing the impact of plantation forestry on plant biodiversity: A comparison of sites in Central Chile and Chilean Patagonia. *Glob. Ecol. Conserv.*, 10, 159–172.

Breiman, L. (2001). Random Forests. *Mach. Learn.*, 45, 5–32.

Brinck, K., Fischer, R., Lehmann, S. & Paula, M.D. De. (2017). High resolution analysis of tropical forest fragmentation and its impact on the global carbon cycle. *Nat. Commun.*, 8.

Brovkin, V., Sitch, S., von Bloh, W., Claussen, M., Bauer, E. & Cramer, W. (2004). Role of land cover changes for atmospheric CO  increase and climate change during the last 150 years. *Glob. Chang. Biol.*, 10, 1253–1266.

Brown, M.E., Pinzón, J.E., Didan, K., Morisette, J.T. & Tucker, C.J. (2006). Evaluation of the consistency of Long-term NDVI time series derived from AVHRR, SPOT-vegetation, SeaWiFS, MODIS, and landsat ETM+ sensors. *IEEE Trans. Geosci. Remote Sens.*, 44, 1787–1793.

Brown, M.E., Delgodo Arias, S., Neumann, T., Jasinski, M.F., Posey, P., Babonis, G., *et al.* (2016). Applications for ICESat-2 Data: From NASA's Early Adopter Program. *IEEE Geosci. Remote Sens. Mag.*, 4, 24–37.

Brusch, S., Lehner, S., Fritz, T., Soccorsi, M., Soloviev, A. & van Schie, B. (2011). Ship Surveillance With TerraSAR-X. *IEEE Trans. Geosci. Remote Sens.*, 49, 1092–1103.

Bucini, G. & Lambin, E.F. (2002). Fire impacts on vegetation in Central Africa: a remote-sensing-based statistical analysis. *Appl. Geogr.*, 22, 27–48.

Buck, O., Millán, V.E.G., Klink, A. & Pakzad, K. (2015). Using information layers for mapping grassland habitat distribution at local to regional scales. *Int. J. Appl. Earth Obs. Geoinf.*, 37, 83–89.

Burton, A.C., Neilson, E., Moreira, D., Ladle, A., Steenweg, R., Fisher, J.T., *et al.* (2015). REVIEW: Wildlife camera trapping: a review and recommendations for linking surveys to ecological processes. *J. Appl. Ecol.*, 52, 675–685.

Butchart, S.H.M., Walpole, M., Collen, B., van Strien, A., Scharlemann, J.P.W., Almond, R.E.A., *et al.* (2010). Global Biodiversity: Indicators of Recent Declines. *Science (80-. ).*, 328, 1164–1168.

Cahalan, R.F. (1992). The Kuwait oil fires as seen by Landsat. *J. Geophys. Res.*, 97, 14565.

Caillault, S., Ballouche, A. & Delahaye, D. (2015). Where are the "bad fires" in West African savannas? Rethinking burning management through a space-time analysis in Burkina Faso. *Geogr. J.*, 181, 375–387.

Campbell, J.B. (1996). *Introduction to remote sensing (2nd Edition)*. Guilford Press.

Carvalho, G.A., Minnett, P.J., Fleming, L.E., Banzon, V.F. & Baringer, W. (2010). Satellite remote sensing of harmful algal blooms: A new multi-algorithm method for detecting the Florida Red Tide (Karenia brevis). *Harmful Algae*, 9, 440–448.

Casadio, S., Arino, O. & Serpe, D. (2012). Gas flaring monitoring from space using the ATSR instrument series. *Remote Sens. Environ.*, 116, 239–249.

Castillo-Santiago, M.A., Ricker, M. & de Jong, B.H.J. (2010). Estimation of tropical forest structure from SPOT-5 satellite images. *Int. J. Remote Sens.*, 31, 2767–2782.

Chambers, J.Q., Asner, G.P., Morton, D.C., Anderson, L.O., Saatchi, S.S., Espírito-Santo, F.D.B., *et al.* (2007). Regional ecosystem structure and function: ecological insights from remote sensing of tropical forests. *Trends Ecol. Evol.*, 22, 414–423.

Chaplin-Kramer, R., Sharp, R.P., Mandle, L., Sim, S., Johnson, J., Butnar, I., *et al.* (2015). Spatial patterns of agricultural expansion determine impacts on biodiversity and carbon storage. *Proc. Natl. Acad. Sci.*, 112, 7402–7407.

Chapman, B., McDonald, K., Shimada, M., Rosenqvist, A., Schroeder, R. & Hess, L. (2015). Mapping Regional Inundation with Spaceborne L-Band SAR. *Remote Sens.*, 7, 5440–5470.

Chassot, E., Bonhommeau, S., Dulvy, N.K., Mélin, F., Watson, R., Gascuel, D., *et al.* (2010). Global marine primary production constrains fisheries catches. *Ecol. Lett.*, 13, 495–505.

Chavez, P.S. (1988). An improved dark-object subtraction technique for atmospheric scattering correction of multispectral data. *Remote Sens. Environ.*, 24, 459–479.

Chen, X., Vierling, L. & Deering, D. (2005). A simple and effective radiometric correction method to improve landscape change detection across sensors and across time. *Remote Sens. Environ.*, 98, 63–79.

Clark, J., Wang, Y. & August, P. V. (2014). Assessing current and projected suitable habitats for tree-of-heaven along the Appalachian Trail. *Philos. Trans. R. Soc. B Biol. Sci.*, 369, 20130192–20130192.

Cohen, W.B. & Goward, S.N. (2004). Landsat's Role in Ecological Applications of Remote Sensing. *Bioscience*, 54, 535–545.

Congalton, R., Gu, J., Yadav, K., Thenkabail, P. & Ozdogan, M. (2014). Global Land Cover Mapping: A Review and Uncertainty Analysis. *Remote Sens.*, 6, 12070–12093.

Connette, G., Oswald, P., Songer, M. & Leimgruber, P. (2016). Mapping Distinct Forest Types Improves Overall Forest Identification Based on Multi-Spectral Landsat Imagery for Myanmar's Tanintharyi Region. *Remote Sens.*, 8, 882.

Corbane, C., Najman, L., Pecoul, E., Demagistri, L. & Petit, M. (2010). A complete processing chain for ship detection using optical satellite imagery. *Int. J. Remote Sens.*, 31, 5837–5854.

Cord, A. & Rödder, D. (2011). Inclusion of habitat availability in species distribution models through multi-temporal remote-sensing data? *Ecol. Appl.*, 21, 3285–3298.

Cornforth, W., Fatoyinbo, T., Freemantle, T. & Pettorelli, N. (2013). Advanced Land Observing Satellite Phased Array Type L-Band SAR (ALOS PALSAR) to Inform the Conservation of Mangroves: Sundarbans as a Case Study. *Remote Sens.*, 5, 224–237.

Cortés, G., Girotto, M. & Margulis, S.A. (2014). Analysis of sub-pixel snow and ice extent over the extratropical Andes using spectral unmixing of historical Landsat imagery. *Remote Sens. Environ.*, 141, 64–78.

Crist, E.P. & Cicone, R.C. (1984). A Physically-Based Transformation of Thematic Mapper Data—The TM Tasseled Cap. *IEEE Trans. Geosci. Remote Sens.*, GE-22, 256–263.

Cui, B.-L. & Li, X.-Y. (2011). Coastline change of the Yellow River estuary and its response to the sediment and runoff (1976–2005). *Geomorphology*, 127, 32–40.

Dahdouh-Guebas, F., Jayatissa, L.P., Di Nitto, D., Bosire, J.O., Lo Seen, D. & Koedam, N. (2005). How effective were mangroves as a defence against the recent tsunami? *Curr. Biol.*, 15, R443–R447.

Deikumah, J.P., McAlpine, C.A. & Maron, M. (2014). Mining matrix effects on West African rainforest birds. *Biol. Conserv.*, 169, 334–343.

Demšar, U., Harris, P., Brunsdon, C., Fotheringham, A.S. & McLoone, S. (2013). Principal Component Analysis on Spatial Data: An Overview. *Ann. Assoc. Am. Geogr.*, 103, 106–128.

Díaz Varela, R.A., Ramil Rego, P., Calvo Iglesias, S. & Muñoz Sobrino, C. (2008). Automatic habitat classification methods based on satellite images: A practical assessment in the NW Iberia coastal mountains. *Environ. Monit. Assess.*, 144, 229–250.

Dierssen, H.M., Zimmerman, R.C., Drake, L.A. & Burdige, D. (2010). Benthic ecology from space: Optics and net primary production in seagrass and benthic algae across the Great Bahama Bank. *Mar. Ecol. Prog. Ser.*, 411, 1–15.

Donato, D.C., Kauffman, J.B., Murdiyarso, D., Kurnianto, S., Stidham, M. & Kanninen, M. (2011). Mangroves among the most carbon-rich forests in the tropics. *Nat. Geosci.*, 4, 293–297.

Dong, J., Xiao, X., Chen, B., Torbick, N., Jin, C., Zhang, G., *et al.* (2013). Mapping deciduous rubber plantations through integration of PALSAR and multi-temporal Landsat imagery. *Remote Sens. Environ.*, 134, 392–402.

Drusch, M., Del Bello, U., Carlier, S., Colin, O., Fernandez, V., Gascon, F., *et al.* (2012). Sentinel-2: ESA's Optical High-Resolution Mission for GMES Operational Services. *Remote Sens. Environ.*, 120, 25–36.

Dubayah, R. & Drake, J. (2000). Lidar remote sensing for forestry.

Dudka, S. & Adriano, D.C. (1997). Environmental Impacts of Metal Ore Mining and Processing: A Review. *J. Environ. Qual.*, 26, 590.

Duffy, J.E., Richardson, J.P. & Canuel, E.A. (2003). Grazer diversity effects on ecosystem functioning in seagrass beds. *Ecol. Lett.*, 6, 637–645.

Duncan, C., Kretz, D., Wegmann, M., Rabeil, T. & Pettorelli, N. (2014). Oil in the Sahara: mapping anthropogenic threats to Saharan biodiversity from space. *Philos. Trans. R. Soc. B Biol. Sci.*, 369, 20130191–20130191.

Eklundh, L., Johansson, T. & Solberg, S. (2009). Mapping insect defoliation in Scots pine with MODIS time-series data. *Remote Sens. Environ.*, 113, 1566–1573.

Elvidge, C.D. & Chen, Z. (1995). Comparison of broad-band and narrow-band red and near-infrared vegetation indices. *Remote Sens. Environ.*, 54, 38–48.

ESA. (2015). SENTINEL-2 User Handbook.

Evans, T.L., Costa, M., Tomas, W.M. & Camilo, A.R. (2014). Large-scale habitat mapping of the Brazilian Pantanal wetland: A synthetic aperture radar approach. *Remote Sens. Environ.*, 155, 89–108.

Everitt, J.H., Yang, C., Fletcher, R. & Deloach, C.J. (2008). Comparison of QuickBird and SPOT 5 Satellite Imagery for Mapping Giant Reed. *J. Aquat. Plant Manag. J. Aquat. Plant Manag.*, 46, 77–82.114

Fahrig, L. (2003). Effects of Habitat Fragmentation on Biodiversity. *Annu. Rev. Ecol. Evol. Syst.*, 34, 487–515.

Fassnacht, F.E., Latifi, H., Ghosh, A., Joshi, P.K. & Koch, B. (2014). Assessing the potential of hyperspectral imagery to map bark beetle-induced tree mortality. *Remote Sens. Environ.*, 140, 533–548.

Fatoyinbo, T.E., Simard, M., Washington-Allen, R.A. & Shugart, H.H. (2008). Landscape-scale extent, height, biomass, and carbon estimation of Mozambique's mangrove forests with Landsat ETM+ and Shuttle Radar Topography Mission elevation data. *J. Geophys. Res. Biogeosciences*, 113, n/a-n/a.

Fatoyinbo, T.E. & Simard, M. (2013). Height and biomass of mangroves in Africa from ICESat/GLAS and SRTM. *Int. J. Remote Sens.*, 34, 668–681.

Felbier, A., Esch, T., Roth, A., Heldens, W., Taubenböck, H. & Schwinger, M. (2012). The Urban Footprint Processor – Concept and Implementation of a Processing Chain within the TanDEM-X Mission. In: *EUSAR*. pp. 15–18.

Fensholt, R., Horion, S., Tagesson, T., Ehammer, A., Ivits, E. & Rasmussen, K. (2015). Global-scale mapping of changes in ecosystem functioning from earth observation-based trends in total and recurrent vegetation. *Glob. Ecol. Biogeogr.*, 24, 1003– 1017.

Forrest, J.L., Wikramanayake, E., Shrestha, R., Areendran, G., Gyeltshen, K., Maheshwari, A., *et al.* (2012). Conservation and climate change: Assessing the vulnerability of snow leopard habitat to treeline shift in the Himalaya. *Biol. Conserv.*, 150, 129–135.

Fourcade, Y., Engler, J.O., Rödder, D. & Secondi, J. (2014). Mapping Species Distributions with MAXENT Using a Geographically Biased Sample of Presence Data: A Performance Assessment of Methods for Correcting Sampling Bias. *PLoS One*, 9, e97122.

Frazier, P.S., Frazier, P.S., Page, K.J. & Page, K.J. (2000). Water Body Detection and Delineation with Landsat TM Data. *Photogramm. Eng. Remote Sens.*, 66, 1461– 1467.

Freemantle, T.P., Wacher, T., Newby, J. & Pettorelli, N. (2013). Earth observation: overlooked potential to support species reintroduction programmes. *Afr. J. Ecol.*, 51, 482–492.

Fretwell, P.T., LaRue, M.A., Morin, P., Kooyman, G.L., Wienecke, B., Ratcliffe, N., *et al.* (2012). An Emperor Penguin Population Estimate: The First Global, Synoptic Survey of a Species from Space. *PLoS One*, 7, e33751.

Fretwell, P.T., Staniland, I.J. & Forcada, J. (2014). Whales from Space: Counting Southern Right Whales by Satellite. *PLoS One*, 9, e88655.

Friedl, M.A., Sulla-Menashe, D., Tan, B., Schneider, A., Ramankutty, N., Sibley, A., *et al.* (2010). MODIS Collection 5 global land cover: Algorithm refinements and characterization of new datasets. *Remote Sens. Environ.*, 114, 168–182.

Fritz, S., See, L., McCallum, I., Schill, C., Obersteiner, M., van der Velde, M., *et al.* (2011). Highlighting continued uncertainty in global land cover maps for the user community. *Environ. Res. Lett.*, 6, 44005.

Gan, T.Y., Zunic, F., Kuo, C.-C. & Strobl, T. (2012). Flood mapping of Danube River at Romania using single and multi-date ERS2-SAR images. *Int. J. Appl. Earth Obs. Geoinf.*, 18, 69–81.

Gao, B. (1996). NDWI—A normalized difference water index for remote sensing of vegetation liquid water from space. *Remote Sens. Environ.*, 58, 257–266.

Garonna, I., Fazey, I., Brown, M.E. & Pettorelli, N. (2009). Rapid primary productivity changes in one of the last coastal rainforests: The case of Kahua, Solomon Islands. *Environ. Conserv.*, 36, 253–260.

Gavier-Pizarro, G.I., Kuemmerle, T., Hoyos, L.E., Stewart, S.I., Huebner, C.D., Keuler, N.S., *et al.* (2012). Monitoring the invasion of an exotic tree (Ligustrum lucidum) from 1983 to 2006 with Landsat TM/ETM + satellite data and Support Vector Machines in Córdoba, Argentina. *Remote Sens. Environ.*, 122, 134–145.

GCOS. (2010). Implementation plan for the global observing system for climate in support of the UNFCCC. *World Meteorol. Organ.*, GCOS-138-, 180.

Geddes, J.A., Murphy, J.G., O'Brien, J.M. & Celarier, E.A. (2012). Biases in long-term NO2 averages inferred from satellite observations due to cloud selection criteria. *Remote Sens. Environ.*, 124, 210–216.

Ghasemi, N., Sahebi, R. & Mohammadzadeh, A. (2011). A review on biomass estimation methods using synthetic aperture radar data. *Int. J. GEOMATICS Geosci.*, 1.

Ghulam, A., Porton, I. & Freeman, K. (2014). Detecting subcanopy invasive plant species in tropical rainforest by integrating optical and microwave (InSAR/PolInSAR) remote sensing data, and a decision tree algorithm. *ISPRS J. Photogramm. Remote Sens.*, 88, 174–192.

Giglio, L., Schroeder, W. & Justice, C.O. (2016). The collection 6 MODIS active fire detection algorithm and fire products. *Remote Sens. Environ.*, 178, 31–41.

Giri, C., Ochieng, E., Tieszen, L.L., Zhu, Z., Singh, A., Loveland, T., *et al.* (2011). Status and distribution of mangrove forests of the world using earth observation satellite data. *Glob. Ecol. Biogeogr.*, 20, 154–159.

Gleeson, E., College, R., Parkway, N., Neill, C.C. & Fiske, G. (2000). *The effects of winter moth defoliation on forest growth and production inferred from satellite imagery and dendrochronology. Unpubl. Pap.*

Gleyzes, M.A., Perret, L. & Kubik, P. (2012). PLEIADES SYSTEM ARCHITECTURE AND MAIN PERFORMANCES. *ISPRS - Int. Arch. Photogramm. Remote Sens. Spat. Inf. Sci.*, XXXIX-B1, 537–542.

Gohin, F., Saulquin, B., Oger-Jeanneret, H., Lozac'h, L., Lampert, L., Lefebvre, A., *et al.* (2008). Towards a better assessment of the ecological status of coastal waters using satellite-derived chlorophyll-a concentrations. *Remote Sens. Environ.*, 112, 3329–3340.

González Taboada, F. & Anadón, R. (2014). Seasonality of North Atlantic phytoplankton from space: impact of environmental forcing on a changing phenology (1998-2012). *Glob. Chang. Biol.*, 20, 698–712.

Green, E.P., Clark, C.D., Mumby, P.J., Edwards, A.J. & Ellis, A.C. (1998). Remote sensing techniques for mangrove mapping. *Int. J. Remote Sens.*, 19, 935–956.

Green, E.P. (Edmund P. & Edwards, A.J. (2000). *Remote sensing handbook for tropical coastal management*. Unesco Pub.

Guanter, L., Kaufmann, H., Segl, K., Foerster, S., Rogass, C., Chabrillat, S., *et al.* (2015). The EnMAP spaceborne imaging spectroscopy mission for earth observation. *Remote Sens.*

Haack, B. & Bechdol, M. (2000). Integrating multisensor data and RADAR texture measures for land cover mapping. *Comput. Geosci.*, 26, 411–421.

Haddad, N.M., Brudvig, L.A., Clobert, J., Davies, K.F., Gonzalez, A., Holt, R.D., *et al.* (2015). Habitat fragmentation and its lasting impact on Earth's ecosystems. *Sci. Adv.*, 1–9.

Hamdan, O., Khali Aziz, H. & Mohd Hasmadi, I. (2014). L-band ALOS PALSAR for biomass estimation of Matang Mangroves, Malaysia. *Remote Sens. Environ.*, 155, 69–78.

Hansen, M.C. & Loveland, T.R. (2012). A review of large area monitoring of land cover change using Landsat data. *Remote Sens. Environ.*, 122, 66–74.

Hansen, M.C., Potapov, P. V, Moore, R., Hancher, M., Turubanova, S., Tyukavina, A., *et al.* (2013). High-resolution global maps of 21st-century forest cover change. *Science*, 342, 850–853.

Hansen, M.C., Krylov, A., Tyukavina, A., Potapov, P. V, Turubanova, S., Zutta, B., *et al.* (2016). Humid tropical forest disturbance alerts using Landsat data. *Environ. Res. Lett.*, 11, 34008.

Hantson, S., Pueyo, S. & Chuvieco, E. (2015). Global fire size distribution is driven by human impact and climate. *Glob. Ecol. Biogeogr.*, 24, 77–86.

Harvey, E.T., Kratzer, S. & Philipson, P. (2015). Satellite-based water quality monitoring for improved spatial and temporal retrieval of chlorophyll-a in coastal waters. *Remote Sens. Environ.*, 158, 417–430.

He, K.S., Rocchini, D., Neteler, M. & Nagendra, H. (2011). Benefits of hyperspectral remote sensing for tracking plant invasions. *Divers. Distrib.*

He, K.S., Bradley, B.A., Cord, A.F., Rocchini, D., Tuanmu, M.N., Schmidtlein, S., *et al.* (2015). Will remote sensing shape the next generation of species distribution models? *Remote Sens. Ecol. Conserv.*, 1, 4–18.

Hedley, J.D. & Mumby, P.J. (2003). A remote sensing method for resolving depth and subpixel composition of aquatic benthos. *Limnol. Oceanogr.*, 48, 480–488.

Hedley, J.D., Harborne, A.R. & Mumby, P.J. (2005). Simple and robust removal of sun glint for mapping shallow-water benthos. *Int. J. Remote Sens.*, 26, 2107–2112.

Hempson, G.P., Parr, C.L., Archibald, S., Anderson, T.M., Mustaphi, C.J.C., Dobson, A.P., *et al.* (2017). Continent-level drivers of African pyrodiversity. *Ecography (Cop.).*

Herawati, H., González-olabarria, J.R., Wijaya, A., Martius, C., Purnomo, H. & Andriani, R. (2015). Tools for Assessing the Impacts of Climate Variability and Change on Wildfire Regimes in Forests. *Forest*, 6, 1476–1499.

Hermas, E.S., Leprince, S. & El-Magd, I.A. (2012). Retrieving sand dune movements using sub-pixel correlation of multi-temporal optical remote sensing imagery, northwest Sinai Peninsula, Egypt. *Remote Sens. Environ.*, 121, 51–60.

Herold, M. & Johns, T. (2007). Linking requirements with capabilities for deforestation monitoring in the context of the UNFCCC-REDD process. *Environ. Res. Lett.*, 2, 45025.

Herold, M., Mayaux, P., Woodcock, C.E., Baccini, A. & Schmullius, C. (2008). Some challenges in global land cover mapping: An assessment of agreement and accuracy in existing 1 km datasets. *Remote Sens. Environ.*, 112, 2538–2556.

Herold, M., Hirata, Y., Laake, P. Van, Asner, G., Heymell, V. & Román-cuesta, R.M. (2011a). A Review of Methods to Measure and Monitor Historical Forest Degradation. *Unasylva*, 62, 1–31.

Herold, M., Romàn-Cuesta, R.M., Mollicone, D., Hirata, Y., Van Laake, P., Asner, G.P., *et al.* (2011b). Options for monitoring and estimating historical carbon emissions from forest degradation in the context of REDD+. *Carbon Balance Manag.*

Hess, L.L., Melack, J.M., Affonso, A.G., Barbosa, C., Gastil-Buhl, M. & Novo, E.M.L.M. (2015). Wetlands of the Lowland Amazon Basin: Extent, Vegetative Cover, and Dual-season Inundated Area as Mapped with JERS-1 Synthetic Aperture Radar. *Wetlands*, 35, 745–756.

Higginbottom, T.P. & Symeonakis, E. (2014). Assessing land degradation and desertification using vegetation index data: Current frameworks and future directions. *Remote Sens.*

Hong, G., Zhang, A., Zhou, F. & Brisco, B. (2014). Integration of optical and synthetic aperture radar (SAR) images to differentiate grassland and alfalfa in Prairie area. *Int. J. Appl. Earth Obs. Geoinf.*, 28, 12–19.

Hooper, A., Zebker, H., Segall, P. & Kampes, B. (2004). A new method for measuring deformation on volcanoes and other natural terrains using InSAR persistent scatterers. *Geophys. Res. Lett.*, 31, 1–5.

Horning, N. (2004). Selecting the appropriate band combination for an RGB image using Landsat imagery.

Hoyos, L.E., Gavier-Pizarro, G.I., Kuemmerle, T., Bucher, E.H., Radeloff, V.C. & Tecco, P.A. (2010). Invasion of glossy privet (Ligustrum lucidum) and native forest loss in the Sierras Chicas of Córdoba, Argentina. *Biol. Invasions*, 12, 3261–3275.

Hu, C., Lee, Z. & Franz, B. (2012). Chlorophyll a algorithms for oligotrophic oceans: A novel approach based on three-band reflectance difference. *J. Geophys. Res. Ocean.*, 117, n/a-n/a.

Huang, C.-Y. & Asner, G.P. (2009). Applications of remote sensing to alien invasive plant studies. *Sensors (Basel).*, 9, 4869–89.

Huang, C., Wylie, B., Homer, C., Yang, L. & Zylstra, G. (2002). Derivation of a Tasseled cap transformation based on Landsat 7 at-satellite reflectance. *Int. J. Remote Sens.*, 23, 1741–1748.

Huete, A., Didan, K., van Leeuwen, W., Miura, T. & Glenn, E. (2010). MODIS Vegetation Indices. Springer, New York, NY, pp. 579–602.

Huete, A., Didan, K., Miura, T., Rodriguez, E.P., Gao, X. & Ferreira, L.G. (2002). Overview of the radiometric and biophysical performance of the MODIS vegetation indices. *Remote Sens. Environ.*, 83, 195–213.

Imam, E., Kushwaha, S.P.S. & Singh, A. (2009). Evaluation of suitable tiger habitat in Chandoli National Park, India, using spatial modelling of environmental variables. *Ecol. Modell.*, 220, 3621–3629.

Imhoff, M.L. (1995). Theoretical analysis of the effect of forest structure on synthetic aperture radar backscatter and the remote sensing of biomass. *IEEE Trans. Geosci. Remote Sens.*, 33, 341–352.

Intergovernmental Panel on Climate Change (IPCC). (2012). *Managing the Risks of Extreme Events and Disasters to Advance Managing the Risks of Extreme Events and Disasters to Advance Climate Change Adaptation. A Special Report of Working Groups I and II of the Intergovernmental Panel on Climate Change. null.*

Jackson, R.D. & Huete, A.R. (1991). Interpreting vegetation indices. *Prev. Vet. Med.*, 11, 185–200.

Jentsch, A. & Beierkuhnlein, C. (2008). Research frontiers in climate change: Effects of extreme meteorological events on ecosystems. *Comptes Rendus Geosci.*, 340, 621–628.

Jetz, W. & Thau, D. (2018). *Research Blog: Map of Life: A preview of how to evaluate species conservation with Google Earth Engine.* Available at: https://research.googleblog.com/2015/01/map-of-life-preview-of-how-to-evaluate.html. Last accessed 27 January 2018.

de Jong, R., de Bruin, S., de Wit, A., Schaepman, M.E. & Dent, D.L. (2011). Analysis of monotonic greening and browning trends from global NDVI time-series. *Remote Sens. Environ.*, 115, 692–702.

Joppa, L.N., O'Connor, B., Visconti, P., Smith, C., Geldmann, J., Hoffmann, M., *et al.* (2016). Filling in biodiversity threat gaps. *Science*, 352, 416–8.

Joshi, N., Baumann, M., Ehammer, A., Fensholt, R., Grogan, K., Hostert, P., *et al.* (2016). A Review of the Application of Optical and Radar Remote Sensing Data Fusion to Land Use Mapping and Monitoring. *Remote Sens.*, 8, 70.

Kachelriess, D., Wegmann, M., Gollock, M. & Pettorelli, N. (2014). The application of remote sensing for marine protected area management. *Ecol. Indic.*, 36, 169–177.

Karjalainen, M., Kankare, V., Vastaranta, M., Holopainen, M. & Hyyppä, J. (2012). Prediction of plot-level forest variables using TerraSAR-X stereo SAR data. *Remote Sens. Environ.*, 117, 338–347.

De Kauwe, M.G., Disney, M.I., Quaife, T., Lewis, P. & Williams, M. (2011). An assessment of the MODIS collection 5 leaf area index product for a region of mixed coniferous forest. *Remote Sens. Environ.*, 115, 767–780.

Keith, D.A., Rodríguez, J.P., Rodríguez-Clark, K.M., Nicholson, E., Aapala, K., Alonso, A., *et al.* (2013). Scientific Foundations for an IUCN Red List of Ecosystems. *PLoS One*, 8, e62111.

Kennedy, R.E., Yang, Z. & Cohen, W.B. (2010). Detecting trends in forest disturbance and recovery using yearly Landsat time series: 1. LandTrendr - Temporal segmentation algorithms. *Remote Sens. Environ.*, 114, 2897–2910.

Kirwan, M.L. & Megonigal, J.P. (2013). Tidal wetland stability in the face of human impacts and sea-level rise. *Nature*.

Klein, I., Gessner, U. & Kuenzer, C. (2012). Regional land cover mapping and change detection in Central Asia using MODIS time-series. *Appl. Geogr.*, 35, 219–234.

Klemas, V. (2011). Remote Sensing Techniques for Studying Coastal Ecosystems: An Overview. *J. Coast. Res.*, 27, 2–17.

Kloiber, S.M., Brezonik, P.L., Olmanson, L.G. & Bauer, M.E. (2002). A procedure for regional lake water clarity assessment using Landsat multispectral data. *Remote Sens. Environ.*, 82, 38–47.

Knudby, A., Roelfsema, C., Lyons, M., Phinn, S. & Jupiter, S. (2011). Mapping fish community variables by Integrating field and satellite data, object-based image analysis and modeling in a traditional Fijian fisheries management area. *Remote Sens.*, 3, 460–483.

Koh, L.P., Miettinen, J., Liew, S.C. & Ghazoul, J. (2011). Remotely sensed evidence of tropical peatland conversion to oil palm. *Proc. Natl. Acad. Sci.*, 108, 5127–5132.

Kratzer, S. & Vinterhav, C. (2010). Improvement of MERIS level 2 products in baltic sea coastal areas by applying the improved Contrast between Ocean and Land Processor (ICOL) - Data analysis and validation. *Oceanologia*, 52, 211–236.

Kuemmerle, T., Perzanowski, K., Chaskovskyy, O., Ostapowicz, K., Halada, L., Bashta, A.T., *et al.* (2010). European Bison habitat in the Carpathian Mountains. *Biol. Conserv.*, 143, 908–916.

Kuemmerle, T., Perzanowski, K., Radeloff, Volker, C., Piotr, K., Taras, S., Khoyetskyy, P., *et al.* (2011). Predicting potential European bison habitat across its former range. *Ecol. Appl.*, 21, 830–843.

Landmann, T. & Dubovyk, O. (2014). Spatial analysis of human-induced vegetation productivity decline over eastern Africa using a decade (2001-2011) of medium resolution MODIS time-series data. *Int. J. Appl. Earth Obs. Geoinf.*, 33, 76–82.

Lang, M.W., Townsend, P.A. & Kasischke, E.S. (2008). Influence of incidence angle on detecting flooded forests using C-HH synthetic aperture radar data. *Remote Sens. Environ.*, 112, 3898–3907.

Langer, M., Westermann, S., Heikenfeld, M., Dorn, W. & Boike, J. (2013). Satellite-based modeling of permafrost temperatures in a tundra lowland landscape. *Remote Sens. Environ.*, 135, 12–24.

LaRue, M.A., Rotella, J.J., Garrott, R.A., Siniff, D.B., Ainley, D.G., Stauffer, G.E., *et al.* (2011). Satellite imagery can be used to detect variation in abundance of Weddell seals (Leptonychotes weddellii) in Erebus Bay, Antarctica. *Polar Biol.*, 34, 1727–1737.

Latty, R.S., Nelson, R., Markham, B., Williams, D. & Toll, D. (1985). Performance Comparisons Between Information Extraction Techniques Using Variable Spatial Resolution Data, 51, 1459–1470.

Lee, S., Ni-Meister, W., Yang, W. & Chen, Q. (2011). Physically based vertical vegetation structure retrieval from ICESat data: Validation using LVIS in White Mountain National Forest, New Hampshire, USA. *Remote Sens. Environ.*, 115, 2776–2785.

Lefsky, M.A. (2010). A global forest canopy height map from the moderate resolution imaging spectroradiometer and the geoscience laser altimeter system. *Geophys. Res. Lett.*, 37.

Lehmann, C.E.R., Anderson, T.M., Sankaran, M., Higgins, S.I., Archibald, S., Hoffmann, W.A., *et al.* (2014). Savanna vegetation-fire-climate relationships differ among continents. *Science (80-. ).*, 343, 548–552.

Leifer, I., Lehr, W.J., Simecek-Beatty, D., Bradley, E., Clark, R., Dennison, P., *et al.* (2012). State of the art satellite and airborne marine oil spill remote sensing: Application to the BP Deepwater Horizon oil spill. *Remote Sens. Environ.*

Leisher, C., Touval, J., Hess, S.M., Boucher, T.M. & Reymondin, L. (2013). Land and forest degradation inside protected areas in latin america. *Diversity*, 5, 779–795.

Leutner, B. & Wegmann, M. (2016). Pre-processing Remote Sensing Data. In: *Remote Sensing and GIS for Ecologists: Using Open Source Software*. Pelagic Publishing, Exeter, UK.

Li, M., Mao, L., Zhou, C., Vogelmann, J.E. & Zhu, Z. (2010). Comparing forest fragmentation and its drivers in China and the USA with Globcover v2.2. *J. Environ. Manage.*, 91, 2572–2580.

Li, P., Zhang, J. & Feng, Z. (2015). Mapping rubber tree plantations using a Landsat-based phenological algorithm in Xishuangbanna, southwest China. *Remote Sens. Lett.*, 6, 49–58.

Liesenberg, V. & Gloaguen, R. (2012). Evaluating SAR polarization modes at L-band for forest classification purposes in eastern Amazon, Brazil. *Int. J. Appl. Earth Obs. Geoinf.*, 21, 122–135.

Liu, G., Strong, A.E. & Skirving, W. (2003). Remote sensing of sea surface temperatures during 2002 Barrier Reef coral bleaching. *Eos, Trans. Am. Geophys. Union*, 84, 137.

Liu, G., Heron, S.F., Mark Eakin, C., Muller-Karger, F.E., Vega-Rodriguez, M., Guild, L.S., *et al.* (2014). Reef-scale thermal stress monitoring of coral ecosystems: New 5-km global products from NOAA coral reef watch. *Remote Sens.*, 6, 11579–11606.

Lobell, D.B. & Asner, G.P. (2002). Moisture Effects on Soil Reflectance. *Soil Sci. Soc. Am. J.*, 66, 722.

Loh, J., Green, R.E., Ricketts, T., Lamoreux, J., Jenkins, M., Kapos, V., *et al.* (2005). The Living Planet Index: using species population time series to track trends in biodiversity. *Philos. Trans. R. Soc. B Biol. Sci.*, 360, 289–295.

Long, S., Fatoyinbo, T.E. & Policelli, F. (2014). Flood extent mapping for Namibia using change detection and thresholding with SAR. *Environ. Res. Lett.*, 9.

Lönnqvist, A., Rauste, Y., Molinier, M. & Häme, T. (2010). Polarimetric SAR data in land cover mapping in boreal zone. *IEEE Trans. Geosci. Remote Sens.*, 48, 3652–3662.

Louzao, M., Pinaud, D., Péron, C., Delord, K., Wiegand, T. & Weimerskirch, H. (2011). Conserving pelagic habitats: Seascape modelling of an oceanic top predator. *J. Appl. Ecol.*, 48, 121–132.

Loveland, T.R. & Dwyer, J.L. (2012). Landsat: Building a strong future. *Remote Sens. Environ.*, 122, 22–29.

Lu, D., Li, G., Moran, E., Dutra, L. & Batistella, M. (2011). A Comparison of Multisensor Integration Methods for Land Cover Classification in the Brazilian Amazon. *GIScience Remote Sens.*, 48, 345–370.

Lu, D., Chen, Q., Wang, G., Liu, L., Li, G. & Moran, E. (2016). A survey of remote sensing-based aboveground biomass estimation methods in forest ecosystems. *Int. J. Digit. Earth*.

Lucas, R., Rebelo, L.-M., Fatoyinbo, T.E., Rosenqvist, A., Itoh, T., Shimada, M., *et al.* (2014). Contribution of L-band SAR to systematic global mangrove monitoring. *Mar. Freshw. Res.*, 65, 589.

Lyzenga, D.R. (1978). Passive remote sensing techniques for mapping water depth and bottom features. *Appl. Opt.*, 17, 379.

Lyzenga, D.R. (1981). Remote sensing of bottom reflectance and water attenuation parameters in shallow water using aircraft and landsat data. *Int. J. Remote Sens.*, 2, 71–82.

Madritch, M.D., Kingdon, C.C., Singh, A., Mock, K.E., Lindroth, R.L. & Townsend, P.A. (2014). Imaging spectroscopy links aspen genotype with below-ground processes at landscape scales. *Philos. Trans. R. Soc. B Biol. Sci.*, 369, 20130194–20130194.

Manson, F.J., Loneragan, N.R., Skilleter, G.A. & Phinn, S.R. (2005). An evaluation of the evidence for linkages between mangroves and fisheries : A synthesis of the literature and identification of research directions. *Oceanogr. Mar. Biol.*, 43, 31.

Martinez, J.M. & Le Toan, T. (2007). Mapping of flood dynamics and spatial distribution of vegetation in the Amazon floodplain using multitemporal SAR data. *Remote Sens. Environ.*, 108, 209–223.

Di Martino, G., Poderico, M., Poggi, G., Riccio, D. & Verdoliva, L. (2014). Benchmarking Framework for SAR Despeckling. *IEEE Trans. Geosci. Remote Sens.*, 52, 1596–1615.

Marvin, D.C., Koh, L.P., Lynam, A.J., Wich, S., Davies, A.B., Krishnamurthy, R., *et al.* (2016). Integrating technologies for scalable ecology and conservation. *Glob. Ecol. Conserv.*

Matson, M. & Dozier, J. (1981). Identification of subresolution high temperature sources using a thermal IR sensor. *Photogramm. Eng. Remote Sensing*, 47, 1311–1318.

Matthews, M.W., Bernard, S. & Winter, K. (2010). Remote sensing of cyanobacteria-dominant algal blooms and water quality parameters in Zeekoevlei, a small hypertrophic lake, using MERIS. *Remote Sens. Environ.*, 114, 2070–2087.

Mattia, F., Satalino, G., Balenzano, A., Rinaldi, M., Steduto, P. & Moreno, J. (2015). Sentinel-1 for wheat mapping and soil moisture retrieval. In: *2015 IEEE International Geoscience and Remote Sensing Symposium (IGARSS)*. IEEE, pp. 2832–2835.

Mayaux, P., Pekel, J.F., Desclée, B., Donnay, F., Lupi, A., Achard, F., *et al.* (2013). State and evolution of the African rainforests between 1990 and 2010. *Philos. Trans. R. Soc. Lond. B. Biol. Sci.*, 368, 20120300.

McDonald, K.C., Chapman, B., Podest, E., Schroeder, R., Flores, S., Willacy, K., *et al.* (2011). Monitoring inundated wetlands ecosystems with satellite microwave remote sensing in support of earth system science research. *34th Int. Symp. Remote Sens. Environ. - GEOSS Era Towar. Oper. Environ. Monit.*, 1–4.

McGarigal, K. (2015). Fragstats Help.Melin, M., Shapiro, A.C. & Glover-kapfer, P. (2017). *Lidar for Ecology and Conservation. WWF Conserv. Technol. Ser.*

Mermoz, S., Le Toan, T., Villard, L., Réjou-Méchain, M. & Seifert-Granzin, J. (2014). Biomass assessment in the Cameroon savanna using ALOS PALSAR data. *Remote Sens. Environ.*, 155, 109–119.

Miettinen, J., Shimabukuro, Y.E., Beuchle, R., Grecchi, R.C., Gomez, M.V., Simonetti, D., *et al.* (2016). On the extent of fire-induced forest degradation in Mato Grosso, Brazilian Amazon, in 2000, 2005 and 2010. *Int. J. Wildl. Fire*, 25, 129–136.

Miller, S.D., Straka, W., Mills, S.P., Elvidge, C.D., Lee, T.F., Solbrig, J., *et al.* (2013). Illuminating the capabilities of the suomi national Polar-orbiting partnership (NPP) visible infrared imaging radiometer suite (VIIRS) day/night Band. *Remote Sens.*, 5, 6717–6766.

Mollicone, D., Eva, H.D. & Achard, F. (2006). Ecology: Human role in Russian wild fires. *Nature*, 440, 436–437.

Morain, S.A. (1998). *People and Pixels.* National Academies Press, Washington, D.C.

Moreira, A., Prats-Iraola, P., Younis, M., Krieger, G., Hajnsek, I. & Papathanassiou, K.P. (2013). A tutorial on synthetic aperture radar. *IEEE Geosci. Remote Sens. Mag.*, 1, 6–43.

Morel, A.C., Saatchi, S.S., Malhi, Y., Berry, N.J., Banin, L., Burslem, D., *et al.* (2011). Estimating aboveground biomass in forest and oil palm plantation in Sabah, Malaysian Borneo using ALOS PALSAR data. *For. Ecol. Manage.*, 262, 1786–1798.

Morrison, M.L., Marcot, B.G. & Mannan, R.W. (2006). *Wildlife-habitat relationships : concepts and applications.*

Morton, D.C., Nagol, J., Carabajal, C.C., Rosette, J., Palace, M., Cook, B.D., *et al.* (2014). Amazon forests maintain consistent canopy structure and greenness during the dry season. *Nature*, 506, 221–224.

Myneni, R.B. (1997). Estimation of global leaf area index and absorbed par using radiative transfer models. *IEEE Trans. Geosci. Remote Sens.*, 35, 1380–1393.

Nagendra, H., Pareeth, S., Sharma, B., Schweik, C.M. & Adhikari, K.R. (2008). Forest fragmentation and regrowth in an institutional mosaic of community, government and private ownership in Nepal. In: *Landscape Ecology*. Springer Netherlands, pp. 41–54.

Nagendra, H., Lucas, R., Honrado, J.P., Jongman, R.H.G., Tarantino, C., Adamo, M., *et al.* (2013). Remote sensing for conservation monitoring: Assessing protected areas, habitat extent, habitat condition, species diversity, and threats. *Ecol. Indic.*, 33, 45–59.

Nathan, R., Schurr, F.M., Spiegel, O., Steinitz, O., Trakhtenbrot, A. & Tsoar, A. (2008). Mechanisms of long-distance seed dispersal. *Trends Ecol. Evol.*

Nayegandhi, A. (2006). Green, waveform lidar in topo-bathy mapping – Principles and Applications.

NOAA/NESDIS. (2014). *Table of of contents. NOAA KLM User's Guid.* Available at: https://www1.ncdc.noaa.gov/pub/data/satellite/publications/podguides/N-15 thru N-19/pdf/0.0 NOAA KLM Users Guide.pdf. Last accessed 28 January 2018.

Nordin, A., Strengbom, J., Witzell, J., Näsholm, T. & Ericson, L. (2005). Nitrogen Deposition and the Biodiversity of Boreal Forests: Implications for the Nitrogen Critical Load. *AMBIO A J. Hum. Environ.*, 34, 20–24.

Ollinger, S. V. & Smith, M.-L. (2005). Net Primary Production and Canopy Nitrogen in a Temperate Forest Landscape: An Analysis Using Imaging Spectroscopy, Modeling and Field Data. *Ecosystems*, 8, 760–778.

Olofsson, P., Foody, G.M., Herold, M., Stehman, S. V, Woodcock, C.E. & Wulder, M.A. (2014). Good practices for estimating area and assessing accuracy of land change. *Remote Sens. Environ.*, 148, 42–57.

Oom, D. & Pereira, J.M.C. (2012). Exploratory spatial data analysis of global MODIS active fire data. *Int. J. Appl. Earth Obs. Geoinf.*, 21, 326–340.

Palmer, S.C.J., Hunter, P.D., Lankester, T., Hubbard, S., Spyrakos, E., N. Tyler, A., *et al.* (2015). Validation of Envisat MERIS algorithms for chlorophyll retrieval in a large, turbid and optically-complex shallow lake. *Remote Sens. Environ.*, 157, 158–169.

Paloscia, S., Pettinato, S., Santi, E., Notarnicola, C., Pasolli, L. & Reppucci, A. (2013). Soil moisture mapping using Sentinel-1 images: Algorithm and preliminary validation. *Remote Sens. Environ.*, 134, 234–248.

Parmesan, C. (2006). Ecological and Evolutionary Responses to Recent Climate Change. *Annu. Rev. Ecol. Evol. Syst.*, 37, 637–669.

Parviainen, M., Zimmermann, N.E., Heikkinen, R.K. & Luoto, M. (2013). Using unclassified continuous remote sensing data to improve distribution models of red-listed plant species. *Biodivers. Conserv.*, 22, 1731–1754.

Pasher, J., Smith, P.A., Forbes, M.R. & Duffe, J. (2014). Terrestrial ecosystem monitoring in Canada and the greater role for integrated earth observation. *Environ. Rev.*, 22, 179–187.

Pasquarella, V.J., Bradley, B.A. & Woodcock, C.E. (2017). Near-real-time monitoring of insect defoliation using Landsat time series. *Forests*, 8, 275.

Pasquarella, V.J., Holden, C.E., Kaufman, L. & Woodcock, C.E. (2016). From imagery to ecology: leveraging time series of all available Landsat observations to map and monitor ecosystem state and dynamics. *Remote Sens. Ecol. Conserv.*, 2, 152–170.

Patterson, P. & Healey, S. (2015). Global ecosystem dynamics investigation (GEDI) LiDAR sampling strategy. In: *Pushing boundaries: new directions in inventory techniques and applications: Forest Inventory and Analysis (FIA) symposium 2015* (eds. Stanton, S.M. & Christensen, G.). U.S. Department of Agriculture, Forest Service, Pacific Northwest Research Station, Portland, OR., p. 245.

Pe'eri, S., Morgan, L. V., Philpot, W.D. & Armstrong, A.A. (2011). Land-Water Interface Resolved from Airborne LIDAR Bathymetry (ALB) Waveforms. *J. Coast. Res.*, 62, 75–85.

Pearson, J. & Stewart, G.R. (1993). The deposition of atmospheric ammonia and its effects on plants. *New Phytol.*, 125, 283–305.

Pekel, J.-F., Cottam, A., Gorelick, N. & Belward, A.S. (2016). High-resolution mapping of global surface water and its long-term changes. *Nature*, 540, 418–422.

Pennec, A., Gond, V.R. & Sabatier, D. (2011). Tropical forest phenology in French Guiana from MODIS time series. *Remote Sens. Lett.*, 2, 337–345.

Pereira, H.M., Ferrier, S., Walters, M., Geller, G.N., Jongman, R.H.G., Scholes, R.J., *et al.* (2013). Essential biodiversity variables. *Science (80-. ).*

Pettorelli, N., Vik, J.O., Mysterud, A., Gaillard, J.M., Tucker, C.J. & Stenseth, N.C. (2005). Using the satellite-derived NDVI to assess ecological responses to environmental change. *Trends Ecol. Evol.*

Pettorelli, N., Chauvenet, A.L.M., Duffy, J.P., Cornforth, W.A., Meillere, A. & Baillie, J.E.M. (2012). Tracking the effect of climate change on ecosystem functioning using protected areas: Africa as a case study. *Ecol. Indic.*, 20, 269–276.

Pettorelli, N. (2013). *The Normalized Difference Vegetation Index. Norm. Differ. Veg. Index.* Oxford University Press, Oxford, UK.

Pettorelli, N., Laurance, W.F., O'Brien, T.G., Wegmann, M., Nagendra, H. & Turner, W. (2014a). Satellite remote sensing for applied ecologists: Opportunities and challenges. *J. Appl. Ecol.*

Pettorelli, N., Safi, K. & Turner, W. (2014b). Satellite remote sensing, biodiversity research and conservation of the future. *Philos. Trans. R. Soc. B Biol. Sci.*, 369, 20130190– 20130190.

Pettorelli, N., Nagendra, H., Williams, R., Rocchini, D. & Fleishman, E. (2015). A new platform to support research at the interface of remote sensing, ecology and conservation. *Remote Sens. Ecol. Conserv.*, 1, 1–3.

Pettorelli, N., Wegmann, M., Skidmore, A., Mücher, S., Dawson, T.P., Fernandez, M., *et al.* (2016). Framing the concept of satellite remote sensing essential biodiversity variables: challenges and future directions. *Remote Sens. Ecol. Conserv.*, 2, 122–131.

Pettorelli, N., Schulte to Bühne, H., Tulloch, A., Dubois, G., Macinnis-Ng, C., Queirós, A.M., *et al.* (2017). Satellite remote sensing of ecosystem functions: opportunities, challenges and way forward. *Remote Sens. Ecol. Conserv.*

Pickett, S.T.A. & Cadenasso, M.L. (2002). The ecosystem as a multidimensional concept: Meaning, model, and metaphor. *Ecosystems.*

Piñeiro, G., Paruelo, J.M., Oesterheld, M. & Jobbágy, E.G. (2010). Pathways of grazing effects on soil organic carbon and nitrogen. *Rangel. Ecol. Manag.*, 63, 109–119.

Pittiglio, C., Skidmorea, A.K., van Gils, H.A.M.J. & Prins, H.H.T. (2012). Identifying transit corridors for elephant using a long time-series. *Int. J. Appl. Earth Obs. Geoinf.*, 14, 61–72.

Platnick, S., King, M.D., Meyer, K.G., Wind, G., Amarasinghe, N., Marchant, B., *et al.* (2014). MODIS Cloud Optical Properties: User Guide for the Collection 6 Level-2 MOD06/MYD06 Product and Associated Level-3 Datasets. *Version 0.9*, 17, 141.

Platonov, N.G., Mordvintsev, I.N. & Rozhnov, V. V. (2013). The possibility of using high resolution satellite images for detection of marine mammals. *Biol. Bull.*, 40, 197–205.

Potapov, P., Yaroshenko, A., Turubanova, S., Dubinin, M., Laestadius, L., Thies, C., *et al.* (2008). Mapping the world's intact forest landscapes by remote sensing. *Ecol. Soc.*, 13.

Potapov, P. V., Turubanova, S.A., Hansen, M.C., Adusei, B., Broich, M., Altstatt, A., *et al.* (2012). Quantifying forest cover loss in Democratic Republic of the Congo, 2000-2010, with Landsat ETM+ data. *Remote Sens. Environ.*, 122, 106–116.

Pouteau, R., Stoll, B. & Chabrier, S. (2010). Support vector machine fusion of multisensor imagery in tropical ecosystems. In: *2010 2nd International Conference on Image Processing Theory, Tools and Applications, IPTA 2010*. IEEE, pp. 325–329.

Prati, C., Ferretti, A. & Perissin, D. (2010). Recent advances on surface ground deformation measurement by means of repeated space-borne SAR observations. *J. Geodyn.*, 49, 161–170.

Press, A. & Laliberte, S. (2003). Automated wildlife counts from remotely sensed imagery. *Wildl. Soc. Bull.*, 31, 362–371.

Prospere, K., McLaren, K. & Wilson, B. (2014). Plant species discrimination in a tropical wetland using in situ hyperspectral data. *Remote Sens.*, 6, 8494–8523.

Rahman, M.M. & Sumantyo, J.T.S. (2010). Mapping tropical forest cover and deforestation using synthetic aperture radar (SAR) images. *Appl. Geomatics*, 2, 113–121.

Raitsos, D.E., Lavender, S.J., Maravelias, C.D., Haralabous, J., Richardson, A.J. & Reid, P.C. (2008). Identifying four phytoplankton functional types from space: An ecological approach. *Limnol. Oceanogr.*, 53, 605–613.

Ramírez, F., Afán, I., Hobson, K.A., Bertellotti, M., Blanco, G. & Forero, M.G. (2014). Natural and anthropogenic factors affecting the feeding ecology of a top marine predator, the Magellanic penguin. *Ecosphere*, 5, art38.

Rautiainen, M., Heiskanen, J. & Korhonen, L. (2012). Seasonal changes in canopy leaf area index and MODIS vegetation products for a boreal forest site in central Finland. *Boreal Environ. Res.*, 17, 72–84.

Reiche, J., de Bruin, S., Hoekman, D., Verbesselt, J. & Herold, M. (2015a). A Bayesian approach to combine landsat and ALOS PALSAR time series for near real-time deforestation detection. *Remote Sens.*, 7, 4973–4996.

Reiche, J., Verbesselt, J., Hoekman, D. & Herold, M. (2015b). Fusing Landsat and SAR time series to detect deforestation in the tropics. *Remote Sens. Environ.*, 156, 276–293.

Richardson, G., Schmitt, K., Covert, M. & Rogers, C. (2015). Small Satellite Trends 2009-2013. *Proc. AIAA/USU Conf. Small Satell.*, SSC15-VII-3.

Richter, R. & Schläpfer, D. (2016). *Atmospheric / Topographic Correction for Satellite Imagery (ATCOR - 2/3 User Guide). ATCOR-2/3 User Guid. Version 6.3.* ReSe Applications Schläpfer, Wil, Switzerland.

Rickbeil, G.J.M., Coops, N.C. & Adamczewski, J. (2015). The grazing impacts of four barren ground caribou herds (Rangifer tarandus groenlandicus) on their summer ranges: An application of archived remotely sensed vegetation productivity data. *Remote Sens. Environ.*, 164, 314–323.

Riitters, K., Wickham, J., Costanza, J.K. & Vogt, P. (2016). A global evaluation of forest interior area dynamics using tree cover data from 2000 to 2012. *Landsc. Ecol.*, 31, 137–148.

Rocchini, D. & Neteler, M. (2012). Let the four freedoms paradigm apply to ecology. *Trends Ecol. Evol.*

Rocchini, D., Leutner, B. & Wegmann, M. (2016a). From Spectral to Ecological Information. In: *Remote Sensing and GIS for Ecologists: Using Open Source Software*. Pelagic Publishing, Exeter, UK, pp. 150–165.

Rocchini, D., Wegmann, M., Leutner, B. & Bevanda, M. (2016b). Spatial Land Cover Pattern Analysis. In: *Remote Sensing and GIS for Ecologists: Using open source software* (eds. Wegmann, M., Leutner, B. & Dech, S.). Pelagic Publishing, Exeter, UK.

Roelfsema, C.M., Phinn, S.R., Udy, N. & Maxwell, P. (2009). An integrated field and remote sensing approach for mapping seagrass cover, moreton bay, Australia. *J. Spat. Sci.*, 54, 45–62.

Rojas, O., Vrieling, A. & Rembold, F. (2011). Assessing drought probability for agricultural areas in Africa with coarse resolution remote sensing imagery. *Remote Sens. Environ.*, 115, 343–352.

Romijn, E., Lantican, C.B., Herold, M., Lindquist, E., Ochieng, R., Wijaya, A., *et al.* (2015). Assessing change in national forest monitoring capacities of 99 tropical countries. *For. Ecol. Manage.*, 352, 109–123.

Roura-Pascual, N., Suarez, A. V., Gomez, C., Pons, P., Touyama, Y., Wild, A.L., *et al.* (2004). Geographical potential of Argentine ants (Linepithema humile Mayr) in the face of global climate change. *Proc. R. Soc. B Biol. Sci.*, 271, 2527–2535.

Roy, D.P., Boschetti, L., Justice, C.O. & Ju, J. (2008a). The collection 5 MODIS burned area product - Global evaluation by comparison with the MODIS active fire product. *Remote Sens. Environ.*, 112, 3690–3707.

Roy, D.P., Ju, J., Lewis, P., Schaaf, C., Gao, F., Hansen, M., *et al.* (2008b). Multi-temporal MODIS-Landsat data fusion for relative radiometric normalization, gap filling, and prediction of Landsat data. *Remote Sens. Environ.*, 112, 3112–3130.

Roy, D.P., Wulder, M.A., Loveland, T.R., C.E., W., Allen, R.G., Anderson, M.C., *et al.* (2014). Landsat-8: Science and product vision for terrestrial global change research. *Remote Sens. Environ.*, 145, 154–172.

Running, S.W., Nemani, R.R., Heinsch, F.A., Zhao, M., Reeves, M. & Hashimoto, H. (2004). A Continuous Satellite-Derived Measure of Global Terrestrial Primary Production. *Bioscience*, 54, 547.

Saatchi, S., Buermann, W., ter Steege, H., Mori, S. & Smith, T.B. (2008). Modeling distribution of Amazonian tree species and diversity using remote sensing measurements. *Remote Sens. Environ.*, 112, 2000–2017.

Sala, O.E., Chapin, F.S., Armesto, J.J., Berlow, E., Bloomfield, J., Dirzo, R., *et al.* (2000). Global biodiversity scenarios for the year 2100. *Science (80-. ).*

Salajanu, D. & Olson Jr., C.E. (2001). The Significance of Spatial Resolution: Identifying Forest Cover from Satellite Data. *J. For.*, 99, 32–38.

Sanderson, E.W., Jaiteh, M., A., L.M., Redford, K.H., Wannebo, A. V. & Woolmer, G. (2002). The Human Footprint and the Last of the Wild. *Bioscience.*

Saura, S. (2004). Effects of remote sensor spatial resolution and data aggregation on selected fragmentation indices. *Landsc. Ecol.*, 19, 197–209.

Sawaya, K.E., Olmanson, L.G., Heinert, N.J., Brezonik, P.L. & Bauer, M.E. (2003). Extending satellite remote sensing to local scales: Land and water resource monitoring using high-resolution imagery. *Remote Sens. Environ.*, 88, 144–156.

Sayre, R., Dangermond, J., Frye, C., Vaughan, R., Aniello, P., Breyer, S.P., *et al.* (2014). *A new map of global ecological land units : an ecophysiographic stratification approach.*

Schaap, M., Kranenburg, R., Curier, L., Jozwicka, M., Dammers, E. & Timmermans, R. (2013). Assessing the sensitivity of the OMI-NO2 product to emission changes across europe. *Remote Sens.*, 5, 4187–4208.

Schmidt, G., Jenkerson, C., Masek, J., Vermote, E. & Gao, F. (2013). Landsat Ecosystem Disturbance Adaptive Processing System (LEDAPS) Algorithm Description. *Open-file Rep. 2013-1057*, 1–27.

Schroeder, T.A., Cohen, W.B., Song, C., Canty, M.J. & Yang, Z. (2006). Radiometric correction of multi-temporal Landsat data for characterization of early successional forest patterns in western Oregon. *Remote Sens. Environ.*, 103, 16–26.

Schulte to Bühne, H. & Pettorelli, N. (2017). Better together: Integrating and fusing multispectral and radar satellite imagery to inform biodiversity monitoring, ecological research and conservation science. *Methods Ecol. Evol.*

Schulte to Bühne, H., Wegmann, M., Durant, S.M., Ransom, C., de Ornellas, P., Grange, S., *et al.* (2017). Protection status and national socio-economic context shape land conversion in and around a key transboundary protected area complex in West Africa. *Remote Sens. Ecol. Conserv.*, 3, 190–201.

Schuur, E.A.G., Vogel, J.G., Crummer, K.G., Lee, H., Sickman, J.O. & Osterkamp, T.E. (2009). The effect of permafrost thaw on old carbon release and net carbon exchange from tundra. *Nature*, 459, 556–559.

Senf, C., Pflugmacher, D., Wulder, M.A. & Hostert, P. (2015). Characterizing spectral-temporal patterns of defoliator and bark beetle disturbances using Landsat time series. *Remote Sens. Environ.*, 170, 166–177.

Senf, C., Pflugmacher, D., Hostert, P. & Seidl, R. (2017). Using Landsat time series for characterizing forest disturbance dynamics in the coupled human and natural systems of Central Europe. *ISPRS J. Photogramm. Remote Sens.*, 130, 453–463.

Shapiro, A.C., Trettin, C., Küchly, H., Alavinapanah, S. & Bandeira, S. (2015). The Mangroves of the Zambezi Delta: Increase in Extent Observed via Satellite from 1994 to 2013. *Remote Sens.*, 7, 16504–16518.

Shapiro, A.C., Aguilar-Amuchastegui, N., Hostert, P. & Bastin, J.F. (2016). Using fragmentation to assess degradation of forest edges in Democratic Republic of Congo. *Carbon Balance Manag.*, 11.

Sheng, Y. & Alsdorf, D.E. (2005). Automated georeferencing and orthorectification of amazon basin-wide SAR mosaics using SRTM DEM data. *IEEE Trans. Geosci. Remote Sens.*, 43, 1929–1940.

Shepherd, J.D. & Dymond, J.R. (2003). Correcting satellite imagery for the variance of reflectance and illumination with topography. *Int. J. Remote Sens.*, 24, 3503–3514.

Shirley, S.M., Yang, Z., Hutchinson, R.A., Alexander, J.D., Mcgarigal, K. & Betts, M.G. (2013). Species distribution modelling for the people: Unclassified landsat TM imagery predicts bird occurrence at fine resolutions. *Divers. Distrib.*, 19, 855–866.

Siegel, D.A., Behrenfeld, M.J., Maritorena, S., McClain, C.R., Antoine, D., Bailey, S.W., *et al.* (2013). Regional to global assessments of phytoplankton dynamics from the SeaWiFS mission. *Remote Sens. Environ.*, 135, 77–91.

Simard, M., Pinto, N., Fisher, J.B. & Baccini, A. (2011). Mapping forest canopy height globally with spaceborne lidar. *J. Geophys. Res. Biogeosciences*, 116.

Simmons, J.A., Currie, W.S., Eshleman, K.N., Kuers, K., Monteleone, S., Negley, T.L., *et al.* (2008). Forest to reclaimed mine land use change leads to altered ecosystem structure and function. *Ecol. Appl.*, 18, 104–118.

Singh, N.J. & Milner-Gulland, E.J. (2011). Conserving a moving target: Planning protection for a migratory species as its distribution changes. *J. Appl. Ecol.*, 48, 35–46.

Sinha, S., Jeganathan, C., Sharma, L.K. & Nathawat, M.S. (2015). A review of radar remote sensing for biomass estimation. *Int. J. Environ. Sci. Technol.*

Skakun, S., Kussul, N., Shelestov, A. & Kussul, O. (2014). Flood Hazard and Flood Risk Assessment Using a Time Series of Satellite Images: A Case Study in Namibia. *Risk Anal.*, 34, 1521–1537.

Small, D. (2011). Flattening gamma: Radiometric terrain correction for SAR imagery. *IEEE Trans. Geosci. Remote Sens.*, 49, 3081–3093.

Sola, I., González-Audícana, M. & Álvarez-Mozos, J. (2016). Multi-criteria evaluation of topographic correction methods. *Remote Sens. Environ.*, 184, 247–262.

Solberg, S., Næsset, E., Gobakken, T. & Bollandsås, O.M. (2014). Forest biomass change estimated from height change in interferometric SAR height models. *Carbon Balance Manag.*, 9.

Souza, C.M. & Roberts, D.A. (2005). Multitemporal Analysis of Degraded Forests in the Southern Brazilian Amazon. *Earth Interact.*, 9, 1–25.

Souza, C.M., Roberts, D.A. & Cochrane, M.A. (2005). Combining spectral and spatial information to map canopy damage from selective logging and forest fires. *Remote Sens. Environ.*, 98, 329–343.

St-Louis, V., Pidgeon, A.M., Kuemmerle, T., Sonnenschein, R., Radeloff, V.C., Clayton, M.K., *et al.* (2014). Modelling avian biodiversity using raw, unclassified satellite imagery. *Philos. Trans. R. Soc. B Biol. Sci.*, 369, 20130197–20130197.

Stabach, J.A., Rabeil, T., Turmine, V., Wacher, T., Mueller, T. & Leimgruber, P. (2017). On the brink of extinction—Habitat selection of addax and dorcas gazelle across the Tin Toumma desert, Niger. *Divers. Distrib.*, 23, 581–591.

Stapleton, S., LaRue, M., Lecomte, N., Atkinson, S., Garshelis, D., Porter, C., *et al.* (2014). Polar bears from space: Assessing satellite imagery as a tool to track arctic wildlife. *PLoS One*, 9.

Stiling, P. & Cornelissen, T. (2005). What makes a successful biocontrol agent? A meta-analysis of biological control agent performance. *Biol. Control.*

Storey, J., Choate, M. & Lee, K. (2014). Landsat 8 operational land imager on-orbit geometric calibration and performance. *Remote Sens.*, 6, 11127–11152.

Suárez, E., Morales, M., Cueva, R., Bucheli, U. V., Zapata-Ríos, G., Toral, E., *et al.* (2009). Oil industry, wild meat trade and roads: Indirect effects of oil extraction activities in a protected area in north-eastern Ecuador. *Anim. Conserv.*, 12, 364–373.

Swenson, J.J., Carter, C.E., Domec, J.C. & Delgado, C.I. (2011). Gold mining in the peruvian amazon: Global prices, deforestation, and mercury imports. *PLoS One*, 6.

De Sy, V., Herold, M., Achard, F., Asner, G.P., Held, A., Kellndorfer, J., *et al.* (2012). Synergies of multiple remote sensing data sources for REDD+ monitoring. *Curr. Opin. Environ. Sustain.*

Tang, H., Brolly, M., Zhao, F., Strahler, A.H., Schaaf, C.L., Ganguly, S., *et al.* (2014). Deriving and validating Leaf Area Index (LAI) at multiple spatial scales through lidar remote sensing: A case study in Sierra National Forest, CA. *Remote Sens. Environ.*, 143, 131–141.

Taubenböck, H., Esch, T., Felbier, A., Wiesner, M., Roth, A. & Dech, S. (2012). Monitoring urbanization in mega cities from space. *Remote Sens. Environ.*, 117, 162–176.

Teixeira, L., Nilsson, M., Hedley, J. & Shapiro, A. (2015). Benthic habitat mapping and biodiversity analysis in the Primeiras and Segundas archipelago reserve. In: *International Archives of the Photogrammetry, Remote Sensing and Spatial Information Sciences - ISPRS Archives*. pp. 1009–1016.

Teixeira, L., Hedley, J., Shapiro, A. & Barker, K. (2016). Comparison of Two Independent Mapping Exercises in the Primeiras and Segundas Archipelago, Mozambique. *Remote Sens.*, 8, 52.

Théau, J., Peddle, D.R. & Duguay, C.R. (2005). Mapping lichen in a caribou habitat of Northern Quebec, Canada, using an enhancement-classification method and spectral mixture analysis. *Remote Sens. Environ.*, 94, 232–243.

Thomas, N., Lucas, R., Itoh, T., Simard, M., Fatoyinbo, T.E., Bunting, P., *et al.* (2014). An approach to monitoring mangrove extents through time-series comparison of JERS- 1 SAR and ALOS PALSAR data. *Wetl. Ecol. Manag.*, 23, 3–17.

Le Toan, T., Quegan, S., Davidson, M.W.J., Balzter, H., Paillou, P., Papathanassiou, K., *et al.* (2011). The BIOMASS mission: Mapping global forest biomass to better understand the terrestrial carbon cycle. *Remote Sens. Environ.*, 115, 2850–2860.

Townsend, P.A., Helmers, D.P., Kingdon, C.C., McNeil, B.E., de Beurs, K.M. & Eshleman, K.N. (2009). Changes in the extent of surface mining and reclamation in the Central Appalachians detected using a 1976-2006 Landsat time series. *Remote Sens. Environ.*, 113, 62–72.

Traganos, D., Cerra, D. & Reinartz, P. (2017). Cubesat-derived detection of seagrasses using planet imagery following unmixing-based denoising: Is small the next big? In: *International Archives of the Photogrammetry, Remote Sensing and Spatial Information Sciences - ISPRS Archives*. pp. 283–287.

Tripathi, R., Sahoo, R.N., Gupta, V.K., Sehgal, V.K. & Sahoo, P.M. (2013). Developing Vegetation Health Index from biophysical variables derived using MODIS satellite data in the Trans-Gangetic plains of India. *Emirates J. Food Agric.*, 25, 376–384.

Tropek, R., Sedláček, O., Beck, J., Keil, P., Musilová, Z., Símová, I., *et al.* (2014). Comment on "High-resolution global maps of 21st-century forest cover change". *Science*, 344, 981.

Trujillo, P., Piroddi, C. & Jacquet, J. (2012). Fish farms at Sea: The ground truth from Google Earth. *PLoS One*, 7.

Tsendbazar, N.E., de Bruin, S., Mora, B., Schouten, L. & Herold, M. (2016). Comparative assessment of thematic accuracy of GLC maps for specific applications using existing reference data. *Int. J. Appl. Earth Obs. Geoinf.*, 44, 124–135.

Tuanmu, M.N., Viña, A., Bearer, S., Xu, W., Ouyang, Z., Zhang, H., *et al.* (2010). Mapping understory vegetation using phenological characteristics derived from remotely sensed data. *Remote Sens. Environ.*, 114, 1833–1844.

Tucker, C.J. (1979). Red and photographic infrared linear combinations for monitoring vegetation. *Remote Sens. Environ.*, 8, 127–150.

Tucker, C.J. (1980). Remote sensing of leaf water content in the near infrared. *Remote Sens. Environ.*, 10, 23–32.

Tucker, C.J., Compton, J., Grant, D.M. & Dykstra, J.D. (2004). NASA's Global Orthorectified Landsat data set. *Am. Soc. Photogramm. Remote Sens.*, 70, 313–322.

Tulloch, V.J.D., Tulloch, A.I.T., Visconti, P., Halpern, B.S., Watson, J.E.M., Evans, M.C., *et al.* (2015). Why do We map threats? Linking threat mapping with actions to make better conservation decisions. *Front. Ecol. Environ.*

Turner, W., Rondinini, C., Pettorelli, N., Mora, B., Leidner, A.K., Szantoi, Z., *et al.* (2015). Free and open-access satellite data are key to biodiversity conservation. *Biol. Conserv.*, 182, 173–176.

Tüshaus, J., Dubovyk, O., Khamzina, A. & Menz, G. (2014). Comparison of medium spatial resolution ENVISAT-MERIS and terra-MODIS time series for vegetation decline analysis: A case study in central Asia. *Remote Sens.*, 6, 5238–5256.

Urbazaev, M., Thiel, C., Mathieu, R., Naidoo, L., Levick, S.R., Smit, I.P.J., *et al.* (2015). Assessment of the mapping of fractional woody cover in southern African savannas using multi-temporal and polarimetric ALOS PALSAR L-band images. *Remote Sens. Environ.*, 166, 138–153.

USGS. (2015). *AST_L1T Product User's Guide.*

USGS. (2016). *Landsat 8 (L8) Data Users Handbook. America (NY).*

USGS. (2017a). *LANDSAT 4-7 Surface Reflectance (LEDAPS) Product.*

USGS. (2017b). *Product guide Landsat 8 surface reflectance code (LASRC) product. Dep. Inter. U.S. Geol. Surv.*

Vågen, T.-G., Winowiecki, L.A., Tondoh, J.E., Desta, L.T. & Gumbricht, T. (2016). Mapping of soil properties and land degradation risk in Africa using MODIS reflectance. *Geoderma*, 263, 216–225.

Vanonckelen, S., Lhermitte, S. & Van Rompaey, A. (2013). The effect of atmospheric and topographic correction methods on land cover classification accuracy. *Int. J. Appl. Earth Obs. Geoinf.*, 24, 9–21.

Venter, O., Sanderson, E.W., Magrach, A., Allan, J.R., Beher, J., Jones, K.R., *et al.* (2016). Sixteen years of change in the global terrestrial human footprint and implications for biodiversity conservation. *Nat. Commun.*, 7.

Verbesselt, J., Hyndman, R., Newnham, G. & Culvenor, D. (2010). Detecting trend and seasonal changes in satellite image time series. *Remote Sens. Environ.*, 114, 106–115.

Vermote S.Y. Kotchenova and J.P. Ray, E.F. (2011). MODIS surface reflectance user's guide. *MODIS L. Surf. Reflectance Sci. Comput. Facil.*

Verpoorter, C., Kutser, T. & Tranvik, L.J. (2012). Automated mapping of water bodies using Landsat multispectral data. *Limnol. Oceanogr. Methods*, 10, 1037–1050.

Vogeler, J.C. & Cohen, W.B. (2016). A review of the role of active remote sensing and data fusion for characterizing forest in wildlife habitat models. *Rev. Teledetección*, 1.

Vogelmann, J.E., Rock, B.N. & Moss, D.M. (1993). Red edge spectral measurements from sugar maple leaves. *Int. J. Remote Sens.*, 14, 1563–1575.

Walker, D.A., Reynolds, M.K., Daniëls, F.J.A., Einarsson, E., Elvebakk, A., Gould, W.A., *et al.* (2005). The Circumpolar Arctic vegetation map. *J. Veg. Sci.*, 16, 267–282.

Wang, F., McShea, W.J., Wang, D., Li, S., Zhao, Q., Wang, H., *et al.* (2014). Evaluating landscape options for corridor restoration between giant panda reserves. *PLoS One*, 9.

Wang, L., Sousa, W.P., Gong, P. & Biging, G.S. (2004). Comparison of IKONOS and QuickBird images for mapping mangrove species on the Caribbean coast of Panama. *Remote Sens. Environ.*, 91, 432–440.

Waske, B. & Braun, M. (2009). Classifier ensembles for land cover mapping using multitemporal SAR imagery. *ISPRS J. Photogramm. Remote Sens.*, 64, 450–457.

Wegmann, M. & Leutner, B. (2016). Introduction to Remote Sensing and GIS. In: *Remote Sensing and GIS for Ecologists: Using Open Source Software* (eds. Wegmann, M., Leutner, B. & Dech, S.). Pelagic Publishing, Exeter, UK.

Werdell, P.J., Bailey, S.W., Franz, B.A., Harding, L.W., Feldman, G.C. & McClain, C.R. (2009). Regional and seasonal variability of chlorophyll-a in Chesapeake Bay as observed by SeaWiFS and MODIS-Aqua. *Remote Sens. Environ.*, 113, 1319–1330.

Wheeler, D., Hammer, D., Kraft, R. & Steele, A. (2014). Satellite-Based Forest Clearing Detection in the Brazilian Amazon: FORMA, DETER, and PRODES. *World Resour. Inst. Issue Br.*, 1–24.

Whittle, M., Quegan, S., Uryu, Y., Stüewe, M. & Yulianto, K. (2012). Detection of tropical deforestation using ALOS-PALSAR: A Sumatran case study. *Remote Sens. Environ.*, 124, 83–98.

Wilfong, B.N., Gorchov, D.L. & Henry, M.C. (2009). Detecting an Invasive Shrub in Deciduous Forest Understories Using Remote Sensing. *Weed Sci.*, 57, 512–520.

Wohlfahrt, C., Bevanda, M., Horning, N., Leutner, B. & Wegmann, M. (2016). Field data for remote sensing data analysis. In: *Remote Sensing and GIS for Ecologists: Using Open Source Software* (eds. Wegmann, M., Leutner, B. & Dech, S.). Pelagic Publishing, Exeter, UK.

Wolter, P.T. & Townsend, P.A. (2011). Multi-sensor data fusion for estimating forest species composition and abundance in northern Minnesota. *Remote Sens. Environ.*, 115, 671–691.

Woodcock, C.E., Allen, R., Anderson, M., Belward, A., Bindschadler, R., Cohen, W., *et al.* (2008). Free access to Landsat imagery. *Science*, 320, 1011.

Wulder, M.A., Masek, J.G., Cohen, W.B., Loveland, T.R. & Woodcock, C.E. (2012a). Opening the archive: How free data has enabled the science and monitoring promise of Landsat. *Remote Sens. Environ.*, 122, 2–10.

Wulder, M.A., White, J.C., Nelson, R.F., Næsset, E., Ørka, H.O., Coops, N.C., *et al.* (2012b). Lidar sampling for large-area forest characterization: A review. *Remote Sens. Environ.*

Wulder, M.A., White, J.C., Loveland, T.R., Woodcock, C.E., Belward, A.S., Cohen, W.B., *et al.* (2016). The global Landsat archive: Status, consolidation, and direction. *Remote Sens. Environ.*, 185, 271–283.

Xin, Q., Olofsson, P., Zhu, Z., Tan, B. & Woodcock, C.E. (2013). Toward near real-time monitoring of forest disturbance by fusion of MODIS and Landsat data. *Remote Sens. Environ.*, 135, 234–247.

Xiuping Jia & Richards, J.A. (1994). Efficient maximum likelihood classification for imaging spectrometer data sets. *IEEE Trans. Geosci. Remote Sens.*, 32, 274–281.

Xu, H. (2006). Modification of normalised difference water index (NDWI) to enhance open water features in remotely sensed imagery. *Int. J. Remote Sens.*, 27, 3025– 3033.

Xu, L., Saatchi, S.S., Shapiro, A., Meyer, V., Ferraz, A., Yang, Y., *et al.* (2017). Spatial Distribution of Carbon Stored in Forests of the Democratic Republic of Congo. *Sci. Rep.*, 7.

Yang, Z., Wang, T., Skidmore, A.K., De Leeuw, J., Said, M.Y. & Freer, J. (2014). Spotting East African mammals in open savannah from space. *PLoS One*, 9.

Young, N.E., Anderson, R.S., Chignell, S.M., Vorster, A.G., Lawrence, R. & Evangelista, P.H. (2017). A survival guide to Landsat preprocessing. *Ecology*, 98, 920–932.

Zhang, C., Li, W. & Travis, D. (2007). Gaps-fill of SLC-off Landsat ETM+ satellite image using a geostatistical approach. *Int. J. Remote Sens.*, 28, 5103–5122.

Zhu, Z., Bi, J., Pan, Y., Ganguly, S., Anav, A., Xu, L., *et al.* (2013). Global Data Sets of Vegetation Leaf Area Index (LAI)3g and Fraction of Photosynthetically Active Radiation (FPAR)3g Derived from Global Inventory Modeling and Mapping Studies (GIMMS) Normalized Difference Vegetation Index (NDVI3g) for the Period 1981 to 2011. *Remote Sens.*, 5, 927–948.

Zhu, W., Yu, Q., Tian, Y.Q., Becker, B.L., Zheng, T. & Carrick, H.J. (2014). An assessment of remote sensing algorithms for colored dissolved organic matter in complex freshwater environments. *Remote Sens. Environ.*, 140, 766–778.

Zhu, Z. & Woodcock, C.E. (2012). Object-based cloud and cloud shadow detection in Landsat imagery. Remote Sens. Environ., 118, 83–94

Zhu, Z., Wang, S. & Woodcock, C.E. (2015). Improvement and expansion of the Fmask algorithm: cloud, cloud shadow, and snow detection for Landsats 4–7, 8, and Sentinel 2 images. *Remote Sens. Environ.*, 159, 269–277.

A natural-colour image acquired by Landsat 8 OLI, showing phytoplankton blooming east of the Shetland Islands (visible on the left). Multispectral remote sensing has been used to monitor primary productivity in the oceans, as well as map shallow benthic habitats. Source: NASA Earth Observatory image by Joshua Stevens, using Landsat data from USGS.